

NASA TECHNICAL TRANSLATION

NASA TT F-15,533

RESULTS AND INFORMATION OBTAINED REGARDING AERODYNAMIC JET
INTERFERENCE ASSOCIATED WITH THE Do 31 V/STOL JET TRANSPORT
AIRCRAFT AND THEIR APPLICATION TO FUTURE V/STOL DEVELOPMENT

D. Welte

NASA-TT-F-15533) RESULTS AND INFORMATION
OBTAINED REGARDING AERODYNAMIC JET
INTERFERENCE ASSOCIATED WITH THE Do 31
V/STOL JET TRANSPORT (Kanner (Leo)
Associates) 149 p HC \$10.50

N74-20669

Unclas
36288

CSCL 01C 63/02

Translation of "Ergebnisse und Erfahrungen zur Aerodynamischen
Strahlinterferenz beim VSTOL-Strahltransportflugzeug Do 31 und
ihre Anwendung auf zukünftige VSTOL-Entwicklungen," Dornier-
Werke G.m.b.H., Friedrichshafen (W. Ger.),
BMVg-FBWT-72-22, 1972, 183 pages



NATIONAL AERONAUTICS AND SPACE ADMINISTRATION
WASHINGTON, D.C. 20546

APRIL 1974

1. Report No. NASA TT F-15,533	2. Government Accession No.	3. Recipient's Catalog No.	
4. Title and Subtitle RESULTS AND INFORMATION OBTAINED REGARDING AERODYNAMIC JET INTERFERENCE ASSOCIATED WITH THE Do 31 V/STOL JET TRANSPORT AIRCRAFT AND THEIR APPLICATION TO FUTURE V/STOL DEVELOPMENT		5. Report Date April 1974	
		6. Performing Organization Code	
7. Author(s) D. Welte, Bonn Bundeswehramt		8. Performing Organization Report No.	
		10. Work Unit No.	
9. Performing Organization Name and Address Leo Kanner Associates Redwood City, California 94063		11. Contract or Grant No. NASW-2481	
		13. Type of Report and Period Covered Translation	
12. Sponsoring Agency Name and Address National Aeronautics and Space Administration, Washington, D.C. 20546		14. Sponsoring Agency Code	
15. Supplementary Notes Translation of "Ergebnisse und Erfahrungen zur Aerodynamischen Strahlinterferenz beim VSTOL-Strahltransportflugzeug Do 31 und ihre Anwendung auf zukünftige VSTOL-Entwicklungen," Dornier-Werke G.m.b.H., Friedrichshafen (W. Ger.), BMVg-FBWT-72-22, 1972, 183 pages			
16. Abstract The most important results concerning jet interference effects for the Do 31 aircraft, resulting from wind tunnel model measurements and flight tests, are presented, and an estimation is given of jet interference effects for future V/STOL project studies. Calculations are based on a single semi-empirical method for determination of jet-induced lift loss in hovering for simple configurations such as the Do 31, and it is possible to calculate the lift loss to within 1% accuracy. The investigation of the jet-induced flow field around the Do 31 during hovering with ground effect and in the transition flight regime yielded a rough estimation of the jet interference effects for future V/STOL studies.			
17. Key Words (Selected by Author(s))		18. Distribution Statement Unclassified-Unlimited	
19. Security Classif. (of this report) Unclassified	20. Security Classif. (of this page) Unclassified	21. No. of Pages 149	22. Price \$10.50

TABLE OF CONTENTS

	<u>Page</u>
I. THE SIGNIFICANCE OF AERODYNAMIC JET INTERFERENCE TO V/STOL ENGINEERING, BASED ON EXPERIENCE OBTAINED FROM Do 31 DEVELOPMENT AND FLIGHT TESTING	1
1. The Significance of Jet Interference Associated with V/STOL Aircraft	1
2. Jet Interference Associated with the Do 31	4
3. Jet Interference Associated with Future V/STOL Aircraft	8
II. MAJOR RESULTS ON AERODYNAMIC INTERFERENCE OBTAINED FROM Do 31 DEVELOPMENT AND FLIGHT TESTING AND THEIR APPLICATION TO FUTURE V/STOL AIRCRAFT	
1. Jet Interference Model Measurements Performed During Do 31 Development and Testing	12
2. Preparation of Measurement Data for the Balance of Forces and Torques in Do 31 Transitions	31
3. Evaluation of Representative Do 31 Transitions with Respect to Jet-Induced Forces and Torques, and Comparison with Model Measurements	47
4. Guidelines for Model Tests for Future V/STOL Development	93
5. Basic Material for Estimating Jet Interference in Hover and in Transition for Future V/STOL Aircraft	109
6. Summary	146

PRECEDING PAGE BLANK NOT FILMED

RESULTS AND INFORMATION OBTAINED REGARDING AERODYNAMIC JET INTERFERENCE ASSOCIATED WITH THE Do 31 V/STOL JET TRANSPORT AIRCRAFT AND THEIR APPLICATION TO FUTURE V/STOL DEVELOPMENT

Dieter Welte,
Bonn Bundeswehramt

I. THE SIGNIFICANCE OF AERODYNAMIC JET INTERFERENCE TO V/STOL ENGINEERING, BASED ON EXPERIENCE OBTAINED FROM Do 31 DEVELOPMENT AND FLIGHT TESTING

/2*

1. The Significance of Jet interference Associated with V/STOL Aircraft

In the design, development and operation of vertical or ultrashort takeoff aircraft, new types of problems, relative to conventional takeoff aircraft, occur which are based on the type of propulsion system or on the generation of thrust through the use of power plant jets directed downward.

The flow fields generated by these downward-directed power plant jets are the cause of effects associated with V/STOL aircraft takeoffs and landings, known as

- recirculation
- ground erosion
- jet interference.

The influence which these effects have on the operation, characteristics and performance of the aircraft is a function of

- the configuration of the aircraft (aircraft geometry and arrangement of power plants) and
- the type of power plant jets (lift generated by rotor, propeller, lift fan, bypass or single-stage power plants of various jet intensity).

Aerodynamic jet interference, or jet interference for short, refers to the effect on external aircraft aerodynamics due to the power plant jets. The cause of this effect is the secondary flow induced by a jet and the interaction of several power plant jets close to the ground.

/3

* Numbers in the margin indicate pagination in the foreign text.

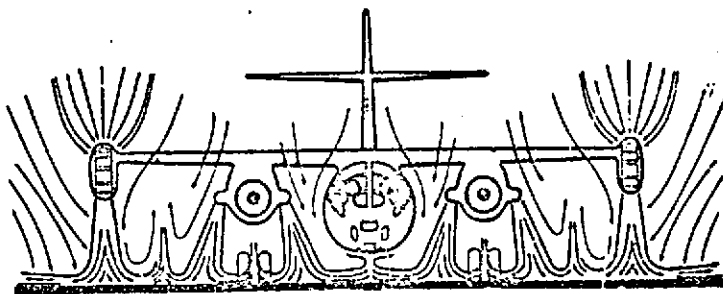
Jet interference produces different effects during various VTOL phases of flight, i.e.

- in hover in the immediate vicinity of the ground (first phase of takeoff, last phase of landing)

- in hover above the ground effect (vertical takeoff and landing)

- in transition flight (takeoff and landing transitions).

In hover close to the ground, the jet effect is due to the three factors shown in the illustration below:



- sink effect

- fountain development

- suction effect (not visible here).

The sink effect is produced by turbulent jet mixing with the surrounding air and primarily generates an underpressure region on the underside of the aircraft. Between neighboring power plants or groups of power plants, energetic exhaust gas fountains from the ground flow against the underside of the aircraft and produce an upward force. Power plant jets which flow between the ground and the underside of the aircraft produce an additional downward force due to the suction effect. The three effects are superimposed on one another in quite different manners in each individual case.

/4

In hover beyond the ground effect, only the sink effect occurs.

In transition flight, beyond the ground effect, jet interference can be broken down into a near field and a far field effect. As outlined in the illustration,

- blockage,

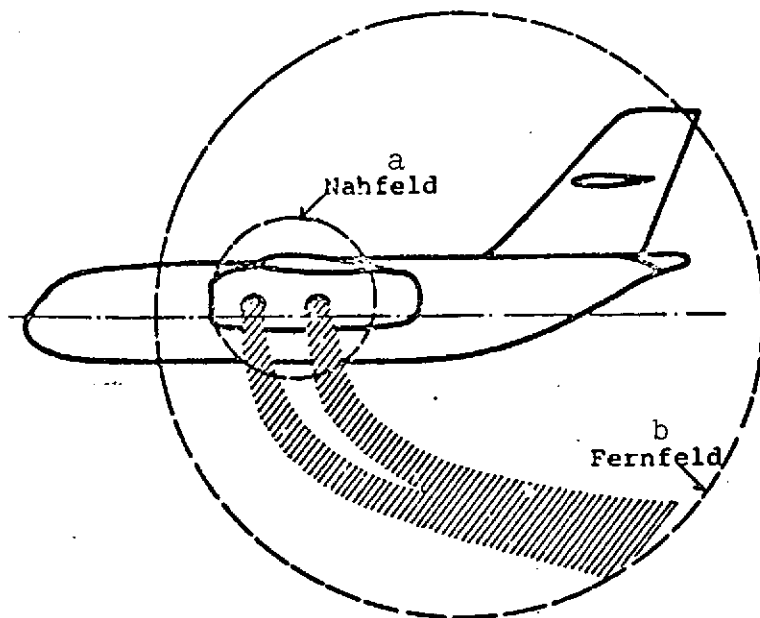
- the wake, and

- the lowering effect

are operant in the near field and

-- downwash induction

is operant in the far field.



Key: a. Near field
b. Far field

The blockage of flow about the aircraft by the presence of the jet produces a relatively small change in pressure distribution in the near field. There is an area of reduced overall pressure in the jet wake, which primarily has its effect in a slight increase in aircraft drag. If the control surfaces are located in the jet wake, flight stability is also influenced.

The sink effect produces a downwash in the near field. A downwash field is induced in the far field by jet mixing and jet deflection. Overall, jet inter-

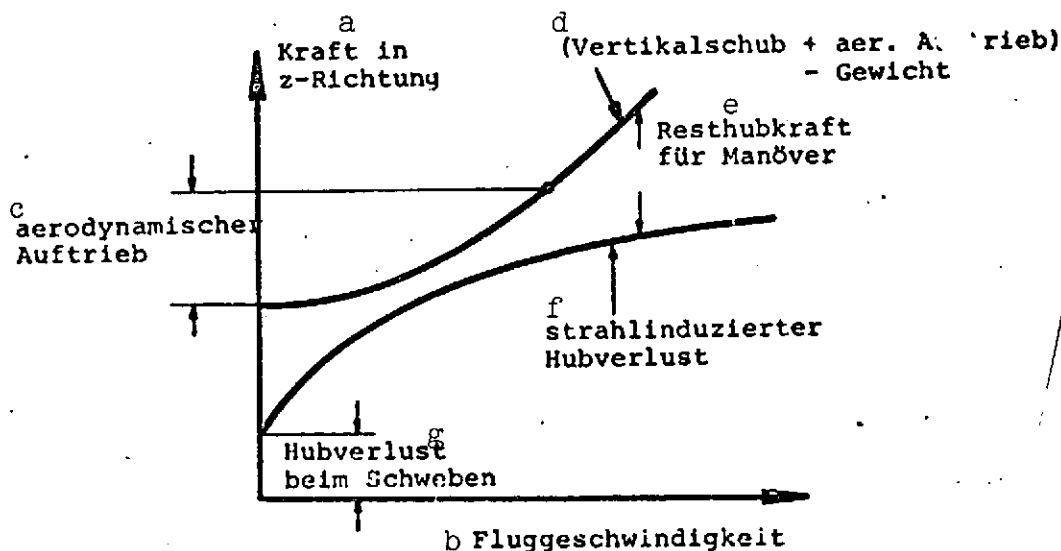
ference generally causes a downward force and a tail-heavy torque during transition flight. When lift fans are used, with their relatively high air throughput, the interference effect of the inlet flow must also be taken into consideration.

All of the jet interference effects described generally reduce the power and the controllability of a V/STOL configuration. During vertical takeoff, the balance of lift must be positive after the subtraction of all losses so that the aircraft can leave the ground. A second condition for vertical takeoff is provision for the failure of the critical power plant. The balanced residual lift must ensure a safe landing. Disruptive torques caused by jet interference are generally small at zero forward speed.

In transition flight, lift loss and disruptive torque normally increase linearly with aircraft speed at first, starting from the value for the hover state; these then become flatter and can decrease again toward the end of the transition phase. Since

/5

aerodynamic lift and aerodynamic control torque increase as the square of air speed, a certain critical speed exists at which residual thrust and/or residual control torque reaches a minimum.



- Key:
- a. Force in z-direction
 - b. Aircraft speed
 - c. Aerodynamic lift
 - d. (Vertical thrust + aerodynamic lift - weight)
 - e. Residual lift for maneuvering
 - f. Jet-induced lift loss
 - g. Lift loss in hover

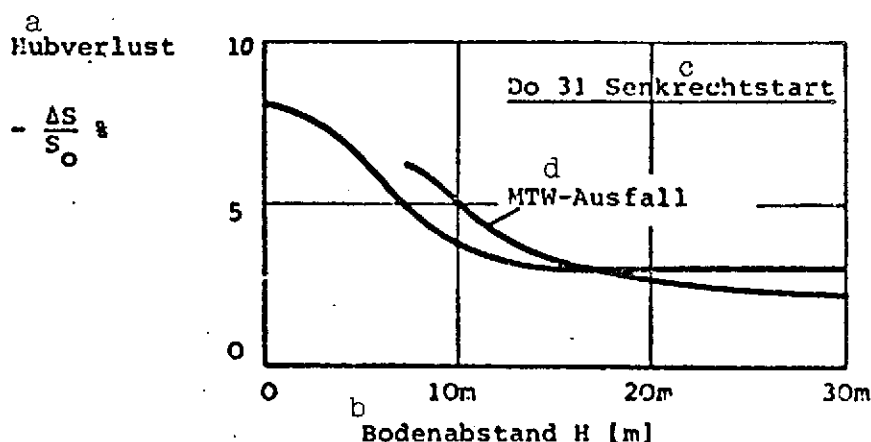
Since a residual control torque and a residual lift necessary for the execution of flight maneuvers are defined in the aircraft approval regulations or recommendations (e.g. FAA, AGARD), an exact knowledge of jet interference effects is important. Aircraft configuration, the position of power plants relative to one another, power plant thrust ratio and jet direction are the significant parameters which determine the magnitude of residual lift and residual control torque and the critical speed.

/6

2. Jet Interference Associated with the Do 31

The aerodynamic problems which occurred in connection with jet interference during Do 31 development were solved primarily by experimental means. The jet-induced forces and torques in hover and transition flight, with and without ground effect, were measured in the wind tunnel.

Lift loss in hover outside of the ground effect is about 3.5% of gross thrust and increases to a maximum of 8% as the ground is approached. An important point is the failure of a cruising power plant. Lift loss is reduced to about 2% outside of the ground effect, since the cruising power plant which has failed, mounted under the inboard wing, induces greater losses than a lift power plant, suspended at the wing tips. Loss increases somewhat more steeply as the ground is approached, however. The jet-induced torques are small in hover with and without the ground effect as measured with the available control torques. /7



Key: a. Lift loss
 b. Ground distance
 c. Vertical takeoff
 d. Failure of cruising power plant
 S = Thrust

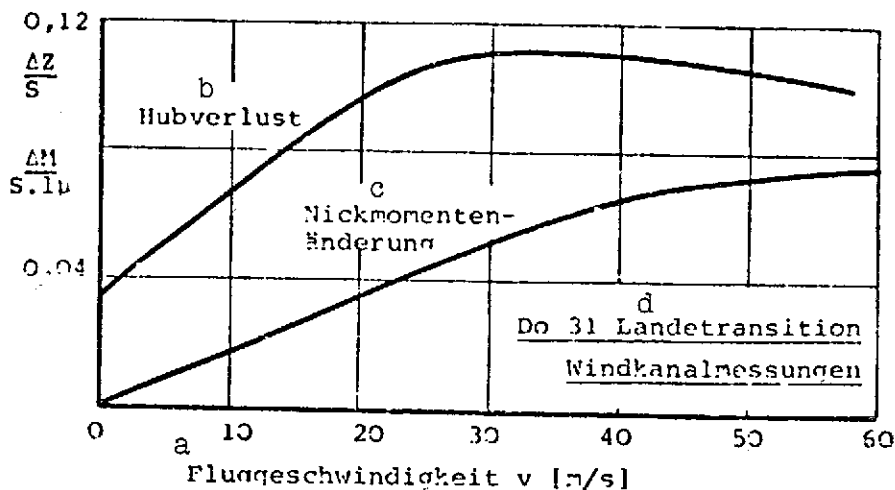
The measured lift losses are taken into consideration in compiling the balance of lifts and/or in determining maximum vertical takeoff weights. The cases indicated in the table below are decisive in the limitation of maximum vertical takeoff weight in the Do 31.

In the first case, 8% is used for lift loss due to jet interference. In addition, a lift loss due to the increase in inlet temperature caused by recirculation must be taken into consideration. The critical case is the failure of a cruising power plant during the takeoff process. Under the condition of an oblique point takeoff, a reliable emergency landing is ensured with a residual lift of 95% of aircraft weight. During an oblique point takeoff, the aircraft climbs away from the takeoff point along a path inclined at 25°. In this case, the values outside the ground effected are used for loss figures.

Case	Thrust requirement	Thrust loss due to jet interference	Increase in inlet temperature	Max. vertical takeoff weight, H = 600 m, ISA
1. VTO All power plants intact	$\frac{F_{\text{tot max}}}{W_t} = 1.03$	$\frac{\Delta F}{F} = 8\%$	$\Delta T_{\text{CPP}} = 15^\circ\text{C}$ $\Delta T_{\text{LPP}} = 5^\circ\text{C}$	21,000 kg
2. VTO one cruising power plant fails	$\frac{F_{\text{Res}}}{W_t} = 0.95$	$\frac{\Delta F}{F} = 2\%$	Zero	19,530 kg

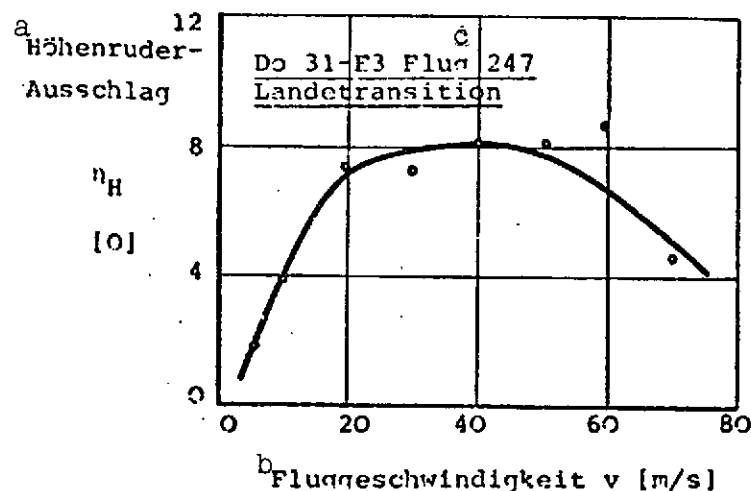
In Do 31 transition flight, the change in normal force and pitch torque due to jet interference initially varies as a linear function of aircraft speed. The change in normal force becomes flatter with increasing aircraft speed and reaches a value of 10 to 12% of total thrust at about the middle of the transition. The change in normal force during transition flight involves no limitation on the maximum vertical takeoff weight of the Do 31, since the above-mentioned condition for vertical takeoff and for power plant failure is appreciably less favorable for oblique point takeoff.

/8



Key: a. Aircraft speed; b. Lift loss; c. Change in pitch torque; d. Landing transition, wind tunnel measurements; S = thrust.

Extreme control-surface positions are necessary to trim the jet-induced pitch torque during the transition. The figure below shows the curve of elevator angle during the landing transition by the Do 31 E3.

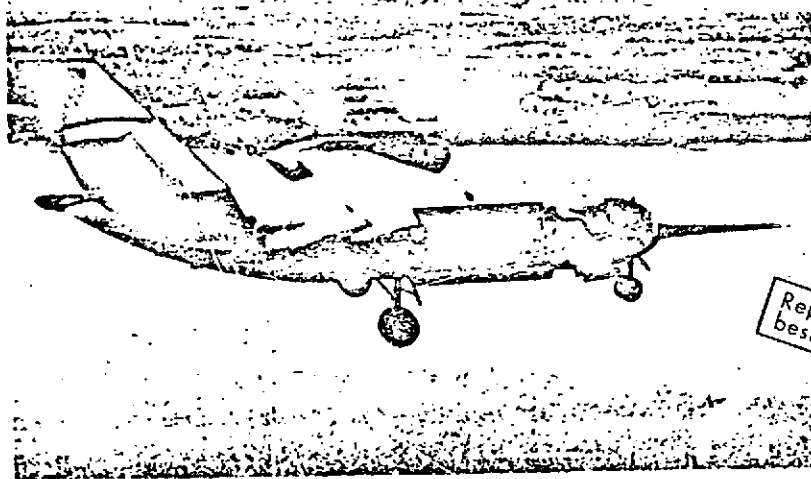


Key: a. Elevator angle; position;
b. Aircraft speed
c. Flight 247, landing transition

Elevator angle is coupled with the gate of the tail control nozzle. At $\eta_H = 12.5^\circ$, the tail control nozzle is wide open and delivers maximum control thrust. The elevator can be angled even farther. Its effectiveness drops off beyond about $\eta_H = 16^\circ$. We see that up to half of the available control torque is required to compensate for jet-induced pitch torque during transition. This example shows that jet interference is a factor which is not to be underestimated in the design of future V/STOL aircraft.

The measurement of jet-induced forces and torques in the wind tunnel made the development of new test techniques necessary. Model and measurement engineering are presented with unconventional tasks. Two wind tunnel models were built and had measurements performed on them during the course of Do 31 development. One model was equipped with electrically driven model motors. In the second model, compressed air was discharged to simulate jets. The latter method proved to be the more effective. It is also to be recommended for interference studies on future V/STOL aircraft for the case of zero forward speed.

A series of takeoff and landing transitions with the Do 31 E3 test aircraft were analyzed with regard to forces and torques. Algorithms programmed for the IBM 360 were developed which calculate instantaneous thrusts, weight and aerodynamic quantities from the measured data. The thrust and torque balance yields the jet-induced forces and torques as residual terms. Since a relatively small difference between several larger numbers is involved, extremely high requirements are placed on the accuracy of the data, but are not always satisfied.



Reproduced from
best available copy.

Agreement between the results of wind-tunnel and flight tests is not satisfactory for all flight states; it is justifiable to conclude, however, that wind tunnel measurements can be reliably applied to the large-scale design.

A prerequisite for applicability is that, in addition to geometric similarity, the momentum densities of thrust and on-coming flow be proportional in the model and in the full-scale design.

3. Jet Interference Associated with Future V/STOL Aircraft

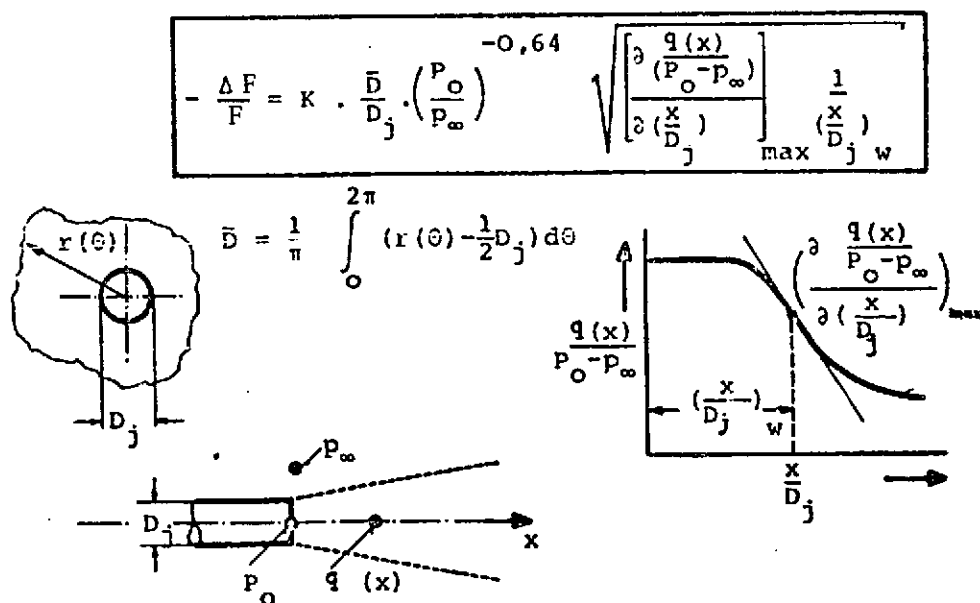
Due to their importance in the designing of a V/STOL aircraft, data on the effects of jet interference upon flight performance and characteristics are necessary while still in the early development stage.

A generally valid calculation of jet-induced forces and torques is possible only for the case of hover outside the ground effect. An empirically determined relation can be given between lift loss $\Delta F/F$, the ratio of aircraft equivalent diameter D to nozzle diameter D_j , and the decrease in stagnation pressure along the jet axis. The Mach number effect in free jet propagation is taken into consideration with an additional term in the form of the ratio of overall jet pressure P_0 to static ambient pressure p_∞ . A value of about $K = 0.0136$ is obtained for the constant from model measurements.

/11

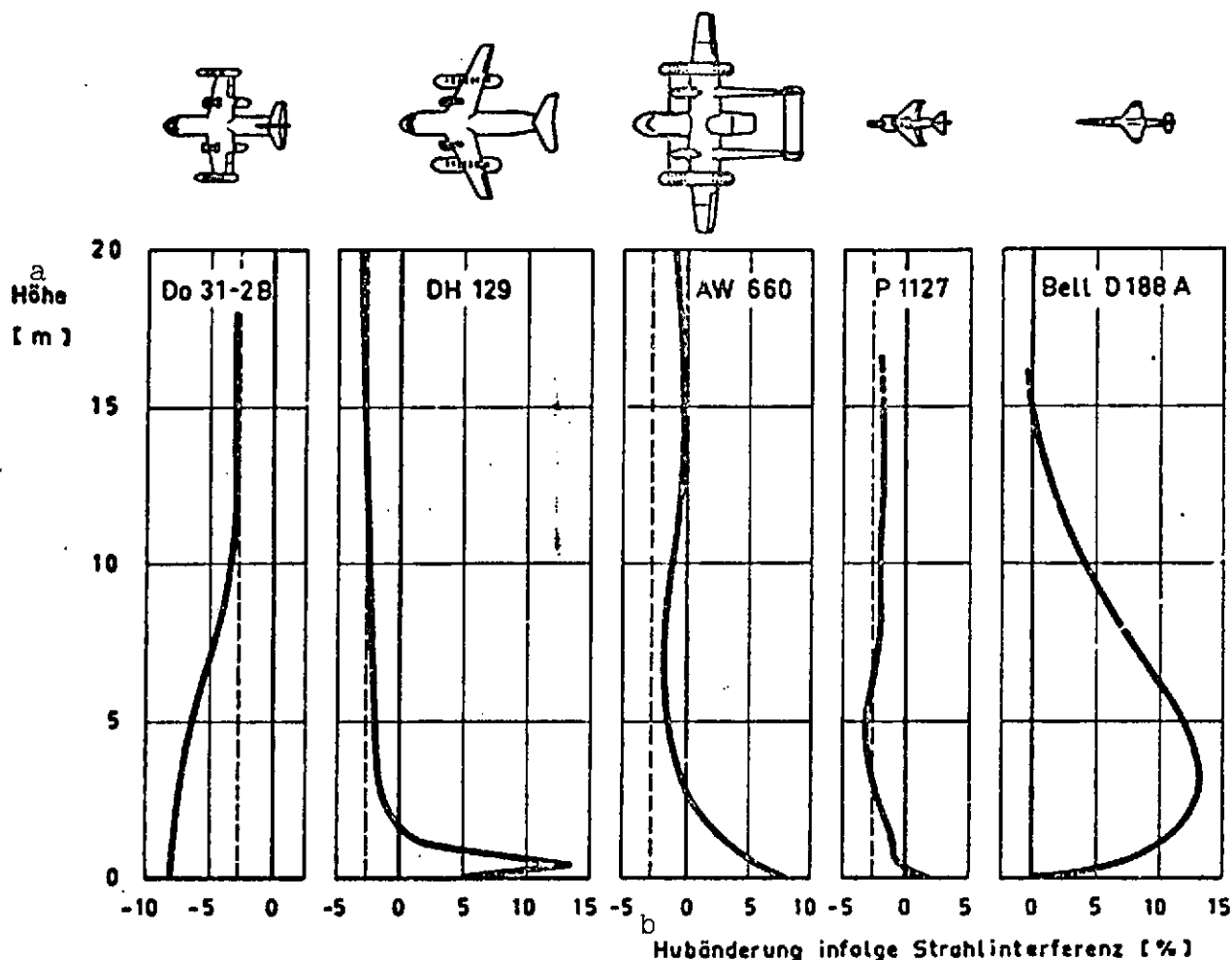
During vertical takeoff, vertical landing, or hovering close to the ground, the fountain effect is superimposed on the sink effect, and its influence on the forces and torques can only be

given in terms of trends for a given V/STOL configuration. The pattern of flow on the ground, including the positions of stagnation points or stagnation lines, and the directions of ascent of the fountains can be roughly determined from simple momentum considerations, so an estimate of the order of magnitude of negative or positive changes in lift and head- or tail-heavy torque is also possible. The flow field close to the ground is relatively easily influenced by small changes in the nozzle angles or in aircraft inclination. Upwash and thus the balance of forces and torques can be effected with relatively small control surfaces on the fuselage. Thus we still have possible means of effecting changes even in advanced stages of development without having to basically alter configuration. In civilian applications, it is possible to use gratings as takeoff surfaces. These serve primarily to lead off the hot exhaust gases; in addition, however, they also cause interference to be reduced to the case of hover outside the ground effect region.



The figure below shows the results of measurements performed on models: change in lift due to jet interference on various VTOL aircraft as a function of altitude. /12

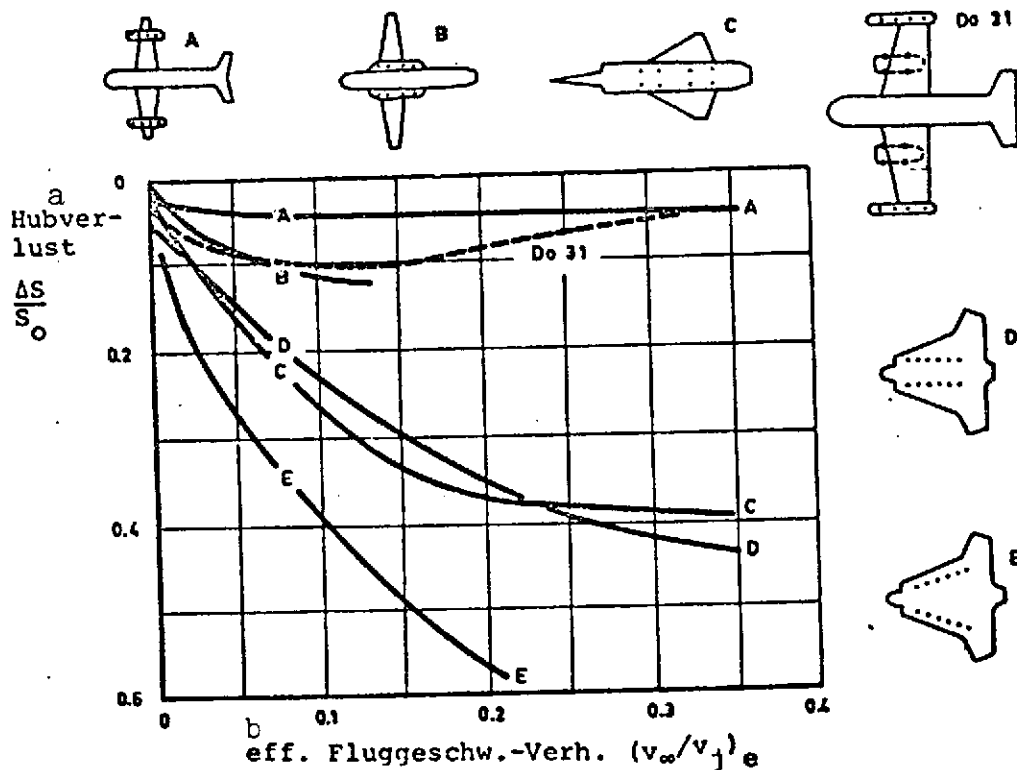
We are so far still a long way from being able to give the design engineer satisfactory data on jet interference, without prior wind tunnel measurements, for the case of transition flight. Although there are a number of potential-theory formulations which include the blockage and sink effects of a jet /13



Key: a. Altitude
b. Change in lift due to jet interference

and yield the induced velocity field, the model representations are still not quite true to reality, and the suction effect and deformation of the jet must be known from measurements. This theory breaks down for power plants arranged in groups on the aircraft. Information is lacking with regard to the propagation of groups of jets with different impinging flow.

A summary of wind tunnel measurements performed on various V/STOL configurations by the British Aircraft Corporation and by Dornier is given in the figure below to provide an overview of the order of magnitude of aerodynamic jet interference in transition flight.



The closer to the margin of the airframe the power plants are located, the smaller jet interference is. The jet-induced torques exhibit similar trends. The power plant component makes up about half of the overall change in torque in the Do 31.

Future V/STOL transport aircraft will primarily employ dual-stage power plants with high bypass ratios or lift fans for the generation of lift. Due to the relatively high air flow rate, not only the thrust jet but also the inlet flow produces an interference effect. In hover, with or without ground effect, the influence of inlet flow upon the balance of forces and torques is still small. Only in transition can changes in torque about the transverse axis and, during side slip, also about the longitudinal axis occur as the result of inlet flow. Interference tests in transition should therefore include not only the simulation of power plant jets but also that of inlet flow. On the basis of the present state of the art, it is recommended that power plants be simulated by means of fans driven electrically via extension shafts.

II. MAJOR RESULTS ON AERODYNAMIC INTERFERENCE OBTAINED FROM Do 31 /15 DEVELOPMENT AND FLIGHT TESTING AND THEIR APPLICATION TO FUTURE V/STOL AIRCRAFT

1. Jet Interference Model Measurements Performed During Do 31 /16 Development and Testing

Overview of Contents

- 1.1. Introduction
- 1.2. Notation
- 1.3. Measurement with the 1:6 Model
- 1.4. Measurements with the 1:20 Model
- 1.5. References

Figures

- 1.1. Do 31 1:6 jet interference model.
- 1.2. Do 31 1:6 jet interference model in the FKFS wind tunnel.
- 1.3. Do 31 jet interference in hover close to ground. Lift loss, pitch torque, roll torque. Configuration for vertical takeoff.
- 1.4. Do 31 jet interference in hover close to ground, with power plant failure. Starboard cruising power plant has failed. Residual thrusts in torque equilibrium. /17
- 1.5. Do 31 jet interference model, 1:20, three views.
- 1.6. Test setup with the Do 31 jet interference model, 1:20, in the Dornier wind tunnel, Immenstaad.
- 1.7. Do 31 jet interference in hover close to ground. Effect of cruising power plant nozzle angle on loss of thrust.
- 1.8. Do 31 jet interference in hover close to ground. Effect of cruising power plant nozzle angle on change in torque.
- 1.9. Do 31 jet interference in transition. Lift, pitch torque. All power plants on takeoff thrust. Angle of attack $\alpha = 0^\circ$.
- 1.10. Do 31 jet-induced downwash at location of lift power plant in transition. All power plants on takeoff thrust. Cruising power plant nozzle angle $\tau_{MTW} = 90^\circ$. Angle of attack $\alpha = 0^\circ$.

- 1.11. Do 31 jet-induced neutral point shift, in transition.
Conditions as in Fig. 1.10.
- 1.12. Do 31 jet interference during short takeoff. Lift,
drag, pitch torque. All power plants on takeoff thrust.
Ground - to - landing gear distance $H/b = 0.025$
Angle of pitch $\theta = 0^\circ$
CPP nozzle angle $\tau_{MTW} = 10^\circ$
LPP nozzle angle $\tau_{HTW} = 75^\circ$
Landing flap angle $\eta_K = 45^\circ$
Angle of attack $\alpha = 0^\circ$

1.1. Introduction

/18

Wind tunnel measurements are an indispensable aid in the development of an aircraft. This is particularly true for a V/STOL project, since certain flow processes can practically be determined here only by experimental means. In particular, the problem involves the phenomena known as jet interference and recirculation.

Jet interference measurements yield the changes in forces, torques and points of force application in all phases of flight and all attitudes; these changes are important for the mechanics of flight. During the developmental phase of the Do 31, these measurements were carried out in the Stuttgart wind tunnel with a 1:6 model. A major portion of the measurements were devoted to the vertical takeoff and vertical landing phases, particularly important in flight testing, including a simulated power plant failure. The most important results are reported in Section 1.3.

In a second phase of jet interference measurements which approximately coincided in time with the beginning of flight testing, the entire range of transition flight of the Do 31 was studied, particularly with regard to comparison with flight test results. The measurements were carried out in the Dornier wind tunnel with a 1:20 model. The most important results are reported in Section 1.4.

1.2. Notation

/19

A	Aerodynamic lift
b	Wing span
C_A, C_W, C_M	Aerodynamic coefficients of lift, drag and pitch torque, respectively
F	Reference area for wing
H	Distance between landing gear and ground
l_μ	Mean aerodynamic wing chord length
L	Roll torque
M	Pitch torque
S_0	Gross thrust
v_∞	Aircraft velocity
v_j	Jet velocity

$$\frac{(v_\infty/v_j)_e}{\sqrt{\frac{v_\infty^2 \rho_\infty}{v_j^2 \rho_j}}} =$$

Effective velocity ratio

α Angle of attack

ϕ	Angle of roll
θ	Angle of pitch
τ	Angle of power plant nozzle rotation ($\tau = 0^\circ$ for jet exhausting rearward)
η_K	Angle of split flaps

1.3. Measurements with the 1:6 Model

/20

The 1:6 model of the Do 31 was designed for the large FKFS (Research Institute for Motor Vehicles and Vehicle Motors) wind tunnel, Stuttgart ($4.8 \times 7.2 \text{ m}^2$) and had the following principal dimensions:

Span (to center of lift power plant pod)	$b = 2.834 \text{ m}$
Wind area	$F = 1.581 \text{ m}^2$
Mean aerodynamic chord	$\bar{x}_\mu = 0.570 \text{ m}$

Fig. 1.1 shows two views of the model, and Fig. 1.2 shows a photograph of the model installed in the wind tunnel, including a wooden panel used for ground simulation.

The cruising power plants were simulated with electrically driven axial compressors with a rated power of 20 hp each at 20,000 rpm. The lift power plant pods were equipped with three outlet nozzles, corresponding to the earlier design. Thrust was generated by one crossflow fan per lift pod, driven by a medium frequency motor at a reduced speed of $n = 8500 \text{ rpm}$. The tests were conducted primarily with the following thrusts:

2 lift power plant pods = 9.36 kp [1 kp = 1 kg force]

2 cruising power plant pods = 14.20 kp.

The power plants were rigidly connected to the model. The electrical lines were led out of the tail of the fuselage via a system that followed the angle of attack.

The lower portion of Fig. 1.2 shows a photograph of the power plants mounted on the calibrating frame. This made it possible to determine power plant thrusts outside the airframe. The jet-induced forces and torques were determined from the difference between model measurement and thrust measurement.

/21

Figs. 1.3 and 1.4 show the most important results from the measurements. Jet-induced lift loss, pitch torque and roll torque are plotted against ground distance in Fig. 1.3. As long as the landing gear is in contact with the ground, lift loss amounts to 8% of gross lift. After liftoff, lift loss decreases relatively rapidly and remains constant at 3 to 3.5% at a distance of 1 wing span or more from the ground.

Pitch torque is slightly nose-heavy in the immediate vicinity of the ground but has a stabilizing effect when changes in the angle of pitch occur. It drops off rapidly upon liftoff and yields a constant, relatively low tail-heavy torque beyond 4 or 5 m. Maximum available jet control torque is

$$M/(S_0 \cdot l_\mu) = \pm 0.125.$$

Roll torque has an unstabilizing effect when an angle of roll exists, but is relatively small compared to the maximum available control torque of $L/S_0 \cdot b/2 = \pm 0.17$ and decreases with altitude above ground. The zero point shift at $\phi = 0^\circ$ is due to the asymmetry of the flow field. Fig. 1.4, analogous to Fig. 1.3, shows conditions accompanying failure of the critical power plant, i.e. the cruising power plant in the case of the Do 31. The thrusts of the remaining power plants are suitably throttled or increased to emergency thrust levels in order to maintain torque equilibrium. Lift loss outside the ground effect has dropped to about 2%. The reason for this is that the lift power plant jets produce less lift loss, in relative terms, than the cruising power plant.

The measurement results have been incorporated into the balances of lifts which were used to determine maximum vertical takeoff weights. Aside from a strength limit, two requirements had to be met here:

/22

a) For vertical takeoff, excess thrust was to amount to at least 3% of takeoff weight; among other things, the loss for jet interference was taken to be 8%.

b) Upon failure of a cruising power plant, a balanced residual thrust of at least 95% of takeoff weight was to remain; among other things, the loss due to jet interference was taken to be 2%, since this case was assumed to occur out of ground effect only.

The corresponding wind tunnel test reports are presented in [1-4].

1.4. Measurements with the 1:20 Model

/23

The 1:20 model of the Do 31 was built for the Dornier wind tunnel ($2.20 \times 3.20 \text{ m}^2$) and had the following principal measurements:

Span	$b = 1.24 \text{ m}$
Wing area	$F = 0.22 \text{ m}^2$
Mean aerodynamic chord	$l_{\mu} = 0.186 \text{ m.}$

Fig. 1.5 shows three views of the model. Compressed air was blown out of nozzles to simulate the power plant jets. The nozzles, with compressed air lines, were rigidly connected to a system which followed the angle of attack and did not make contact with the Do 31 model. Fig. 1.6 shows the test setup. A base panel, 3 m in diameter, adjustable in height and inclination, was used for ground simulation.

A detailed report on the measurements can be found in [5].

A summary of the most important results is given for hover in Figs. 1.7 and 1.8, for transition flight in Figs. 1.9 through 1.11, and for short takeoff in Fig. 1.12.

Figs. 1.7 and 1.8 show the curves of lift and torque variation with ground distance for three angles of rotation $\tau_{\text{cpp}} = 60^\circ$, 90° and 120° for the cruising power plants. The effect of angles of pitch which occur in practice during the takeoff and landing processes ($-10^\circ < \theta < +10^\circ$) is indicated by hatched regions. The effects of nozzle angle of rotation and the angle of pitch are on the same order of magnitude. Overall, however, the disturbances are no greater than those measured with the 1:6 model and can be easily controlled.

Fig. 1.9 shows the curves of changes in lift and torque versus effective velocity ratio. The latter is a parameter commonly used in jet interference studies and is the root of the ratio of momentum densities in the oncoming flow and power plant jets. The angle of nozzle rotation on the cruising power plants appears as an additional parameter. /24

At $(v_\infty/v_j)_e = 0$, the familiar losses associated with hover occur.

The interference effects of power plant jets exhausting normally from a wing can, in highly simplified terms, be broken down into a near field and a far field. In the near field, the stagnation of oncoming flow upstream from the nozzle jet, the dead-water region in the lee of the jet, and the suction effect of the jet lead primarily to a change in the pressure distribution on the wing and cause a change in lift and torque. In the far field, which might be defined as the region where the jet is already deflected into the oncoming flow to a large degree, the suction effect of the jet induces a downwash field which contributes to the change in torque primarily at the elevator. The change in downwash angle at the location of the Do 31 lift power plants was

determined by the probe-surface method and is plotted against effective velocity ratio in Fig. 1.10.

Fig. 1.11 shows the curves of neutral point shift versus velocity.

Finally, Fig. 1.12 shows the effect of the coefficient of thrust upon the aerodynamic coefficients of longitudinal motion close to the ground, as required for short takeoff calculations.

An exact description of the tests is given in [5].

REFERENCES

1. Esch, P., "Do 31 2 B wind tunnel tests, measurement period II: 25 measurements with and without thrust," Dornier VW 313-B2.
2. Esch, P., "Do 31 2 B wind tunnel tests, measurement period III: measurements with thrust," Dornier VW 313-B3.
3. Esch, P., "Do 31 2 B wind tunnel tests, measurement period IV: ground effect measurements," Dornier VW 352-B2.
4. Esch, P., "Do 31 2 B wind tunnel tests, measurement period V: ground effect measurements," Dornier VW 352-B6.
5. Esch, P. and Joos, R., "Do 31 2 B interference and ground effect measurements in the DW wind tunnel," Dornier VW 537-B1.

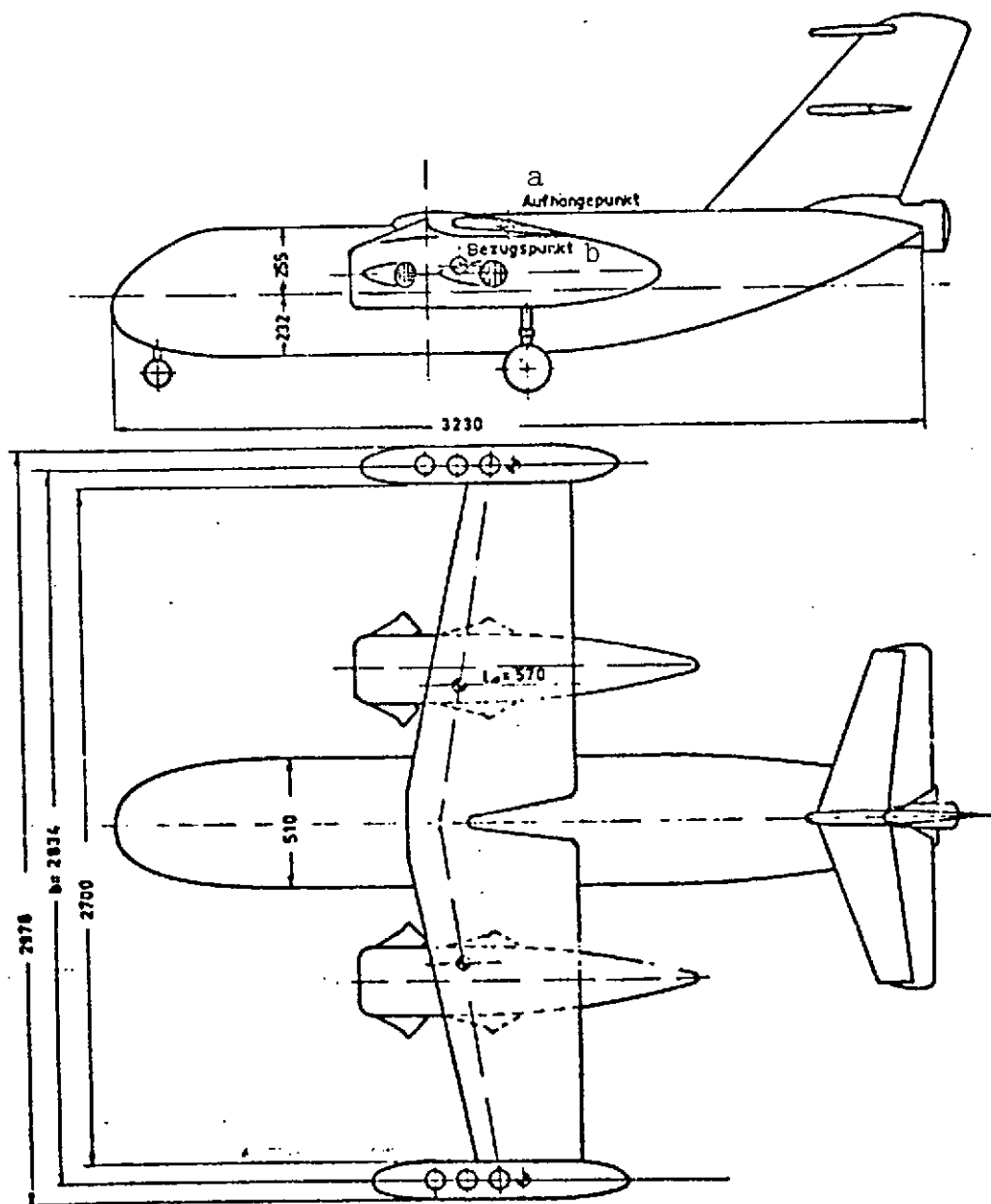
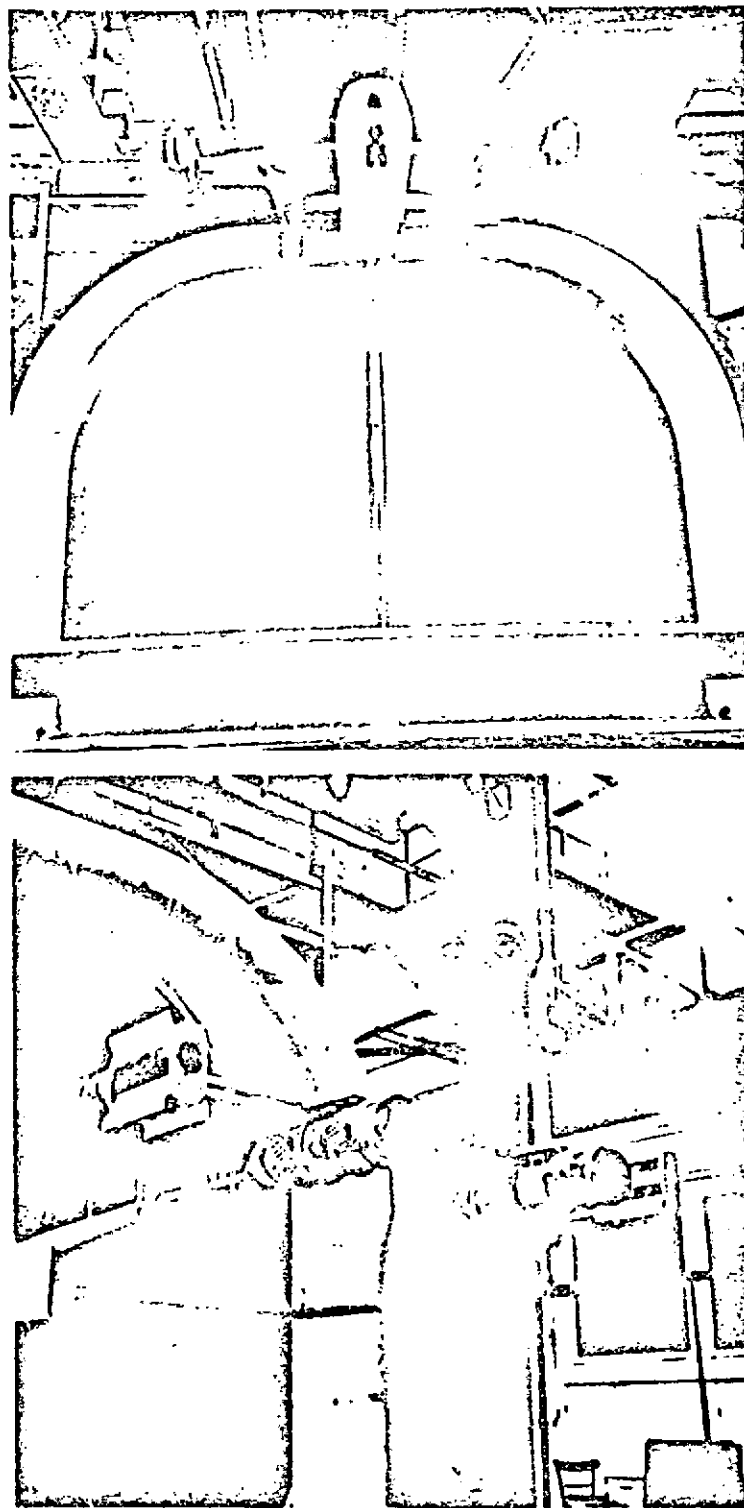


Fig. 1.1. Do 31 1:6 jet interference model.

Key: a. Suspension point
b. Reference point



Reproduced from
best available copy.

Fig. 1.2. Do 31 1:6 jet interference model in the FKFS wind tunnel.

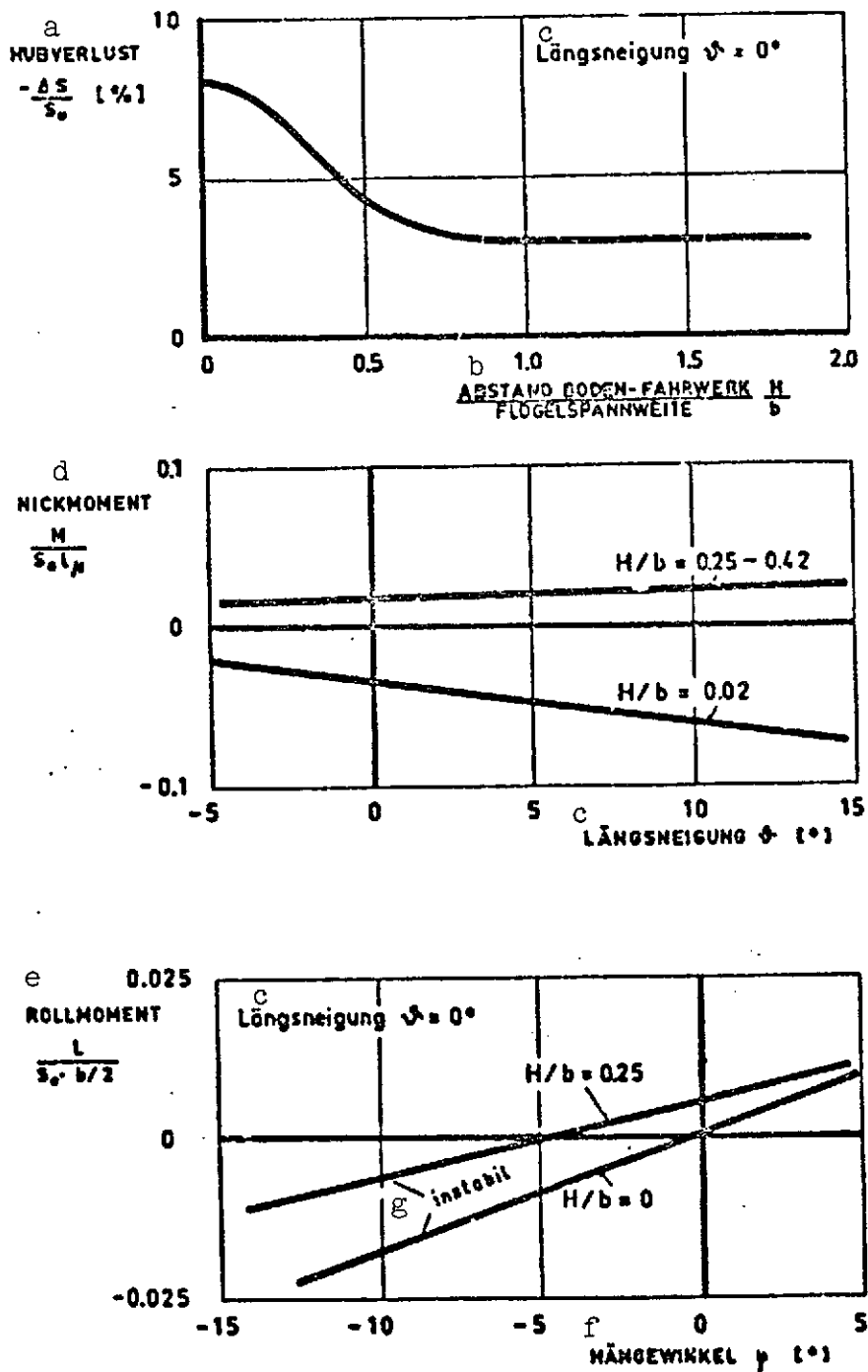


Fig. 1.3. Do 31 jet interference in hover close to ground. Lift loss, pitch torque, roll torque. Configuration for vertical takeoff.

- Key:
- a. Lift loss
 - b. (Ground- to - landing gear distance)/(wing span)
 - c. Angle of pitch
 - d. Pitch torque
 - e. Roll torque
 - f. Angle of roll
 - g. Unstable

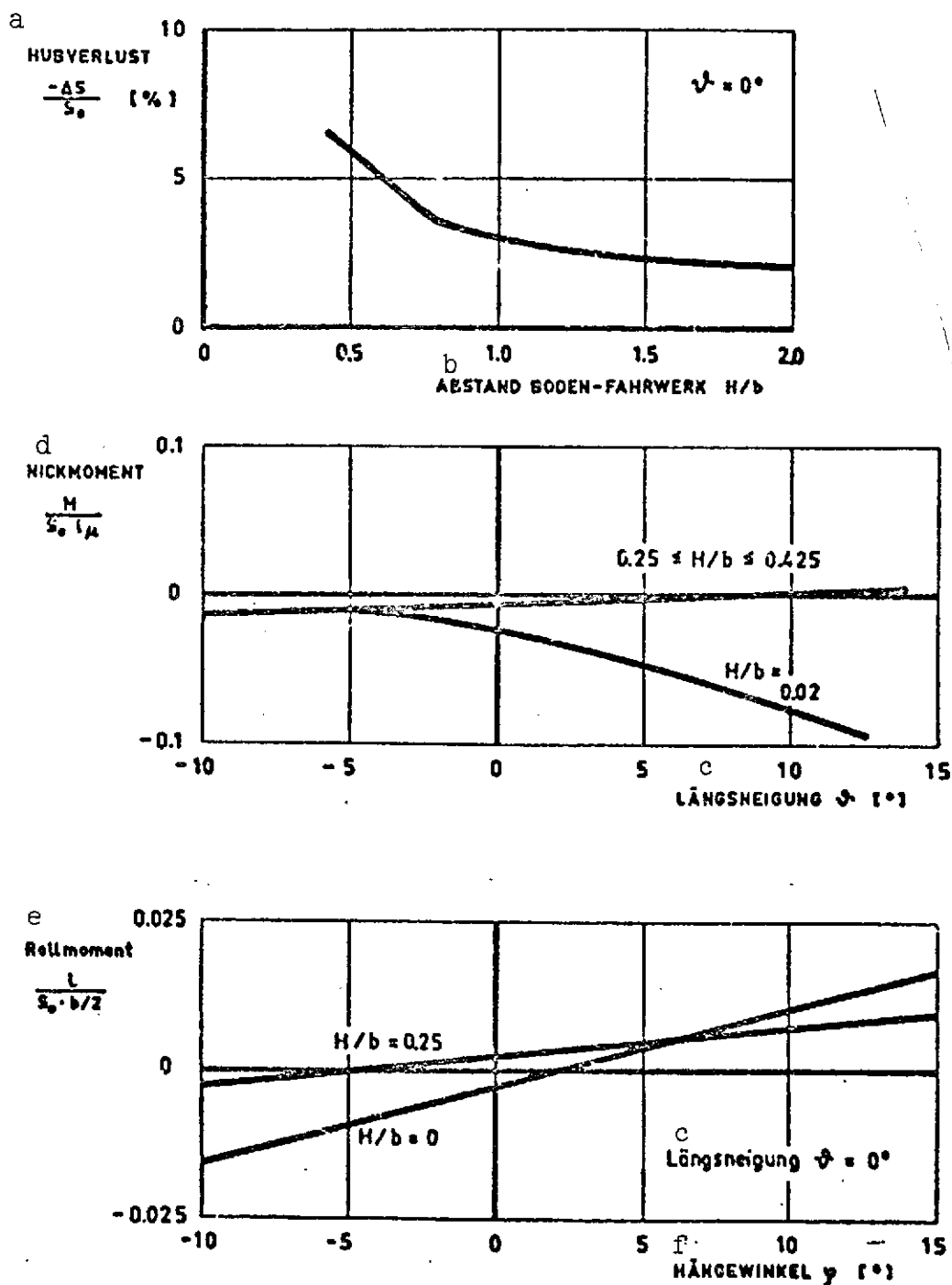
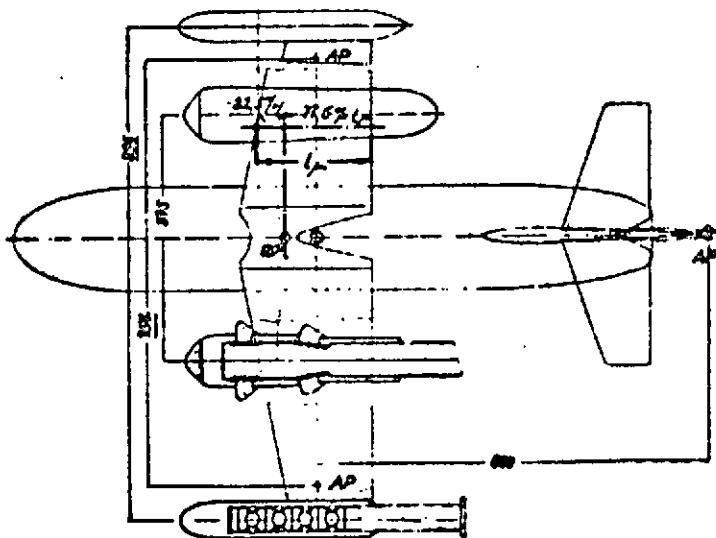


Fig. 1.4. Do 31 jet interference in hover close to ground, with power plant failure. Starboard cruising power plant has failed. Residual thrusts in torque equilibrium.

- Key:
- a. Lift loss
 - b. (Ground - to - landing gear distance)
 - c. Angle of pitch
 - d. Pitch torque
 - e. Roll torque
 - f. Angle of roll



[Note: Commas in numerals are equivalent to decimal points.]

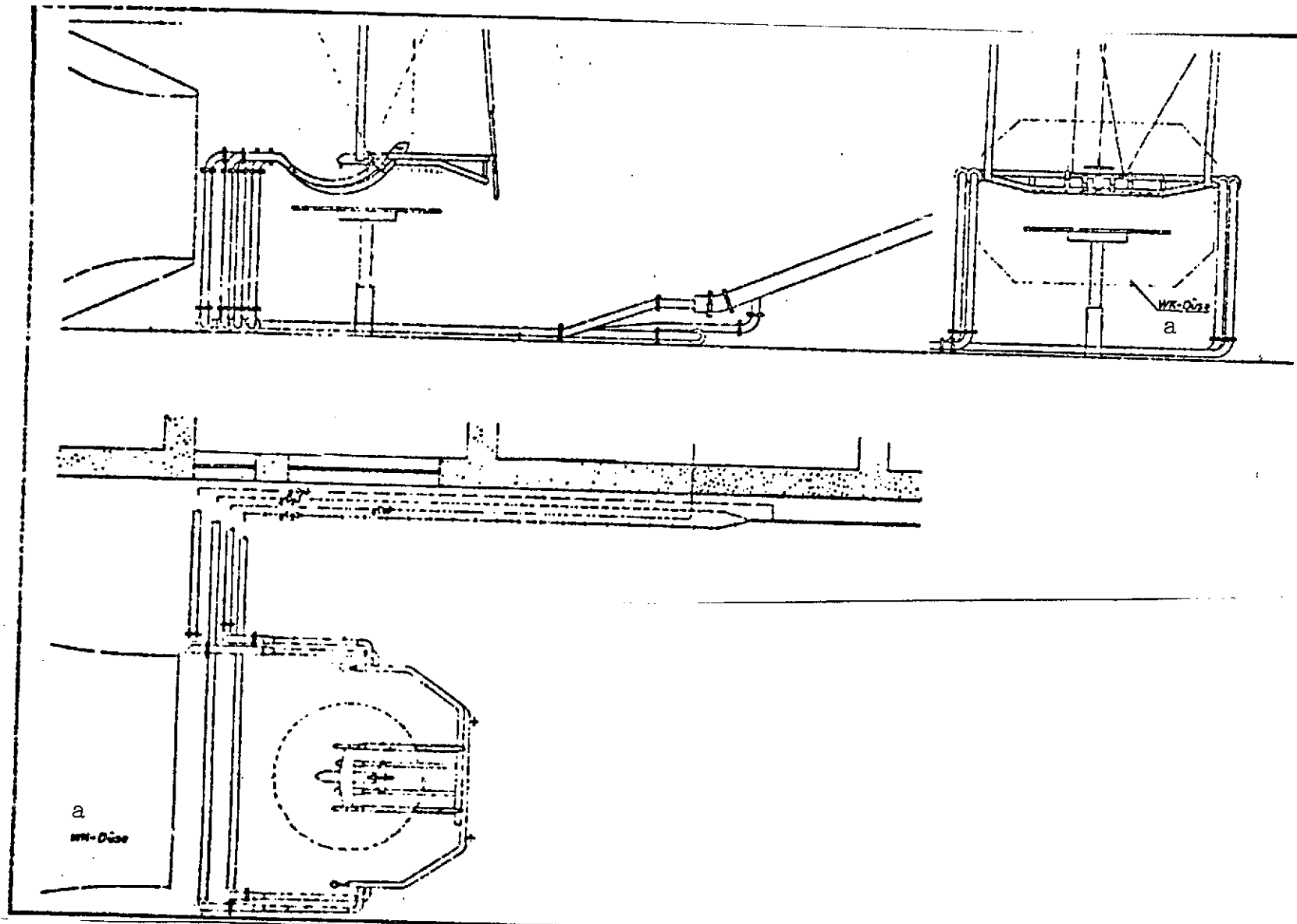


Fig. 1.6. Test setup with the Do 31 jet interference model, 1:20, in the Dornier wind tunnel, Immenstaad.

Key: a. Wind tunnel nozzle

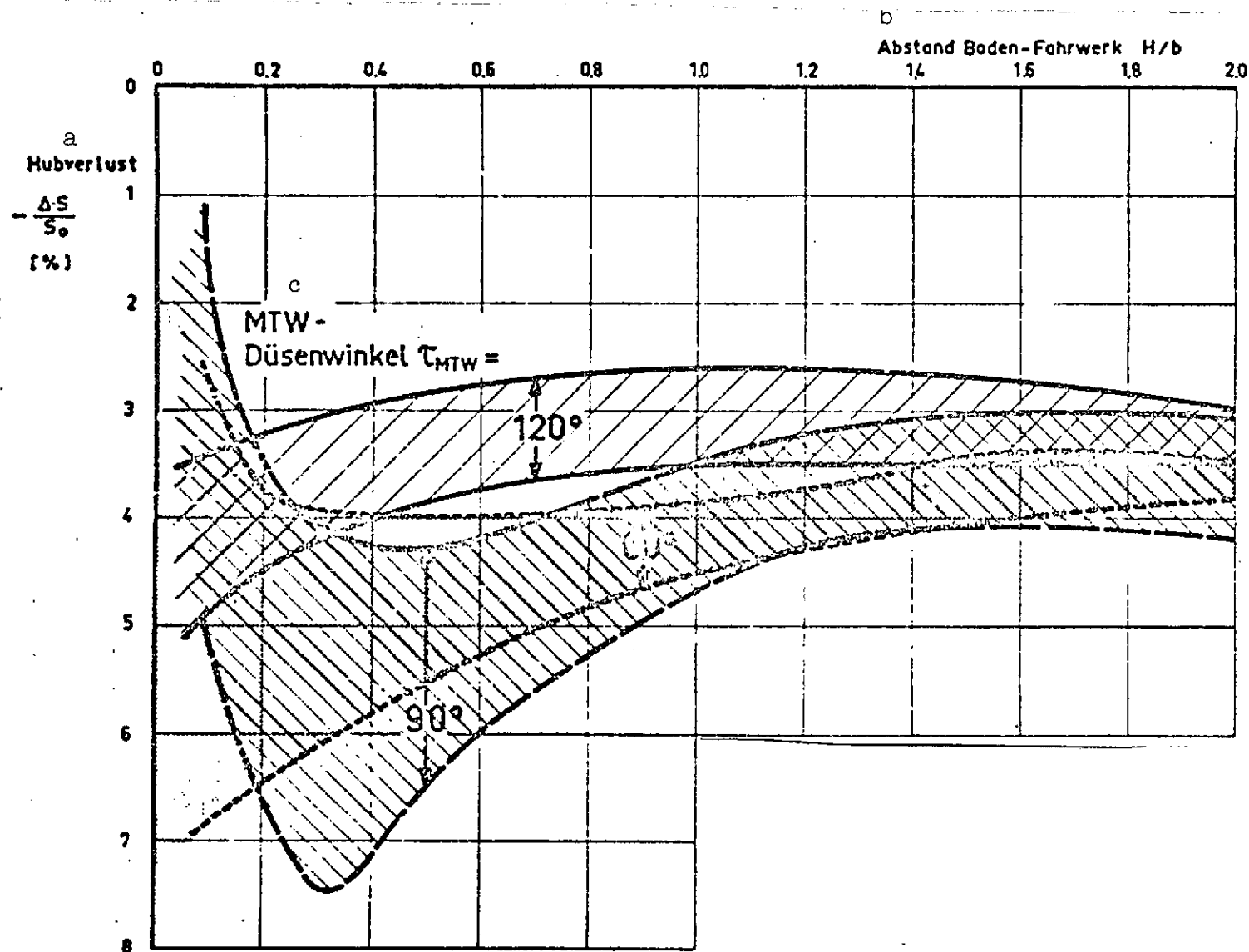


Fig. 1.7. Do 31 jet interference in hover close to ground. Effect of cruising power plant nozzle angle. All power plants on takeoff thrust. Angle of pitch: $-10^\circ < \theta < +10^\circ$.

Key: a. Lift loss; b. Ground - to - landing gear distance;
c. Cruising power plant nozzle angle

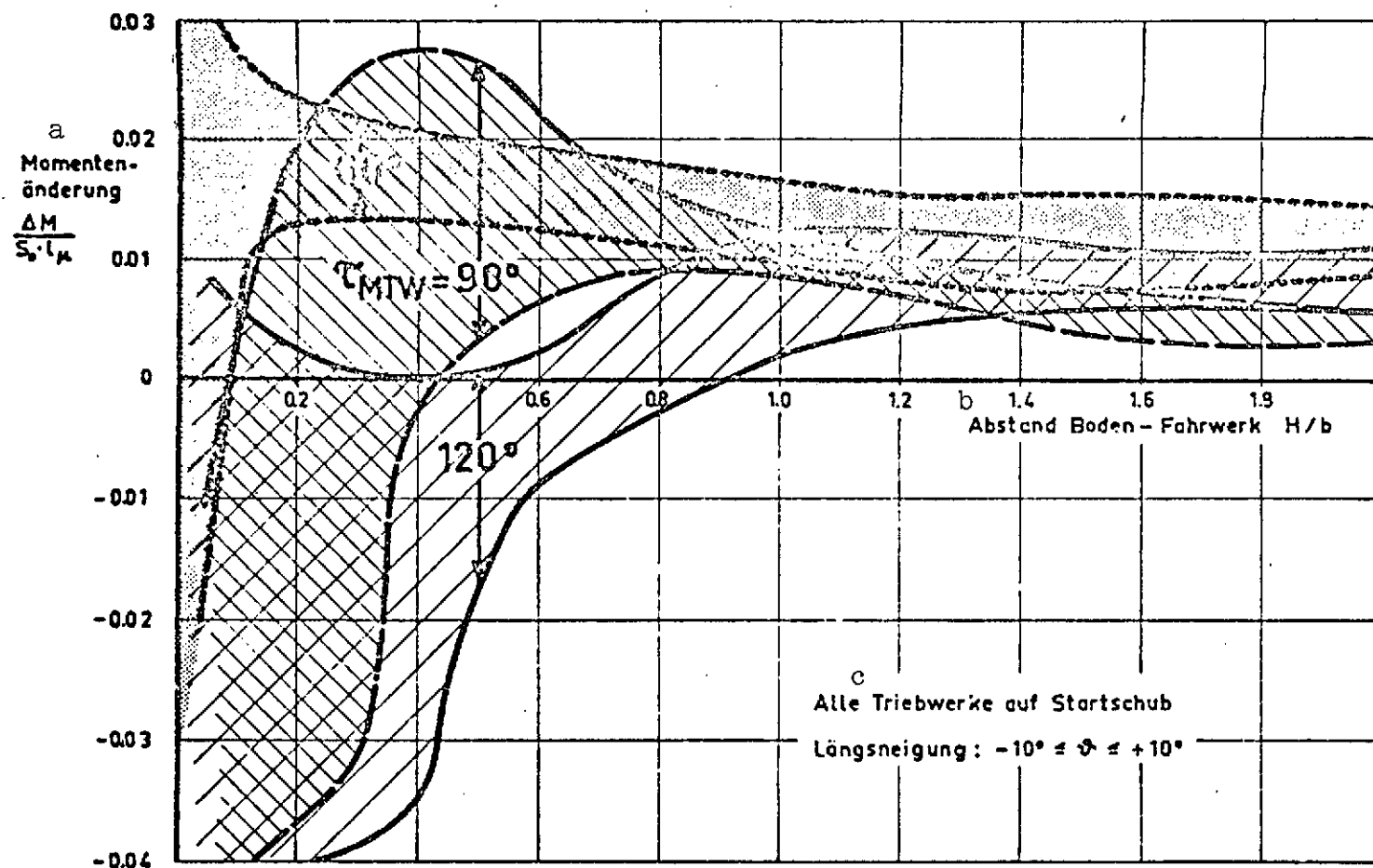


Fig. 1.8. Do 31 jet interference in hover close to ground.
Effect of cruising power plant nozzle angle.

Key: a. Change in torque
b. Ground - to - landing gear distance
c. All power plants on takeoff thrust. Angle of pitch: ...

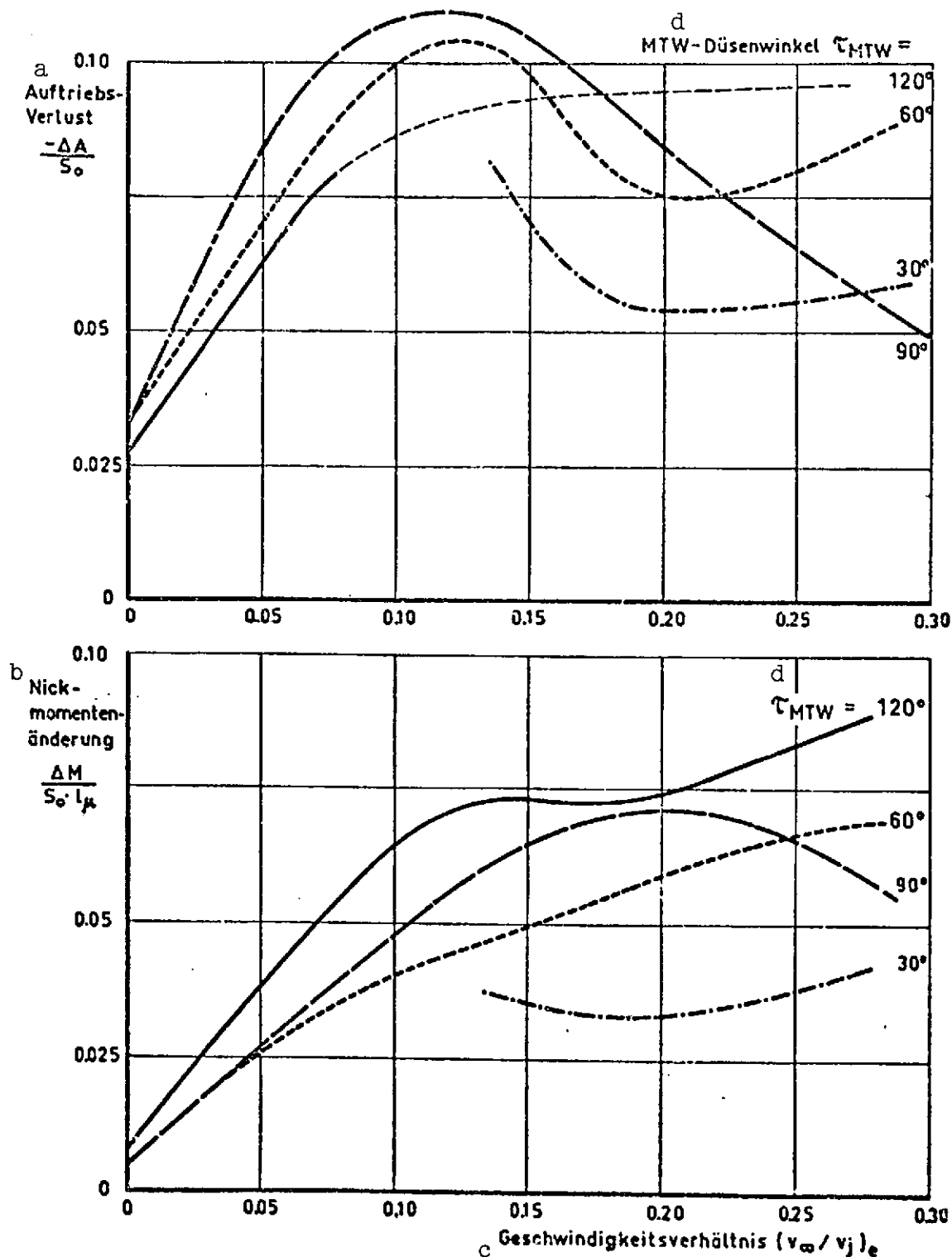


Fig. 1.9. Do 31 jet interference in transition. Lift, pitch torque. All power plants on takeoff thrust. Angle of attack $\alpha = 0^\circ$.

Key: a. Lift loss
 b. Change in pitch torque
 c. Velocity ratio
 d. Cruising power plant nozzle angle

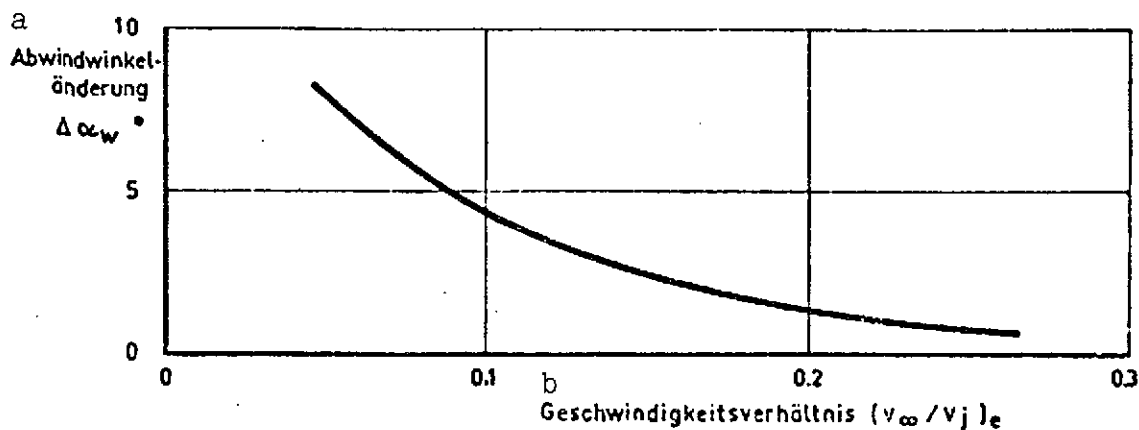


Fig. 1.10. Do 31 jet-induced downwash at location of lift power plants in transition. All power plants on takeoff thrust. Cruising power plant nozzle angle $\tau_{MTW} = 90^\circ$. Angle of attack $\alpha = 0^\circ$.

Key: a. Change in downwash angle
b. Velocity ratio

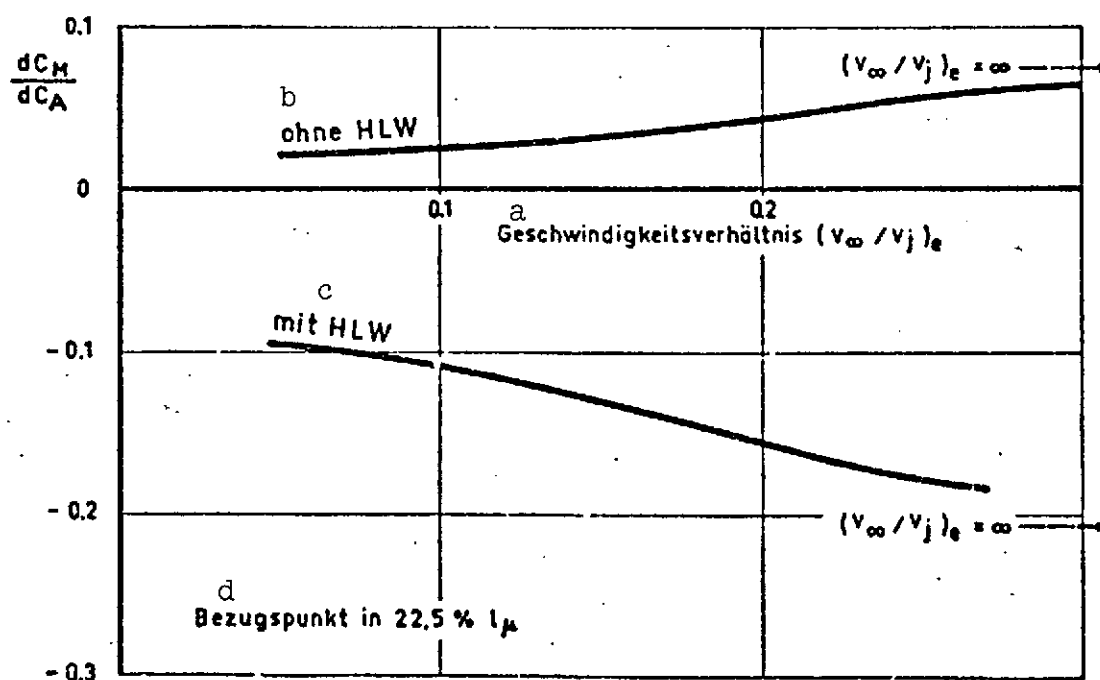


Fig. 1.11. Do 31 jet-induced neutral point shift, in transition. Conditions as in Fig. 1.10.

Key: a. Velocity ratio
b. Without lift power plants
c. With lift power plants
d. Reference point at 22.5% l_μ

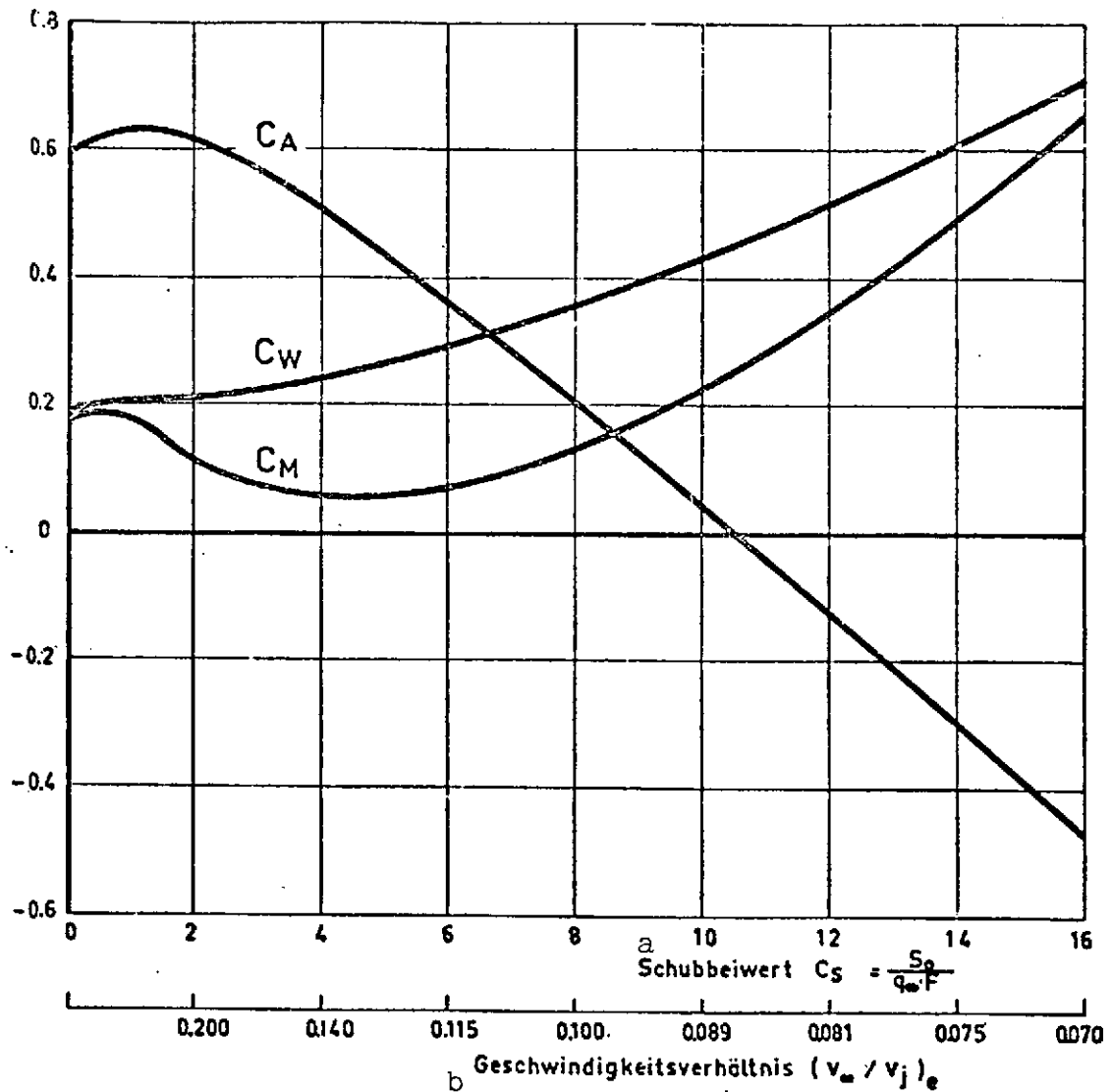


Fig. 1.12. Do 31 jet interference during short takeoff. Lift, drag, pitch torque. All power plants on takeoff thrust.

Ground - to - landing gear distance	$H/b = 0.025$
Angle of pitch	$\theta = 0^\circ$
CPP nozzle angle	$\tau_{MTW} = 10^\circ$
LPP nozzle angle	$\tau_{HTW} = 75^\circ$
Landing flap angle	$\eta_K = 45^\circ$
Angle of attack	$\alpha = 0^\circ$

Key: a. Coefficient of thrust
b. Velocity ratio

2. Preparation of Measurement Data for the Balances of Forces and Torques in Do 31 Transitions

/37

Overview of Contents

- 2.1. Introduction
 - 2.2. Notation
 - 2.3. Data Preparation
 - 2.4. Calculation of Jet Interference
- References

Tables

- 2.1. Do 31 geometry and moments of inertia
- 2.2. Aerodynamic coefficients

Figures

- 2-1. Do 31 E1/E3 test aircraft in flight and on ground.
- 2-2. Comparison of gross thrusts for cruising power plants and thrust power plants determined by various methods of computation. Do 31 E3 trial 243, takeoff phase.
- 2-3. Comparison of measured and smoothed acceleration in z-direction (coordinates fixed relative to aircraft). Do 31 E3 trial 243, takeoff phase.
- 2-4. Comparison of measured, smoothed and corrected angles of attack.

2.1. Introduction

/39

The development of a new aircraft generally requires a large number of model tests in both the initial and advanced stages, and it provisionally terminates in the testing of a prototype. One goal of this testing is also to check information obtained in model tests with regard to its usability for the full-scale version. This is particularly applicable if new engineering is employed.

During the course of Do 31 development, jet interference proved to be an important factor influencing VTOL performance and flight characteristics. An evaluation of the flight tests initially encountered serious problems, however, which stemmed in part from the measurement system and in part from the methods of evaluation. In the course of time, however, improvements were achieved in both areas, so it was possible to undertake an evaluation with some promise of success.

2.2. Notation

/40

C_A, C_W, C_M	Aerodynamic coefficients of lift, drag, and torque, respectively
E	Inlet momentum
F	Reference area for wing
G	Instantaneous gross aircraft weight
g	Acceleration due to gravity
I_y	Moment of inertia
l_u	Mean aerodynamic wing chord
M_{inter}	Jet-induced pitch torque
M_S	Pitch torque due to power plant thrust
M_E	Pitch torque due to inlet momentum
q_{dyn}	Dynamic pressure in flight, from Pitot tube
S_O	Gross thrust from power plants
$\dot{u}_{tot}, \dot{w}_{tot}$	Normal accelerations
\dot{q}	Angular acceleration
X_S, Z_S	Distance between center of gravity and reference point
α	Angle of attack

Subscripts:

X, Y, Z	Coordinates fixed with respect to the aircraft (positive downward and forward)
HTW	Lift power plants
MTW	Lift/thrust power plants (cruising power plants)

2.3. Data Preparation

/41

The evaluation of flight tests with regard to jet interference proved to be so difficult because the jet-induced forces and torques were obtained as differences between several large quantities [1]. In order to keep error in jet interference small, all measured quantities involved in the calculation had to be known with the highest possible accuracy. In addition, it is possible to improve the results by suitable mathematical and statistical methods. This entire approach is of course also applicable to wind tunnel tests and was likewise practiced in the initial period, but in the separation of model and power plants we find the much simpler possibility here of directly measuring jet interference, at least in hover.

Reference has already been made to the importance of a high-quality measurement system. Decisive improvements could then also be made during the course of flight testing, not least of all through our own developments. As an example of this, Fig. 2-1 shows the Do 31 with attached Dornier Fluglog ["flight-log"] for the combined measurement of angle of attack, angle of sideslip, and aircraft speed.

Unfortunately, the Fluglog, in the form in which it was used with the Do 31, is also an example of poor data acquisition. In the acquisition of aircraft speed, excessive integration time and imprecisely known access time results in time lags which are no longer tolerable for this evaluation. For the evaluation of jet interference, we therefore relied on the determination of aircraft speed from dynamic pressure measurements which were also carried out, in conjunction with the measurement of ambient pressure and ambient temperature.

Due to its exposed position well ahead of the nose of the fuselage, angle measurements with the Log are inaccurate if the aircraft executes rotary movements about its transverse or vertical axis. This inaccuracy is of course particularly serious at low aircraft speeds and was therefore corrected during data preparation. The effect of this correction is clear in Fig. 2-4, about which more will be said in another connection.

/42

The success of jet interference calculations depends upon the accuracy of the method for calculating thrust. In the course of

testing the Do 31, two methods were developed for each type of power plant; although these do not agree completely, their accuracy is such an improvement over earlier methods that an evaluation appears reasonable. Fig. 2-2 shows a comparison of the various methods. In the case of lift power plants, only the rpm method can be considered for jet interference evaluation, since the thrust of each power plant is required for the balance of torques, not just overall pod thrust as provided by the fuel flow method. In the case of cruising power plants, the rpm method yield a somewhat flatter thrust curve, so the rpm method was selected for calculating thrust both for this reason and for the sake of uniformity.

A second important factor in the calculation of jet interference is the determination of weight. Weight is determined from known takeoff weight and fuel consumption. Unfortunately, a shortcoming must be mentioned here, too, as the measurement of consumption by the right thrust power plant pod occasionally involves error; a slight consumption level is indicated with the power plants not running. Since the evaluation of jet interference is made for relatively short phases of flight, on the order of 2 or 3 min, the erroneous consumption figures were taken, and the initial weight for the corresponding phase of flight, manually corrected by the difference in consumptions between left and right lift pods, was just inserted into the preparation program.

In each set of measurements, the data exhibit a certain dispersion, and stray values are also possible. The principal goal of data preparation is thus to ensure a certain degree of balance. If only occasional stray values occur, an appreciable improvement can be expected if an adapted smoothing method is used to eliminate roughness in the data. The method used here (cf. [2]) uses a cubic parabola for smoothing, the coefficients for which are determined by the method of least squares. The measured data to the left and right of the position being considered are made use of here, with all values being assigned a weight corresponding to the Gaussian error function. For this purpose, in turn, the number of points is preselected, and the interval thereby determined is assigned to the so-called 3σ limits. The weights have then thereby been determined. Test calculations with different numbers of points naturally yielded a smoother curve as the number of points was increased. It must be noted, however, that actual effects are then also obliterated; for example, rotation of the cruising power plants begins with a discontinuity which is no longer manifested after smoothing. The number of points was taken at 31 for preparation; at a data frequency of 5 Hz -- most of the recordings earmarked for evaluation are available in this form -- this corresponds to a time interval of 3 sec before and after the point in time which is under consideration. More is probably no longer reasonable, since changes in the state of

flight can be made during this time span by the pilot for which the approximation with a cubic parabola is no longer adequate.

A continuous curve is obtained by smoothing the data. This, in turn, eliminates the need for an evaluation at the frequency with which the data are available. The evaluations, to be discussed below, were made at a frequency of 1 Hz, which has proven to be a usable value. On the other hand, unnecessary computations are avoided -- unnecessary because the state of flight has changed too little; on the other hand "fast" changes in the state of flight are still covered with a sufficient number of points. /44

Smoothing is done without regard to whether data which are related to one another also match. For example, no attention was paid to whether smoothed acceleration, once integrated, yields the smoothed velocity. It is simply assumed that the measured data are dispersed about the correct value.

As an example of smoothing, Fig. 2-3 first shows measured acceleration, with the aircraft as a fixed reference, in the Z-direction as compared with the smoothed value. The evening effect of smoothing is quite discernible, but so is the fact that pronounced obliteration has not yet occurred. The same applies to Fig. 2-4, in which smoothing of the angle of attack is shown. The angle of attack correction described above is also shown.

All measured data which are required for calculating thrust and weight were excluded from smoothing. In these cases, the calculation was first made and then the results smoothed. In the calculation of weight, it makes no difference what approach we use, since the consumption data are already relatively smooth. In the calculation of thrust, a still more precise study would be necessary, although here, too, the calculated values are already rather smooth, as Fig. 2-2 also shows. The reason for this approach lies in the assumed lower time consumption.

These extensive measures taken for data acquisition and the abundance of data themselves can only be handled by a program for an electronic computer, quite aside from the fact that the initial values are stored on magnetic tape. One FORTRAN program each was /45 therefore written for the described preparation procedure and for the evaluation which followed. These programs are supported by three others which are not necessary for the actual calculations but do offer certain opportunities for control and further processing. The entire program [3] is designed for use on an IBM/360 computer.

2.4. Calculation of Jet Interference

The equations of motion in six degrees of freedom form the basis for calculating jet interference from the flight test data.

Since lift loss and jet-induced torque, only, are of primary interest for vertical takeoff and landing engineering, it is sufficient to make the calculations in the vertical plane. It is also sufficient to calculate the aerodynamic components in the remaining three equations with simplified coefficients, since velocity is low in the transition region, so the effect of compressibility can be ignored. The nonsteady derivatives are also neglected, due to their normally small effect. Instantaneous total gross thrust was chosen as the reference quantity for jet-induced forces, so that interference parameters in a coordinate system fixed relative to the aircraft can be calculated from the following equations [1].

$$\begin{aligned}\frac{\dot{x}_{inter}}{s_o} &= \frac{G}{s_o} \cdot \frac{\dot{u}_{tot}}{g} - \frac{s_x - E \cdot \cos \alpha}{s_o} \\ &\quad + (C_A \cdot \sin \alpha - C_W \cos \alpha) \cdot \frac{q_{dyn} \cdot F}{s_o} \\ \frac{\dot{z}_{inter}}{s_o} &= \frac{G}{s_o} \cdot \frac{\dot{w}_{tot}}{g} - \frac{s_z - E \cdot \sin \alpha}{s_o} \\ &\quad - (C_A \cdot \cos \alpha + C_W \sin \alpha) \cdot \frac{q_{dyn} \cdot F}{s_o}\end{aligned}$$

/46

$$\begin{aligned}\frac{M_{inter}}{s_o} &= \frac{I_y}{s_o \cdot l_u} \cdot \dot{q} + \frac{G}{s_o} \left(\left(\frac{x_s}{l_u} \right)^2 + \left(\frac{z_s}{l_u} \right)^2 \right) \cdot \frac{\dot{q} \cdot l_u}{g} \\ &\quad + \frac{G}{s_o} \left(\frac{\dot{u}_{tot}}{g} \cdot \frac{z_s}{l_u} + \frac{\dot{w}_{tot}}{g} \cdot \frac{x_s}{l_u} \right) \\ &\quad - \frac{M_S + M_E}{s_o \cdot l_u} + C_M \cdot \frac{q_{dyn} \cdot F}{s_o}\end{aligned}$$

The torque reference point is the aerodynamic reference point corresponding to 22.5% l_u . These equations form the content of a computer program which makes use of the measurement values prepared as described in the preceding section and the data compiled in Tables 2.1, 2.2 and 2.3 for aircraft geometry, moments of inertia and aerodynamic coefficients.

The results of these calculations are given as computer printouts in list form. In addition, a certain level of interpretation of the results can immediately be made by the computer.

For this purpose, certain classes were introduced for the two most important parameters of jet interference in the case of the Do 31, the angle τ of nozzle rotation of the cruising power plants and the ratio S_{HTW}/S_{MTW} of lift power plant thrusts to cruising power plant thrusts, and dimensionless jet-induced lift or jet-induced torque was expressed as a function of effective velocity ratio $(V_{\infty}/V_j)_{eff}$ in the form of a print plot.

Ten Do 31 E3 flights were available for evaluation, with a total of three vertical takeoffs, eight vertical landings and nine simulated landing approaches and other flight maneuvers, on whose results a report will be given in Section 3.

2.5. REFERENCES

1. "The calculation of jet interference for the Do 31 from flight tests," EA-31/2429.
2. "Method for smoothing series of equidistant data," EA-31/2449.
3. "Program description for the program system LiDA31, DAUF31, DALP31, SAF31, PLOS31 for calculating jet interference for the Do 31 from flight tests," EA/P-0182/71.

TABLE 2.1. Do 31 GEOMETRY AND MOMENTS OF INERTIA

/48

Wing area	F	= 57.0	m ²
Span	b	= 17.0	m
Aspect ratio	Λ	= 5.07	--
Reference chord length	ℓ_μ	= 33.415	m
Distance of cruising power plant inlet momentum from transverse plane	X_{ME}	= 11.60	m
from horizontal plane	Z_{ME}	= -0.39	m
Distance of cruising power plant gross thrust, cold, from transverse plane	X_{MBC}	= 0.30	m
from horizontal plane	Z_{MBC}	= 0.267	m
Distance of cruising power plant gross thrust, hot, from transverse plane	X_{MBH}	= -1.70	m
from horizontal plane	Z_{MBH}	= -0.267	m
Distance of lift power plant inlet momentum from transverse plane			
Lift power plants 1 and 5	$X_{HE1,5}$	= 0.55	m
Lift power plants 2 and 6	$X_{HE2,6}$	= -0.26	m
Lift power plants 3 and 7	$X_{HE3,7}$	= -1.07	m
Lift power plants 4 and 8	$X_{HE4,8}$	= -1.88	m
from horizontal plane	Z_{HE}	= -2.06	m
Distance of lift power plant gross thrust from transverse plane			
Lift power plants 1 and 5	$X_{HB1,5}$	= 0.25	m
Lift power plants 2 and 6	$X_{HB2,6}$	= -0.56	m
Lift power plants 4 and 8	$X_{HB3,7}$	= -1.37	m
Lift power plants 4 and 8	$X_{HB4,8}$	= -2.18	m
from horizontal plane	Z_{HB}	= -0.78	m
Distance of tail control nozzle from transverse plane	X_{HD}	= -12.569	m
from horizontal plane	Z_{HD}	= -1.655	m

[Table 2.1 continued on following page.]

TABLE 2.1. (CONTINUED)

/49

Coordinates of Center of Gravity from the Following Equations:

Landing gear retracted:

$$\begin{aligned}
 17250 < G < 18450 \quad x_s &= 13 \cdot 10^{-6} \cdot G - 0,157 \text{ m} \\
 &z_s = 47 \cdot 10^{-6} \cdot G - 0,713 \text{ m} \\
 18450 < G < 19670 \quad x_s &= 20 \cdot 10^{-6} \cdot G - 0,286 \text{ m} \\
 &z_s = 47 \cdot 10^{-6} \cdot G - 0,713 \text{ m} \\
 19670 < G < 24500 \quad x_s &= 11 \cdot 10^{-6} \cdot G - 0,1085 \text{ m} \\
 &z_s = 34 \cdot 10^{-6} \cdot G - 0,457 \text{ m}
 \end{aligned}$$

Landing gear extended: allowances for all weight ranges

$$\begin{aligned}
 \Delta x_s &= -3,4 \cdot 10^{-6} \cdot G + 0,13 \text{ m} \\
 \Delta z_s &= -4,0 \cdot 10^{-6} \cdot G + 0,17 \text{ m}
 \end{aligned}$$

Moments of inertia from the following equations:

$$\begin{aligned}
 \text{Landing gear extended:} \quad I_y &= 0,1125 \cdot G + 25\,900 \text{ rkps}^2 \\
 \text{Landing gear retracted:} \quad I_y &= 0,0734 \cdot G + 26\,130 \text{ mkps}^2
 \end{aligned}$$

TABLE 2.2. AERODYNAMIC COEFFICIENTS
(Fl = FLAPS, Lg = LANDING GEAR)

$$c_A = \left(\frac{dc_A}{d\alpha} + \Delta \left(\frac{dc_A}{d\alpha} \right)_{Fl} \right) \cdot (\alpha - \alpha_o - \Delta\alpha_o Fl - \Delta\alpha_o Lg)$$

$$c_W = (c_{W_o} + \Delta c_{W Fl} + \Delta c_{W Lg} + \Delta c_{W HTW}) + \frac{c_A}{\pi \Gamma A} (K_1 + K_2 \cdot c_A)$$

$$c_M = (c_{M_o} + \Delta c_{M_o Fl} + \Delta c_{M_o Lg}) + \left(\frac{dc_M}{d\alpha} + \Delta \left(\frac{dc_M}{d\alpha} \right)_{Lg} \right) \times \\ \times (\alpha - \alpha_o - \Delta\alpha_o Fl - \Delta\alpha_o Lg) + \frac{dc_M}{d\eta} \eta_H$$

/50

where

$\alpha_o = -2.13^\circ$	$K_1 = -(0.290 + 0.881 \cdot \frac{\eta_K}{45^\circ})$
$\Delta\alpha_o Fl = -3.52^\circ \cdot \frac{\eta_K}{45^\circ}$	$K_2 = (1.304 + 0.267 \cdot \frac{\eta_K}{45^\circ})$
$\Delta\alpha_o Lg = 0.34^\circ$	$c_{M_o} = 0.058$
$\frac{dc_A}{d\alpha} = 5.127$	$\Delta c_{M_o Fl} = 0.13 \cdot \frac{\eta_K}{45^\circ}$
$\Delta \left(\frac{dc_A}{d\alpha} \right)_{Fl} = 0.368$	$\Delta c_{M_o Lg} = -0.015$
$c_{W_o} = 0.042$	$\frac{dc_M}{d\alpha} = -0.505$
$\Delta c_{W Fl} = 0.058 \cdot \frac{\eta_K}{45^\circ}$	$\Delta \left(\frac{dc_M}{d\alpha} \right)_{Lg} = -0.125$
$\Delta c_{W Lg} = 0.073$	$\frac{dc_M}{d\eta} = -1.432$
$\Delta c_{W HTW} = 0.018$ with lift pod flaps open	

[Table 2.2. continued on following page]

TABLE 2.2 (CONTINUED)

in the range of validity

451

$$- (4^{\circ} \frac{\eta_K}{45^{\circ}} + 10^{\circ}) \leq \alpha \leq (13^{\circ} + 3^{\circ} \frac{\eta_K}{45^{\circ}})$$

and

$$Ma \leq 0.3$$

The values listed above were obtained from flight tests; C_A and C_W are trimmed values. The elevator component is therefore also absent. The C_M values were subjected to preparation and represent C_M values for $\eta_H = 0$; thus the additional term for elevator torque.

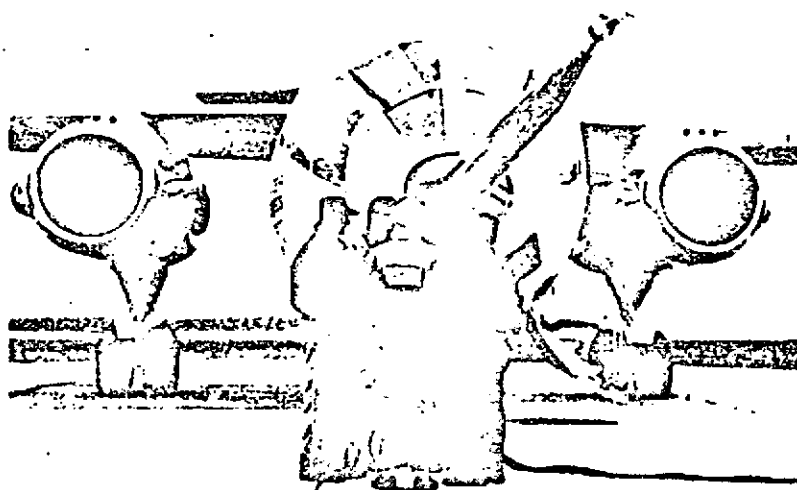
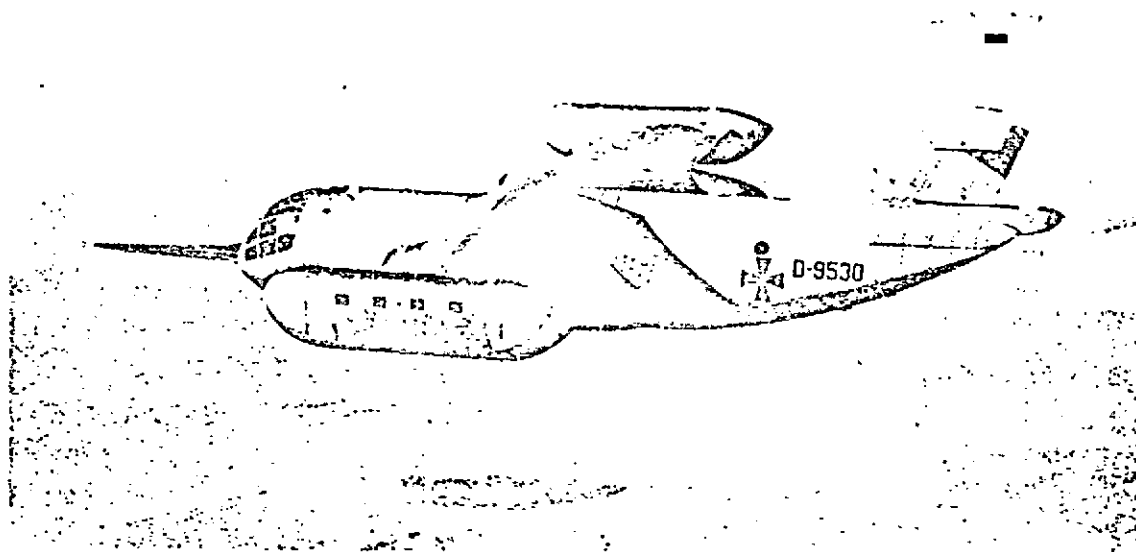


Fig. 2-1. Do 31 E1/E3 test aircraft in flight and on ground.

Reproduced from
best available copy.

Cruising power plant
cold thrust

- rpm method
- + nozzle pressure method

Cruising power plant
hot thrust

- rpm method
- x nozzle pressure method

Lift power plant thrust
(pod)

- o rpm method
- x nozzle pressure method

/53

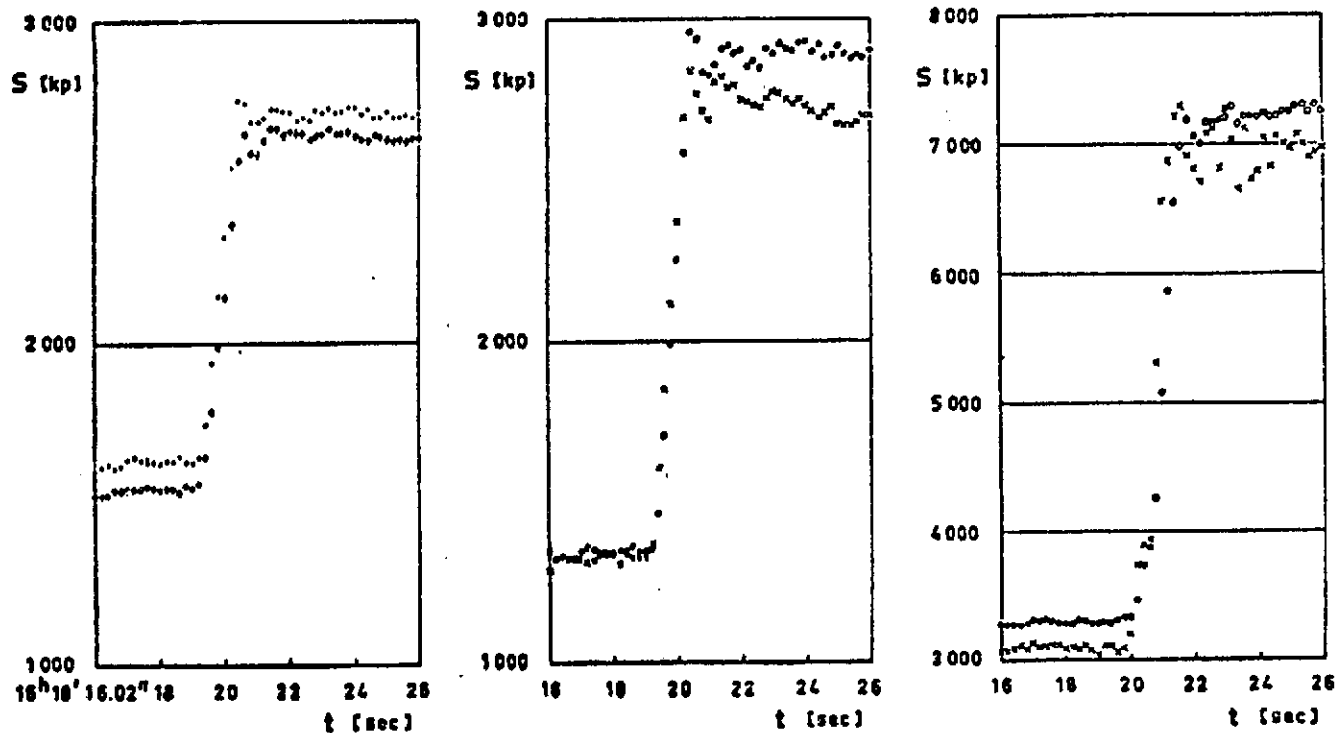


Fig. 2-2. Comparison of gross thrusts for cruising power plants and thrust power plants determined by various methods of computation. Do 31 E3 trial 243, takeoff phase.

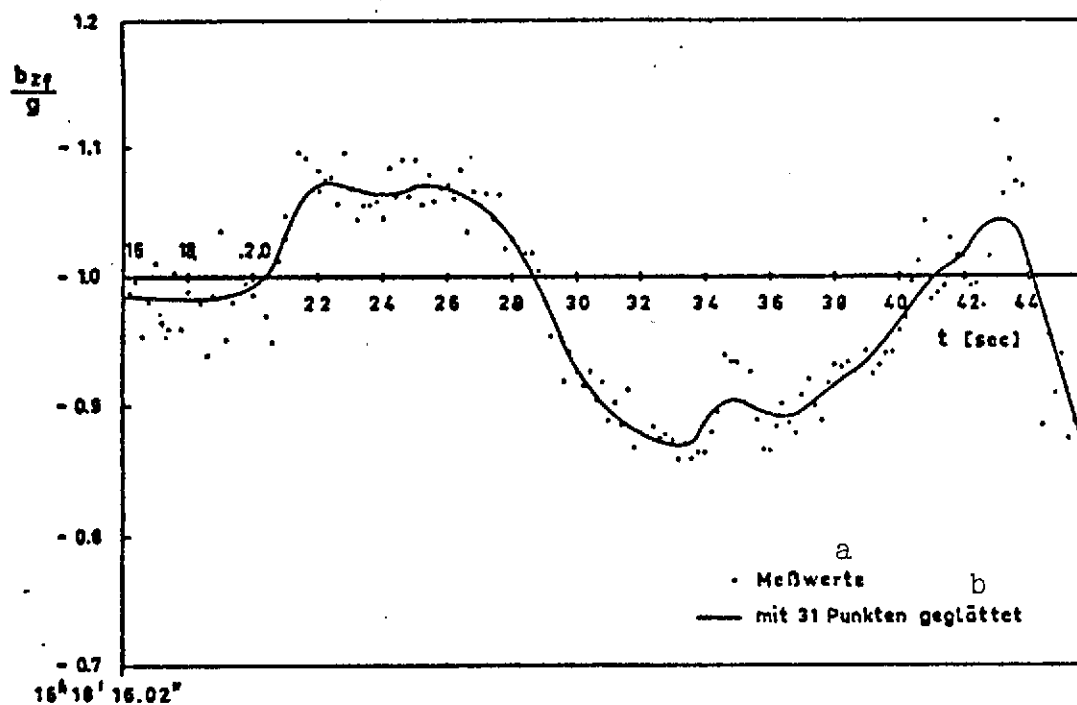


Fig. 2-3. Comparison of measured and smoothed acceleration in z-direction (coordinates fixed relative to aircraft). Do 31 E3 trial 243, takeoff phase.

Key: a. Measured values
 b. Smoothed with 31 points
 B_{zf} = acceleration in z-direction of coordinate system
 fixed relative to aircraft

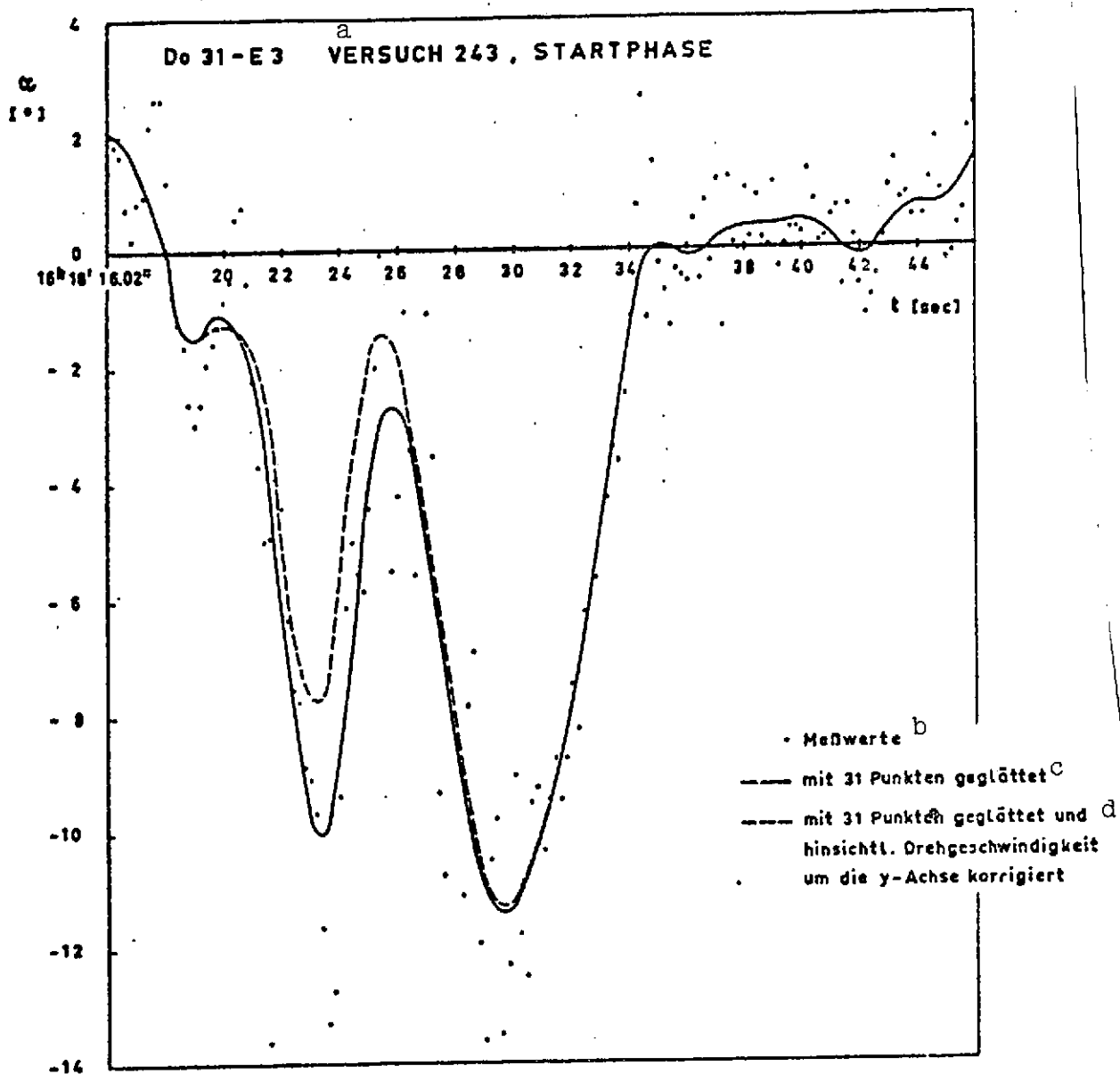


Fig. 2-4. Comparison of measured, smoothed and corrected angles of attack.

Key: a. Trial 243, takeoff phase
 b. Measured values
 c. Smoothed with 31 points
 d. Smoothed with 31 points and corrected with respect to angular velocity about the y-axis

3. Evaluation of Representative Do 31 Transitions with Respect to Jet-Induced Forces and Torques, and Comparison with Model Measurements

/56

Overview of Contents

- 3.1. Introduction
- 3.2. Notation
- 3.3. Evaluation of Do 31 Transitions
- 3.4. Comparison of Test Flight and Wind Tunnel Measurements

Tables

- 3.1. Listing of Do 31 flights evaluated with respect to jet interference
- 3.2. Jet interference evaluation, Do 31 E3, trial 247, takeoff

Figures

/57

- 3.1. Jet-induced normal force, Do 31 E3 trial 247.
- 3.2. Jet-induced torque, Do 31 E3 trial 247.
- 3.3. Time curves of a number of data for a portion of the landing phase, Do 31 E3 trial 247.
- 3.4. Jet-induced normal force, Do 31 E3, all flights listed in Table 3.1.
- 3.5. Jet-induced torque, Do 31 E3.
- 3.6. Do 31 E3 flights, mean jet-induced normal force from Fig. 3.4.
- 3.7. Jet-induced normal force, Do 31 E3 trial 247 with α_0 correction.
- 3.8. Jet-induced torque, Do 31 E3 trial 247 with α_0 and c_{M0} correction.
- 3.9. Do 31 E3 trial 247: jet-induced normal force coefficient versus angle of attack.
- 3.10. Do 31: jet-induced normal forces during vertical landing. Comparison between wind tunnel and flight test.

- 3.11. Do 31: jet-induced pitch torque during vertical landing.
Comparison between wind tunnel and flight test.
- 3.12. Do 31: jet-induced normal force due to ground effect /58
during four vertical landings.
- 3.13. Do 31: jet-induced pitch torque due to ground effect
during four vertical landings.

3.1. Introduction

/59

This is not the first time that VTOL flights by the Do 31 have been studied with regard to jet interference. Back toward the end of Do 31 flight testing in 1968, an attempt was made to determine the jet-induced forces and torques from measurement data stored on magnetic tape. The data for interference evaluation were at that time more or less byproducts of the actual test assignments, for which reason the required accuracy of certain measured quantities, particularly thrusts, was inadequate. The results of jet interference evaluation were therefore likewise unsatisfactory. The dispersion of the results was sometimes so great that no conclusions could be drawn.

A method for more accurately determining thrust was developed by Dornier for the study of Do 31 VTOL landing techniques carried out in the years 1969/70 under a NASA contract.

Reprocessing of the aerodynamic coefficients on the basis of conventional flights by the Do 31 E3 was accomplished as part of the Do 31 simulation program at NASA.

A considerable improvement in starting conditions for a renewed jet interference evaluation was thereby obtained. Additional measures for improving accuracy and for smoothing the data were carried out as part of these studies and are explained in Section 2.

3.2. Notation

/60

B	Wing span
c_z	Coefficient of normal forces (positive: downward)
c_M	Coefficient of pitch torque (positive: tail-heavy)
F	Wing area
H	Distance between landing gear and ground
ℓ_μ	Mean aerodynamic chord length
M	Pitch torque
q_∞	Flight dynamic pressure
S_H	Thrust of Do 31 lift power plants
S_M	Thrust of Do 31 cruising power plants
S_O	Gross thrust of power plants
v_∞	Aircraft speed
v_j	Initial velocity of nozzle jet

$$v_{\text{eff}} = \sqrt{\frac{v_{\infty}^2 \rho_{\infty}}{v_j^2 \rho_j}}$$

Effective velocity ratio

X	Tangential force (coordinates fixed relative to aircraft) positive forward
Z	Normal force (coordinates fixed relative to aircraft) positive downward
α	Angle of attack
τ	Angle of cruising power plant nozzle rotation; $\tau = 0$ when jet is directed rearward
η_K	Angle of special flaps
θ	Aircraft angle of pitch

3.3. Evaluation of Do 31 Transitions

/61

This evaluation is limited to so-called NASA flights performed in 1970, since usable magnetic tapes of measured data are still available only for these flights and, moreover, the method of thrust determination is usable only for these flights, as already mentioned. The test program at that time was oriented almost exclusively toward the study of landing methods for vertical landings, so the parameters which are important for jet interference processes cover only a relatively narrow range. Table 3.1 shows a compilation of the evaluated Do 31 E3 flights, including time intervals and flight maneuvers.

The measured data are treated by the method described in Section 2. The results are available for each flight in the form of a list which contains the most important flight data and the jet-induced normal forces $ZI = \Delta Z/S_0$, tangential force $XI = \Delta X/S_0$ and pitch torque $MI = \Delta M/S_0 \cdot l_u$, referred to instantaneous gross thrust S_0 and mean aerodynamic chord length l_u , at intervals of 1 sec. In addition, $\Delta Z/S_0$ and $\Delta M/S_0 \cdot l_u$ are plotted over effective velocity ratio

$$v_{\text{eff}} = \sqrt{\frac{v_{\infty}^2 \cdot g_{\infty}}{v_j^2 \cdot g_j}}$$

in a print plot. The angle τ of cruising power plant nozzle rotation and the ratio S_H/S_M of lift and cruising power plant thrusts are divided into different classes here. Altitudes of $H/b < 0.8$ are eliminated in the print plot, since the ground effect is treated separately.

Table 3.2 shows the vertical takeoff and vertical landing in trial 247 as an example. Figs. 3.1 and 3.2 show jet-induced normal force and pitch torque in a print plot. Fig. 3.3 shows the time curves of the most important parameters of the state of flight during a portion of the landing phase to touchdown.

The takeoff phase to lift power plant shutdown lasts only about 20 sec. After vertical liftoff, the flight path is rather flat, so the aircraft is not entirely outside the ground effect ($H/b > 0.8$) until 13 sec have elapsed. This is the reason for the small number of measurement points for the takeoff phase in Figs. 3.1 and 3.2. At $H/b < 0.05$, the aircraft is standing on the ground. A conspicuous feature in the list is that a dynamic pressure of about 4 kp/m^2 , corresponding to a $V_{\text{eff}} = 0.03$, is indicated both prior to takeoff and after landing. /62

The average behavior of jet-induced normal force in Fig. 3.1 corresponds qualitatively to the wind tunnel results. The level in flight measurements is higher, however. A conspicuous feature is the constant behavior of torque in Fig. 3.2. Otherwise, the dispersion in measured data is relatively small compared to earlier evaluations. Individual stray values can be ascribed to highly unsteady phases of flight (increase in thrust, rotation of nozzles), as one can see from the list.

The print plots for all evaluated flights are collected in Figs. 3.4 and 3.5. Unfortunately, the concentration of measurement points about a mean value which was hoped for under equivalent conditions did not occur; rather, the range of dispersion was enlarged considerably. In order to obtain a qualitative impression of the effect of the principal parameters τ and S_H/S_M , the means are taken from Fig. 3.4 and plotted as curves in Fig. 3.6. Jet-induced normal force is always smaller for throttled cruising power plants; this is reasonable, since the cruising power plant jets exhausting under the inboard wing cause considerably more interference than the lift power plants mounted on the wing tips. The predominant effect of the cruising power plants on $\Delta Z/S_0$ can also be seen from the pronounced dependence upon angle of rotation.

Analysis of the lists of VTOL landings for all evaluated flights yields the following information:

a) After touchdown on the ground ($H/B < 0.05$), dynamic pressure is still $q_\infty = 4 \text{ to } 10 \text{ kp/m}^2$, corresponding to a $V_{\text{eff}} = 0.03 \text{ to } 0.05$; see table below. /63

Since no statements are made in the flight records concerning wind velocities, it is assumed that a shift in the zero point is involved and that the actual value is $V_{\text{eff}} = 0$.

b) At $H/B = 0.8$, V_{eff} is approximately the same as at $H/B = 0.05$. The considerations discussed under item a) thus apply. At the same time, jet-induced normal force fluctuates over $0.036 < \Delta Z/S_0 < 0.097$ from one flight to another. Since the value of $\Delta Z/S_0$ would have to be the same for all flights under the given identical boundary conditions, a shift in zero points is assumed to have occurred for one or more measured values. An error on this order of magnitude is eliminated in the case of weight determination. An error in normal acceleration is eliminated for the reasons to be presented under item c). A shift in the level of thrust is supported by the fact, presented in Section 2, that appreciable differences in magnitude exist between cruising power plant thrust as determined by the rpm method and by the nozzle pressure method and/or between lift power plant thrust as determined by the rpm method and by the fuel flow method.

VTOL Landings			
Trial	$H/B = 0.05$		$H/B = 0.8$
No.	V_{eff}	V_{eff}	$\Delta Z/S_0$
231	0,047	0,033	0,095
240	0,031	0,027	0,036
243	0,050	0,054	0,097
247	0,042	0,037	0,072

It follows from the wind tunnel measurements that a thrust loss of $\Delta Z/S_0 = 0.036$ must be expected in hover outside the ground effect.

c) For the state of flight at the beginning of the landing phase, prior to starting the lift power plants, $\tau = 10^\circ$, $\eta_K = 45^\circ$, landing gear extended, the aerodynamic coefficients were determined from earlier Do 31 E1 flights under the assumption, as mentioned earlier, that no jet interference occurs. In the present evaluation, five different flights yield a jet-induced normal force of $\Delta Z = 1200$ to 1400 kp at $q = 320$ to 350 kp/m² dynamic pressure for the specified phase of flight. Similar conclusions apply to jet-induced pitch torque. Since a deviation which is approximately constant for several flights is involved, a correction can be used for the aerodynamic coefficients. Since a dependence upon α cannot be detected (to be sure, the range of stagnation pressures and thus the range of α are very narrow), a shift in the zero-point direction of lift and zero-point torque is suspected. /64

In contrast to the Do 31 E3, the flaps of the lift power plant pod and the deflection cascade on the lift power plant inlet were not extendible in the E1, so the aerodynamic coefficients determined with the E1 do not include these effects. In particular, a shift in c_{M0} is justified for this reason.

d) Highly nonsteady phases of flight, produced during changes in thrust or during nozzle rotation, for example, produced stray values in spite of smoothing of the data and should be omitted from evaluation.

Trial 247 was reanalyzed, taking items a) through d) into consideration. In accordance with item c), residual force is $\Delta Z = 1250 \text{ kp}$ for $q = 350 \text{ kp/m}^2$. This corresponds to a normal force coefficient of $\Delta C_z = -0.0626$ which is neutralized as a shift in the zero-point lift direction by $\Delta \alpha_0 = -0.75^\circ$. Accordingly, a shift by $\Delta C_{M0} = -0.067$ is introduced. Thus the interference computation for flight 247 yields freedom from interference on the basis of the assumptions in the conventional landing state of flight. Evaluation of the vertical landing with modified coefficients is shown in Fig. 3.7 and 3.8. As was to be expected, the effects of the change were in the form of an increase in normal force and in torque with increasing dynamic pressure. /65

On the basis of a dispersion in the $\Delta Z/S_0$ values observed, in particular, at higher values of V_{eff} , it was suspected that jet interference is a function of angle of attack. For this reason, the jet-induced normal force coefficient ΔC_z is plotted in Fig. 3.9 against angle of attack for various phases of flight in flight 247. The plot indicates a dependence upon α . A change in the increase in lift has already been observed in wind tunnel measurements, for which reason the wind tunnel results are given for $\alpha = 0^\circ$. The measured data plotted in Fig. 3.9 are not suitable for correcting the flight measurements to $\alpha = 0^\circ$, since dispersion is too great and, moreover, a portion of the dependence upon α may be credited to a correction in the conventional aerodynamic coefficients.

Regarding the evaluation of jet interference in the flight tests, it can be stated, in closing, that usable values for the magnitude of jet-induced normal force and of pitch torque were obtained both for the transition outside the ground effect and for vertical landings. The values associated with hover outside the ground effect ($H/B > 0.8$) are the least reliable. There is apparently an error in the method for determining thrust. At the higher aircraft speeds, toward the end of the transition, inaccuracies in the interference-free aerodynamic coefficients used as input become highly noticeable. A more precise evaluation of jet interference for future flight tests is only possible if

- a) the determination of thrust is further improved,
- b) the interference-free aerodynamic coefficients are determined as precisely as possible from flights with the test aircraft,
- c) special flight maneuvers are flown for jet interference studies,
- d) wind velocity and direction are determined precisely during the takeoff and landing processes.

3.4. Comparison of Test Flight and Wind Tunnel Measurements

/66

Due to the difference in magnitude of $\Delta Z/S_0$ in hover outside the ground effect mentioned under item b) in Section 3.3, this flight state was selected as a reference point for comparison.

In Figs. 3.10 and 3.11, the normal force induced in transition and pitch torque are plotted over V_{eff} . The uncorrected values and those corrected for α_0 and c_{M0} are higher for the flight test values than for the wind tunnel. The uncorrected torque curve was not drawn in, since there is no dependence upon V_{eff} . The corrected torque curve, on the other hand, is not far from the wind tunnel curve. From this example we see how markedly a relatively small change in the aerodynamic coefficients affects the determination of jet interference, particularly at high aircraft speeds.

For comparison, the maximum available control torque, consisting of jet control and aerodynamic elevator control, is plotted in the lower portion of Fig. 3.11.

The effect of ground distance upon jet-induced normal force and pitch torque is shown in Figs. 3.12 and 3.13. Results from four vertical landings are plotted. The state associated with hover outside the ground effect ($H/B > 0.8$) has been chosen as a reference point.

The reason for the great band width of the plotted wind tunnel measurements is that the angle of pitch was varied over $-10^\circ < \theta < 10^\circ$. A finer breakdown of the θ effect is not profitable, since the unstable flow field close to the ground reacts sensitively to changes in θ , and nonreproducible measurement results exist in some cases.

The figures provide an impression of the disturbances in normal force and in pitch torque occurring during vertical landings and exhibit satisfactory agreement with the wind tunnel measurements.

TABLE 3.1. LISTING OF Do 31 E3 FLIGHTS EVALUATED WITH RESPECT
TO JET INTERFERENCE

Trial No.	Time interval				Flight maneuver
		From		To	
231	16 ^h 2'	54.02"	16 ^h 5'	57.02"	Vertical landing
237	16 ^h 24'	38.02"	16 ^h 26'	51.02"	Simulated landings
	16 ^h 30'	51.02"	16 ^h 22'	10.02"	
238	10 ^h 2'	23.02"	10 ^h 3'	54.02"	Simulated landings
	10 ^h 6'	38.02"	10 ^h 7'	53.02"	
239	12 ^h 8'	30.02"	12 ^h 10'	31.02"	Simulated landings
	12 ^h 14'	39.02"	12 ^h 17'	0.02"	
	12 ^h 21'	1.02"	12 ^h 23'	37.02"	
					Vertical landing
240	14 ^h 49'	15.02"	14 ^h 52'	15.02"	Vertical landing
243	16 ^h 18'	13.02"	16 ^h 19'	0.02"	Vertical takeoff
	16 ^h 18'	19.02"	16 ^h 19'	57.02"	Climb without lift power plants
	16 ^h 27'	2.22"	16 ^h 28'	57.22"	
	16 ^h 36'	45.02"	16 ^h 38'	30.02"	Vertical landing
244	11 ^h 19'	21.02"	11 ^h 21'	31.02"	Simulated landing
	11 ^h 25'	50.02"	11 ^h 27'	53.02"	Vertical landing
246 B	10 ^h 51'	22.02"	10 ^h 53'	10.02"	Vertical landing with forward speed
247	14 ^h 18'	50.02"	14 ^h 19'	20.02"	Vertical takeoff
	14 ^h 32'	2.02"	14 ^h 35'	0.02"	Vertical landing
248	16 ^h 4'	15.02"	16 ^h 4'	41.02"	Vertical takeoff
	16 ^h 10'	0.02"	16 ^h 11'	13.02"	Simulated landing
	16 ^h 16'	0.02"	16 ^h 18'	10.86"	Vertical landing

Three vertical takeoffs
Eight vertical landings
Nine simulated landings

TABLE 3.2a. JET INTERFERENCE EVALUATION, Do 31 E3, TRIAL 247, TAKEOFF

KL1, KH3															Feb. 4, 1972	
Hr	Min	Sec	Weight	Thrust	Dyn. pres.	Alpha	Theta	H/b	Tau	SH/SM	V _{eff}	ZI	XI	MI	Landing gear	
14	18	50.02	21024.	23499.	3.44	0.8	0.4	0.03	74.0	1.485	0.026	0.0522	-0.0440	0.0739	Extended	
14	18	51.02	21017.	23564.	3.99	1.2	1.5	0.06	73.3	1.476	0.034	0.0467	-0.0356	0.0750	↓	
14	18	52.02	21011.	23344.	7.41	1.2	2.3	0.10	65.1	1.497	0.036	0.0457	-0.0445	0.0978		
14	18	53.02	21005.	22510.	14.36	2.6	3.2	0.15	50.6	1.521	0.053	0.0477	-0.0399	0.0940	↓	
14	18	54.02	20998.	22634.	26.11	1.3	3.9	0.19	40.2	1.500	0.072	0.0451	-0.0389	0.0951		
14	18	55.02	20992.	22585.	36.42	1.7	3.9	0.22	36.0	1.472	0.085	0.0546	-0.0306	0.0990	Retracted	
14	18	56.07	20985.	22510.	45.67	4.1	4.3	0.22	34.9	1.467	0.095	0.0595	-0.0330	0.0697		
14	18	57.02	20979.	22670.	55.98	4.2	4.9	0.22	34.8	1.467	0.105	0.0670	-0.0370	0.0660	↓	
14	18	58.02	20972.	22693.	66.26	3.5	5.1	0.24	33.3	1.460	0.115	0.0666	-0.0397	0.0679		
14	18	59.02	20966.	22492.	76.83	3.3	5.3	0.29	33.0	1.462	0.124	0.0696	-0.0426	0.0669	↓	
14	19	00.02	20959.	22324.	90.77	3.0	5.6	0.38	28.4	1.464	0.135	0.0664	-0.0509	0.0646		
14	19	01.02	20953.	22305.	105.99	2.1	5.8	0.49	27.3	1.462	0.145	0.0620	-0.0545	0.0637	↓	
14	19	02.02	20947.	22193.	120.66	0.7	5.4	0.64	25.4	1.461	0.156	0.0393	-0.0595	0.0743		
14	19	03.02	20940.	21961.	136.02	0.4	5.1	0.84	22.2	1.461	0.167	0.0460	-0.0677	0.0799	↓	
14	19	04.02	20934.	21667.	149.79	0.7	5.1	1.13	18.8	1.465	0.176	0.0490	-0.0718	0.0554		
14	19	05.02	20927.	21317.	161.33	1.0	5.3	1.36	14.9	1.467	0.186	0.0446	-0.0744	0.0502	↓	
14	19	06.02	20921.	21268.	173.47	1.1	5.4	1.48	11.9	1.430	0.192	0.0327	-0.0810	0.0696		
14	19	07.02	20914.	21687.	191.90	0.2	5.4	1.69	11.0	1.358	0.200	0.0116	-0.0910	0.0666	↓	
14	19	08.02	20907.	22063.	216.35	-0.4	5.3	1.96	11.1	1.315	0.210	0.0009	-0.0719	0.0651		
14	19	09.02	20900.	22260.	244.67	-0.6	5.2	2.26	11.1	1.313	0.221	0.0215	-0.0536	0.0664	↓	
14	19	10.02	20894.	22437.	267.29	-1.1	5.0	2.59	11.0	1.321	0.232	0.0415	-0.0664	0.0553		
14	19	11.02	20887.	21747.	255.53	-1.3	4.9	2.95	10.9	1.235	0.247	0.0769	-0.0741	0.0566	↓	
14	19	12.02	20881.	19799.	323.43	-1.0	4.8	3.33	11.0	1.025	0.271	0.0816	-0.0541	0.0449		
14	19	13.02	20875.	18599.	345.42	-0.6	5.0	3.69	10.9	0.906	0.299	0.0773	-0.0797	0.0076	↓	
14	19	14.02	20870.	17961.	366.92	0.2	5.3	4.02	10.9	0.868	0.302	0.1223	-0.1604	-0.0527		
14	19	15.02	20866.	15444.	381.43	1.0	5.6	4.33	10.9	0.553	0.333	0.1270	-0.1755	-0.0563	↓	
14	19	16.02	20862.	12674.	396.53	2.0	6.0	4.60	10.9	0.155	0.375	0.0263	-0.1771	-0.0892		
14	19	17.02	20860.	11862.	416.13	2.7	6.4	4.80	10.9	0.009	0.397	-0.0774	-0.0927	0.3063	↓	
14	19	18.02	20858.	11893.	433.86	2.9	6.7	4.98	10.9	0.010	0.405	-0.0953	-0.1157	0.0251		
14	19	19.02	20856.	11937.	447.20	2.9	7.0	5.20	10.8	0.001	0.411	-0.1025	-0.1168	0.0219	↓	
14	19	20.02	20854.	11954.	462.55	3.2	7.7	5.45	10.8	0.0	0.291	-0.0797	-0.1716	0.0026		

TABLE 3.2b. LANDING

/69

KL1, KH3

Feb. 4, 1972

Hr	Min	Sec	Weight	Thrust	Dyn. pres.	Alpha	Theta	H/b	Tau	SH/SM	V _{eff}	ZI	XI	MI	Landing gear
															Extended
14	32	2.02	19157.	6668.	361.16	5.2	2.5	25.96	10.5	0.0	0.344	-0.1665	-0.1665	-0.2177	
14	32	3.02	19155.	6674.	359.08	5.3	2.3	26.94	10.6	0.0	0.343	-0.1440	-0.1735	-0.2254	
14	32	4.02	19154.	6678.	359.35	5.3	2.3	26.96	10.6	0.0	0.343	-0.1266	-0.1748	-0.2300	
14	32	5.02	19153.	6617.	355.50	4.8	2.3	26.99	10.5	0.0	0.343	-0.1805	-0.1769	-0.2168	
14	32	6.02	19152.	6595.	353.80	4.4	2.0	26.71	10.6	0.0	0.343	-0.2029	-0.1841	-0.2043	
14	32	7.02	19151.	6609.	352.93	4.5	1.8	26.28	10.6	0.0	0.342	-0.2023	-0.1952	-0.2052	
14	32	8.02	19150.	6599.	350.59	4.8	1.6	26.22	10.5	0.0	0.341	-0.2137	-0.1917	-0.2097	
14	32	9.02	19149.	6603.	350.68	5.1	1.7	26.44	10.6	0.0	0.341	-0.2142	-0.1857	-0.2097	
14	32	10.02	19148.	6605.	350.81	5.2	2.0	26.49	10.6	0.0	0.341	-0.2024	-0.1867	-0.2072	
14	32	11.02	19147.	6602.	350.16	5.1	2.3	26.35	10.6	0.0	0.341	-0.1861	-0.1819	-0.1987	
14	32	12.02	19146.	6619.	350.44	4.9	2.4	26.20	10.6	0.0	0.340	-0.1947	-0.2003	-0.1990	
14	32	13.02	19145.	6621.	348.56	4.6	2.4	26.08	10.5	0.0	0.340	-0.2460	-0.1694	-0.1995	
14	32	14.02	19144.	6610.	346.15	4.7	2.4	25.94	10.5	0.0	0.339	-0.2629	-0.1915	-0.1970	
14	32	15.02	19143.	6622.	344.27	5.2	2.6	25.75	10.6	0.0	0.337	-0.2083	-0.1964	-0.1978	
14	32	16.02	19142.	6616.	341.34	5.8	3.1	25.54	10.6	0.001	0.457	-0.1798	-0.1539	-0.1955	
14	32	17.02	19141.	6565.	342.29	5.8	3.3	25.35	10.5	0.007	0.454	-0.2440	-0.1290	-0.1892	
14	32	18.02	19140.	6592.	345.25	5.4	3.3	25.18	10.6	0.007	0.456	-0.3129	-0.1091	-0.1801	
14	32	19.02	19138.	6896.	345.74	4.9	3.3	24.96	10.5	0.101	0.475	-0.2751	-0.1044	-0.1694	
14	32	20.02	19136.	7496.	347.41	4.6	3.4	24.81	10.5	0.261	0.457	-0.1560	-0.0741	-0.1603	
14	32	21.02	19134.	8479.	348.82	4.1	3.5	24.75	10.6	0.445	0.430	-0.0917	-0.0536	-0.1297	
14	32	22.02	19131.	10172.	346.51	3.0	3.3	24.72	10.5	0.825	0.392	-0.0557	-0.0484	-0.0774	
14	32	23.02	19127.	11879.	346.68	1.8	2.5	24.69	10.6	1.134	0.362	-0.0123	-0.0641	-0.0447	
14	32	24.02	19124.	12608.	350.44	1.3	1.9	24.58	10.6	1.260	0.354	0.0106	-0.0733	-0.0403	
14	32	25.02	19120.	12713.	353.59	1.5	1.7	24.43	10.5	1.279	0.354	0.0364	-0.0844	-0.0422	
14	32	26.02	19116.	12758.	353.58	1.7	2.0	24.32	10.6	1.283	0.353	0.0575	-0.0797	-0.0406	
14	32	27.02	19112.	12792.	350.67	1.5	2.1	24.24	10.6	1.294	0.351	0.0507	-0.0808	-0.0324	
14	32	28.02	19108.	12786.	347.73	1.3	2.0	24.13	10.5	1.289	0.350	0.0468	-0.0902	-0.0279	
14	32	29.02	19104.	12767.	346.91	1.2	1.8	24.03	10.2	1.289	0.351	0.0229	-0.0933	-0.0159	
14	32	30.02	19100.	12757.	350.53	1.3	1.9	23.97	9.7	1.283	0.352	0.0154	-0.0972	-0.0405	
14	32	31.02	19096.	13073.	349.44	0.9	2.0	23.90	14.7	1.293	0.347	0.0029	-0.0704	-0.0311	
14	32	32.02	19092.	13849.	354.14	0.1	1.9	23.56	27.9	1.312	0.339	0.0028	-0.0475	-0.0259	
14	32	33.02	19008.	14426.	356.05	-0.2	1.6	22.95	39.2	1.308	0.333	0.0431	-0.0607	-0.0148	
14	32	34.02	19084.	14678.	352.17	-0.9	1.2	22.59	47.9	1.318	0.329	0.0294	-0.0707	0.0286	
14	32	35.02	19080.	14874.	344.56	-2.0	0.7	22.69	58.8	1.324	0.323	-0.0173	-0.0759	0.0424	
14	32	36.02	19076.	14934.	333.12	-2.4	0.7	23.19	56.0	1.317	0.317	-0.0102	-0.0794	0.0459	
14	32	37.02	19073.	14928.	326.77	-2.4	-0.2	23.63	67.2	1.316	0.314	0.0297	-0.0719	0.0440	
14	32	38.02	19069.	14935.	324.56	-2.1	-0.5	23.66	66.9	1.317	0.313	0.0879	-0.0655	0.0497	
14	32	39.02	19065.	14903.	315.80	-1.3	-0.6	23.55	66.8	1.316	0.309	0.1264	-0.0711	0.0541	
14	32	40.02	19061.	14935.	309.98	-1.3	-0.7	23.46	66.8	1.308	0.308	0.0965	-0.0771	0.0509	
14	32	41.02	19057.	15022.	312.10	-1.7	-0.9	23.41	67.2	1.304	0.306	0.0273	-0.0725	0.0544	
14	32	42.02	19053.	14671.	307.30	-0.0	-0.4	23.38	65.8	1.320	0.307	0.1706	-0.0727	0.0389	
14	32	43.02	19049.	13747.	299.29	2.3	1.4	23.34	61.0	1.360	0.313	0.3778	-0.1000	-0.0228	
14	32	44.02	19045.	13855.	292.40	-0.1	1.0	23.29	61.9	1.348	0.308	0.1080	-0.0351	-0.0085	
14	32	45.02	19042.	14656.	286.65	-1.3	-0.7	23.17	66.5	1.306	0.296	0.0730	-0.0679	0.0513	
14	32	46.02	19038.	14801.	281.19	-0.6	-0.8	22.90	67.2	1.296	0.292	0.0784	-0.0446	0.0605	
14	32	47.02	19034.	14689.	274.38	-0.5	-0.6	22.60	66.8	1.298	0.290	0.0531	-0.0744	0.0570	
14	32	48.02	19030.	14630.	268.22	-1.0	-0.7	22.47	66.7	1.296	0.297	0.0423	-0.0722	0.0581	
14	32	49.02	19026.	14631.	263.86	-0.9	-1.1	22.30	66.8	1.290	0.295	0.0812	-0.0643	0.0606	
14	32	50.02	19022.	14621.	257.54	0.4	-1.1	22.07	66.9	1.286	0.292	0.1069	-0.0747	0.0571	
14	32	51.02	19018.	14593.	255.18	0.9	-0.4	21.46	65.8	1.295	0.281	0.0986	-0.0771	0.0505	
14	32	52.02	19014.	14581.	258.66	0.7	0.3	20.85	66.8	1.281	0.281	0.0994	-0.0773	0.0526	
14	32	53.02	19010.	14465.	252.42	0.3	0.6	20.79	66.8	1.269	0.280	0.0654	-0.0711	0.0603	
14	32	54.02	19007.	14662.	247.67	-1.4	-0.3	21.14	66.2	1.207	0.276	-0.0014	-0.0998	0.0715	
14	32	55.02	19002.	16221.	249.45	-3.9	-2.7	21.45	66.2	1.538	0.261	-0.0229	-0.0515	0.0846	
14	32	56.02	18952.	18638.	249.65	-5.2	-5.1	21.38	73.5	1.824	0.246	0.0250	-0.0595	0.0898	

TABLE 3.2c. LANDING (CONTINUED)

/70

KL1, KH3

Feb. 4, 1972

Hr	Min	Sec	Weight	Thrust	Dyn. pres.	Alpha	Theta	H/b	Tau	SH/SM	V _{eff}	ZI	XI	MI	Landing gear Extended
14	33	57.02	18992.	20198.	248.27	-1.5	-6.3	21.21	90.0	1.751	0.235	0.0803	-0.0583	0.0835	
14	33	58.02	18987.	20996.	246.89	-1.6	-6.3	21.07	102.0	1.555	0.230	0.1154	-0.0541	0.0751	
14	33	59.02	18981.	21086.	239.68	-1.7	-6.4	20.88	104.3	1.493	0.226	0.1311	-0.0579	0.0718	
14	33	0.02	18976.	21038.	229.52	-1.7	-6.2	20.61	103.6	1.501	0.222	0.1292	-0.0540	0.0735	
14	33	1.02	18970.	21007.	218.17	-1.7	-6.2	20.31	103.4	1.502	0.216	0.1261	-0.0521	0.0763	
14	33	2.02	18964.	20974.	206.76	-1.8	-6.3	20.03	103.1	1.497	0.211	0.1269	-0.0472	0.0772	
14	33	3.02	18959.	20897.	198.63	-1.9	-7.1	19.78	104.4	1.499	0.207	0.1237	-0.0479	0.0765	
14	33	4.02	18953.	20700.	192.86	-1.9	-7.9	19.51	108.3	1.503	0.205	0.1368	-0.0470	0.0798	
14	33	5.02	18947.	20570.	187.29	-1.7	-8.3	19.25	110.0	1.501	0.202	0.1509	-0.0429	0.0766	
14	33	6.02	18942.	20375.	181.87	-1.9	-7.9	18.83	109.3	1.473	0.200	0.1541	-0.0444	0.0717	
14	33	7.02	18936.	19795.	176.29	-1.9	-7.5	18.41	108.9	1.402	0.200	0.1568	-0.0388	0.0703	
14	33	8.02	18931.	19206.	171.24	-2.8	-7.4	18.05	109.0	1.330	0.200	0.1625	-0.0361	0.0698	
14	33	9.02	18926.	18801.	167.88	-2.3	-7.3	17.66	109.4	1.278	0.200	0.1638	-0.0470	0.0681	
14	33	10.02	18921.	18409.	164.02	-1.9	-7.4	17.22	107.2	1.235	0.200	0.1554	-0.0555	0.0657	
14	33	11.02	18916.	18303.	158.83	-1.7	-7.5	16.79	107.8	1.226	0.198	0.1540	-0.0400	0.0673	
14	33	12.02	18911.	18280.	155.10	-1.9	-7.6	16.36	108.9	1.223	0.195	0.1572	-0.0288	0.0680	
14	33	13.02	18906.	18128.	153.01	-1.9	-7.9	15.91	108.9	1.207	0.195	0.1549	-0.0312	0.0695	
14	33	14.02	18902.	18050.	150.42	-1.2	-8.1	15.47	108.8	1.196	0.194	0.1650	-0.0337	0.0712	
14	33	15.02	18897.	18286.	147.02	-0.1	-7.6	15.00	108.8	1.216	0.190	0.1715	-0.0331	0.0690	
14	33	16.02	18892.	18723.	143.66	0.4	-7.0	14.49	108.8	1.269	0.186	0.1726	-0.0296	0.0697	
14	33	17.02	18887.	18955.	140.06	1.0	-6.4	14.01	108.7	1.305	0.182	0.1796	-0.0321	0.0724	
14	33	18.02	18881.	19108.	135.52	1.1	-5.9	13.59	108.8	1.321	0.179	0.1716	-0.0536	0.0715	
14	33	19.02	18876.	19364.	130.87	0.2	-5.3	13.26	108.8	1.354	0.174	0.1586	-0.0280	0.0702	
14	33	20.02	18871.	19526.	126.76	-0.5	-5.2	13.01	109.7	1.391	0.171	0.1559	-0.0279	0.0725	
14	33	21.02	18866.	19551.	123.14	-0.9	-5.5	12.77	109.7	1.382	0.168	0.1524	-0.0269	0.0753	
14	33	22.02	18860.	19568.	119.26	-1.3	-5.7	12.52	108.7	1.377	0.166	0.1516	-0.0255	0.0737	
14	33	23.02	18855.	19570.	115.63	-1.4	-5.6	12.25	108.7	1.376	0.163	0.1529	-0.0267	0.0705	
14	33	24.02	18850.	19469.	111.66	-1.5	-5.7	11.99	108.7	1.371	0.161	0.1563	-0.0295	0.0731	
14	33	25.02	18844.	19353.	106.85	-0.6	-5.9	11.74	108.7	1.362	0.159	0.1659	-0.0305	0.0752	
14	33	26.02	18839.	19342.	104.04	0.2	-6.0	11.50	108.7	1.357	0.156	0.1609	-0.0287	0.0744	
14	33	27.02	18834.	19348.	103.08	-0.2	-6.2	11.26	108.7	1.357	0.155	0.1471	-0.0291	0.0744	
14	33	28.02	18829.	19315.	101.36	-0.8	-6.3	11.03	109.7	1.355	0.154	0.1520	-0.0287	0.0739	
14	33	29.02	18823.	19256.	96.62	-0.2	-6.2	10.93	109.7	1.358	0.150	0.1644	-0.0264	0.0735	
14	33	30.02	18818.	19262.	91.12	1.1	-5.9	10.63	108.7	1.362	0.146	0.1618	-0.0353	0.0735	
14	33	31.02	18813.	18980.	88.45	0.0	-6.0	10.42	108.7	1.331	0.145	0.1362	-0.0366	0.0750	
14	33	32.02	18808.	18488.	88.73	-1.0	-6.4	10.19	108.7	1.764	0.147	0.1151	-0.0279	0.0747	
14	33	33.02	18803.	18174.	90.84	-1.1	-6.6	9.95	108.7	1.221	0.150	0.1441	-0.0270	0.0730	
14	33	34.02	18798.	18060.	90.92	0.8	-6.5	9.71	108.7	1.213	0.151	0.1673	-0.0294	0.0715	
14	33	35.02	18793.	18055.	88.05	1.9	-6.4	9.46	108.7	1.211	0.148	0.1567	-0.0330	0.0727	
14	33	36.02	18788.	18076.	86.43	1.6	-6.3	9.21	108.7	1.209	0.147	0.1448	-0.0307	0.0745	
14	33	37.02	18783.	18085.	86.63	0.6	-6.3	8.93	108.7	1.208	0.147	0.1355	-0.0231	0.0552	
14	33	38.02	18778.	18099.	85.27	0.3	-6.2	8.62	108.7	1.199	0.146	0.1410	-0.0270	0.0564	
14	33	39.02	18773.	18112.	84.24	0.8	-5.8	8.31	108.7	1.705	0.145	0.1359	-0.0321	0.0524	
14	33	40.02	18768.	18600.	66.28	1.6	-5.4	7.99	108.7	1.250	0.144	0.1454	-0.0276	0.0835	
14	33	41.02	18763.	19343.	87.53	3.2	-4.9	7.66	108.7	1.324	0.143	0.1637	-0.0313	0.0727	
14	33	42.02	18758.	19500.	84.43	3.0	-4.6	7.37	108.7	1.368	0.140	0.1441	-0.0329	0.0733	
14	33	43.02	18752.	19248.	80.57	0.9	-5.0	7.13	108.6	1.356	0.137	0.1235	-0.0293	0.0754	
14	33	44.02	18747.	19142.	81.64	-1.1	-5.5	6.92	108.6	1.338	0.139	0.1138	-0.0265	0.0748	
14	33	45.02	18742.	19165.	84.24	-1.1	-5.9	6.71	108.7	1.337	0.141	0.1104	-0.0244	0.0742	
14	33	46.02	18737.	19148.	84.02	0.9	-5.8	6.49	108.6	1.341	0.141	0.1650	-0.0272	0.0751	
14	33	47.02	18732.	19068.	82.82	1.0	-5.5	6.24	108.5	1.331	0.140	0.1473	-0.0298	0.0727	
14	33	48.02	18726.	18887.	81.53	-0.3	-5.4	6.01	108.6	1.309	0.139	0.1412	-0.0227	0.0727	
14	33	49.02	18721.	18500.	75.87	-0.2	-5.6	5.82	112.2	1.300	0.139	0.1536	-0.0266	0.0748	
14	33	50.02	18716.	18277.	77.40	1.0	-5.8	5.61	117.7	1.295	0.138	0.1555	-0.0223	0.0745	
14	33	51.02	18711.	18284.	74.61	2.1	-5.5	5.36	119.1	1.302	0.136	0.1524	-0.0313	0.0717	

TABLE 3.2d. LANDING (CONTINUED)

/71

KL1, KH3

Feb. 4, 1972

Hr Min Sec	Weight	Thrust	Dyn. pres.	Alpha	Theta	H/b	Tau	SH/SM	V _{eff}	ZI	XI	MI	Landing gear Extended
14 33 52.02	18706.	18401.	72.94	2.9	1.5.1	3.08	118.6	1.324	0.133	0.1497	-0.0306	0.0698	
14 33 53.02	18701.	18474.	69.84	2.3	1.4.9	4.83	113.5	1.331	0.130	0.1492	-0.0175	0.0697	
14 33 54.02	18655.	18477.	68.48	1.8	1.3.1	4.59	114.6	1.325	0.127	0.1475	-0.0158	0.0718	
14 33 55.02	18590.	18420.	61.64	3.3	1.3.2	4.20	118.4	1.317	0.123	0.1621	-0.0264	0.0722	
14 33 56.02	18685.	18407.	57.47	7.6	1.2.2	4.60	119.9	1.310	0.119	0.1967	-0.0376	0.0696	
14 33 57.02	18680.	18596.	53.69	11.8	1.1.7	3.71	118.2	1.332	0.114	0.2144	-0.0446	0.0651	
14 33 58.02	18674.	19301.	50.18	12.4	1.0.0	3.47	112.0	1.401	0.108	0.1911	-0.0484	0.0628	
14 33 59.02	18669.	20295.	47.61	8.8	2.3	3.39	104.7	1.452	0.103	0.1598	-0.0383	0.0688	
14 34 0.02	18663.	20761.	44.81	6.3	2.2	3.18	100.3	1.478	0.099	0.1435	-0.0306	0.0734	
14 34 1.02	18658.	20664.	41.56	3.2	1.8	3.11	99.2	1.461	0.095	0.1340	-0.0281	0.0732	
14 34 2.02	18652.	20472.	39.01	1.6	1.6	3.10	99.0	1.440	0.093	0.1327	-0.0304	0.0720	
14 34 3.02	18647.	20109.	37.57	1.5	1.5	3.10	99.6	1.404	0.092	0.1376	-0.0317	0.0710	
14 34 4.02	18641.	19403.	36.03	2.7	1.3	3.08	98.8	1.320	0.091	0.1406	-0.0307	0.0720	
14 34 5.02	18636.	18785.	34.33	3.9	1.2	3.04	98.9	1.237	0.091	0.1328	-0.0367	0.0729	
14 34 6.02	18631.	18524.	34.16	4.8	1.5	2.97	98.9	1.237	0.091	0.1311	-0.0434	0.0740	
14 34 7.02	18626.	18530.	34.11	7.0	2.2	2.87	98.8	1.219	0.091	0.1338	-0.0394	0.0715	
14 34 8.02	18621.	18786.	33.83	9.0	2.7	2.78	98.8	1.249	0.090	0.1277	-0.0370	0.0691	
14 34 9.02	18616.	19044.	33.45	9.5	2.4	2.70	98.8	1.239	0.089	0.1323	-0.0403	0.0734	
14 34 10.02	18611.	18893.	31.70	9.6	2.3	2.63	98.7	1.248	0.087	0.1386	-0.0390	0.0741	
14 34 11.02	18606.	18492.	29.72	9.2	2.7	2.57	98.8	1.204	0.085	0.1335	-0.0400	0.0723	
14 34 12.02	18601.	18387.	28.06	7.9	3.2	2.51	98.8	1.194	0.081	0.1248	-0.0367	0.0702	
14 34 13.02	18596.	18857.	26.03	9.2	3.5	2.42	98.8	1.248	0.079	0.1214	-0.0305	0.0719	
14 34 14.02	18591.	18544.	25.75	11.0	4.0	2.33	98.8	1.329	0.077	0.1331	-0.0379	0.0719	
14 34 15.02	18586.	18913.	26.00	12.1	4.6	2.25	98.8	1.363	0.077	0.1370	-0.0477	0.0701	
14 34 16.02	18580.	18587.	26.44	5.5	4.0	2.19	98.8	1.397	0.074	0.0999	0.0018	0.0729	
14 34 17.02	18575.	18753.	28.06	1.0	2.4	2.17	98.6	1.451	0.082	0.0993	0.0860	0.0761	
14 34 18.02	18570.	18738.	24.96	5.3	3.0	2.15	97.2	1.354	0.077	0.1388	0.0392	0.0761	
14 34 19.02	18565.	19123.	20.67	6.1	4.4	2.12	95.2	1.255	0.079	0.1234	-0.0300	0.0702	
14 34 20.02	18560.	18336.	19.46	7.9	4.7	2.07	94.3	1.261	0.087	0.1162	-0.0364	0.0703	
14 34 21.02	18555.	19491.	18.64	10.5	4.8	2.01	94.1	1.302	0.086	0.1137	-0.0345	0.0721	
14 34 22.02	18549.	19506.	17.10	12.0	4.9	1.95	93.9	1.313	0.083	0.1106	-0.0355	0.0724	
14 34 23.02	18544.	19377.	16.52	11.7	4.9	1.91	94.0	1.245	0.082	0.1102	-0.0393	0.0724	
14 34 24.02	18539.	19206.	16.52	8.6	5.1	1.87	94.0	1.263	0.082	0.1000	-0.0321	0.0704	
14 34 25.02	18534.	19168.	16.91	6.3	5.4	1.82	93.9	1.264	0.083	0.1053	-0.0245	0.0668	
14 34 26.02	18529.	19239.	18.47	8.9	5.6	1.76	93.9	1.268	0.086	0.1335	-0.0737	0.0675	
14 34 27.02	18524.	19547.	18.37	12.5	5.8	1.70	93.8	1.308	0.085	0.1349	-0.0798	0.0695	
14 34 28.02	18519.	20037.	16.45	10.4	5.9	1.63	93.8	1.364	0.081	0.1075	-0.0284	0.0703	
14 34 29.02	18517.	20258.	15.71	7.4	5.9	1.58	93.9	1.377	0.089	0.1045	-0.0217	0.0704	
14 34 30.02	18507.	20186.	15.42	7.2	6.1	1.55	93.9	1.372	0.089	0.1143	-0.0227	0.0679	
14 34 31.02	18502.	19921.	14.66	6.6	6.4	1.53	93.8	1.350	0.085	0.1114	-0.0208	0.0660	
14 34 32.02	18497.	19569.	14.35	6.8	6.4	1.51	93.9	1.301	0.087	0.1134	-0.0204	0.0680	
14 34 33.02	18492.	19216.	14.08	6.7	6.4	1.49	93.8	1.264	0.087	0.1071	-0.0240	0.0640	
14 34 34.02	18486.	19056.	13.28	6.9	6.2	1.53	93.7	1.233	0.086	0.1017	-0.0240	0.0667	
14 34 35.02	18481.	19100.	12.49	9.5	6.1	1.58	93.8	1.226	0.084	0.1043	-0.0213	0.0665	
14 34 36.02	18476.	19293.	11.62	11.2	6.2	1.42	93.8	1.260	0.082	0.0974	-0.0227	0.0663	
14 34 37.02	18471.	19618.	10.38	10.6	6.3	1.27	93.7	1.308	0.049	0.0865	-0.0240	0.0666	
14 34 38.02	18466.	19720.	9.26	8.0	6.1	1.22	93.8	1.320	0.046	0.0804	-0.0228	0.0650	
14 34 39.02	18460.	19437.	8.91	7.7	5.4	1.18	93.8	1.279	0.045	0.0844	-0.0237	0.0663	
14 34 40.02	18455.	19189.	9.24	7.4	5.8	1.13	93.7	1.248	0.047	0.0781	-0.0208	0.0673	
14 34 41.02	18450.	19242.	8.67	6.0	6.1	1.08	93.7	1.252	0.045	0.0762	-0.0176	0.0611	
14 34 42.02	18445.	19124.	7.65	6.9	6.0	1.03	93.7	1.243	0.042	0.0691	-0.0178	0.0629	
14 34 43.02	18440.	18927.	7.37	6.9	6.2	0.97	93.6	1.218	0.042	0.0729	-0.0172	0.0604	
14 34 44.02	18435.	19050.	7.04	9.8	6.4	0.91	93.7	1.215	0.041	0.0781	-0.0200	0.0614	
14 34 45.02	18430.	19212.	5.97	11.8	6.7	0.83	93.8	1.246	0.037	0.0763	-0.0252	0.0615	
14 34 46.02	18425.	19388.	5.21	10.5	6.9	0.76	93.7	1.281	0.035	0.0703	-0.0230	0.0619	

TABLE 3.2e. LANDING (CONTINUED)

/72

KL1, KH3

Feb. 4, 1972

Hr	Min	Sec	Weight	Thrust	Dyn. pres.	Alpha	Theta	H/b	Tau	SH/SM	V _{eff}	ZI	XI	MI	Landing gear
															Extended
14	34	47.02	18419.	18752.	5.20	5.2	6.9	0.61	93.7	1.317	0.034	0.0699	-0.0197	0.0636	
14	34	48.02	18414.	20066.	5.20	5.2	6.7	0.61	93.7	1.353	0.034	0.0711	-0.0189	0.0636	
14	34	49.02	18408.	20081.	5.12	5.2	6.5	0.56	93.6	1.357	0.034	0.0776	-0.0192	0.0651	
14	34	50.02	18403.	19921.	4.88	5.2	6.4	0.51	93.7	1.341	0.033	0.0778	-0.0188	0.0643	
14	34	51.02	18398.	19798.	4.27	5.2	6.2	0.45	93.6	1.329	0.031	0.0756	-0.0215	0.0649	
14	34	52.02	18392.	19375.	3.59	5.2	6.2	0.39	93.6	1.342	0.029	0.0464	-0.0214	0.0623	
14	34	53.02	18387.	20293.	3.15	5.2	6.3	0.32	93.7	1.397	0.026	0.1046	-0.0156	0.0581	
14	34	54.02	18381.	20600.	3.49	-10.0	6.4	0.24	93.7	1.468	0.029	0.1106	-0.0096	0.0543	
14	34	55.02	18376.	20568.	4.04	-4.8	6.0	0.15	93.8	1.571	0.030	0.1187	-0.0005	0.0437	
14	34	56.02	18370.	19742.	2.84	-1.8	4.2	0.08	96.3	1.730	0.030	0.0795	-0.0027	0.0392	
14	34	57.02	18365.	14252.	5.66	-1.2	1.6	0.05	92.9	1.677	0.042	-0.2106	-0.0464	0.0756	
14	34	58.02	18362.	5048.	6.49	2.0	0.7	0.03	98.7	1.000	0.077	-2.3736	-0.1727	0.1658	
14	34	59.02	18361.	1632.	4.81	0.7	0.9	0.03	17.1	0.183	0.115	-10.7420	-0.2104	0.4504	
14	35	0.02	18361.	1578.	4.46	-5.8	0.8	0.03	7.0	0.109	0.113	-11.7074	-0.1144	0.5584	

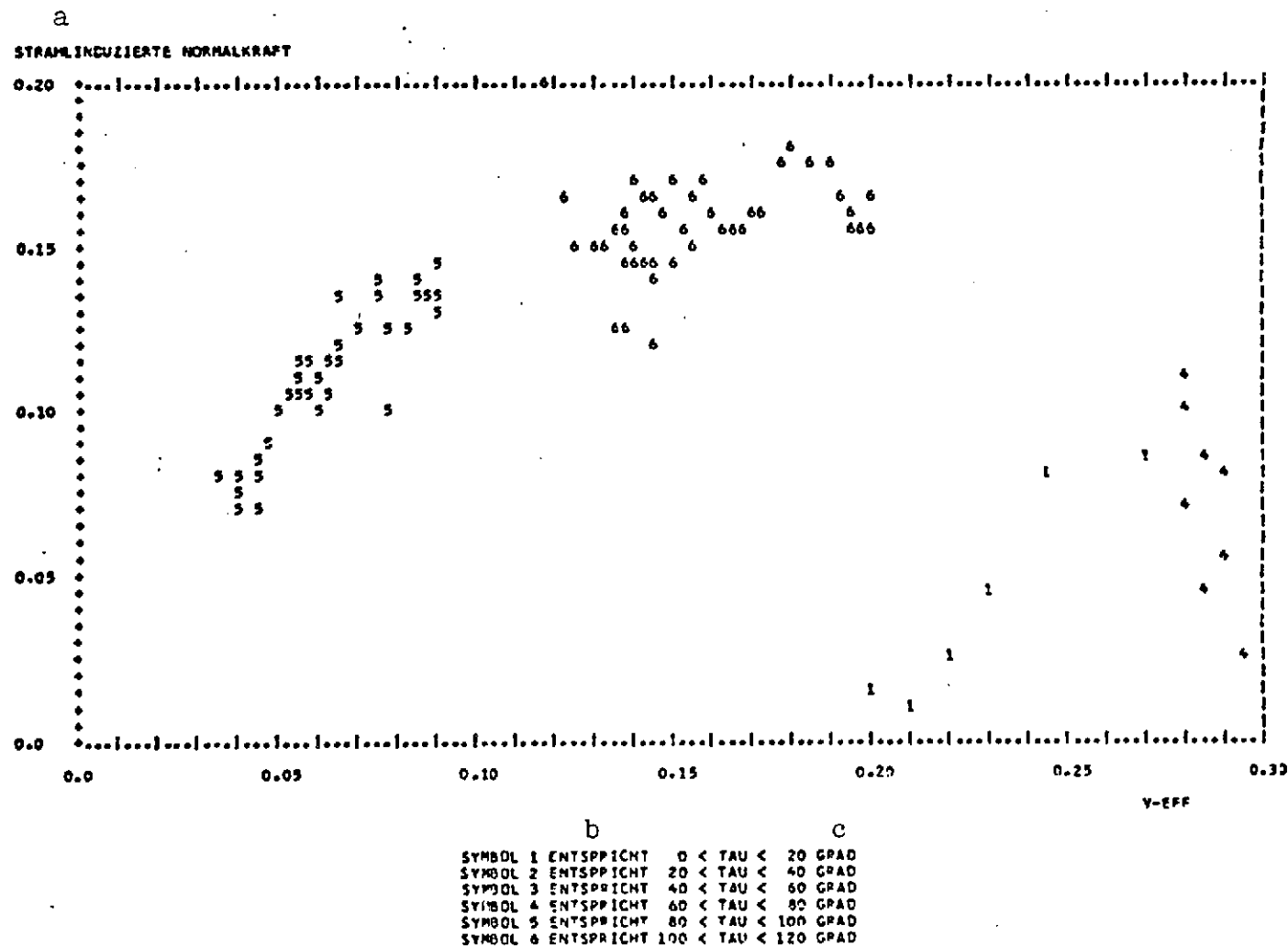


Fig. 3.1.a. Jet-induced normal force, Do 31 E3, trial 247. Thrust ratio SH/S_M of 1.000 to 1.400, without ground effect ($H/b > 0.8$).

Key: a. Jet-induced normal force; b. Corresponds to; c. Degrees

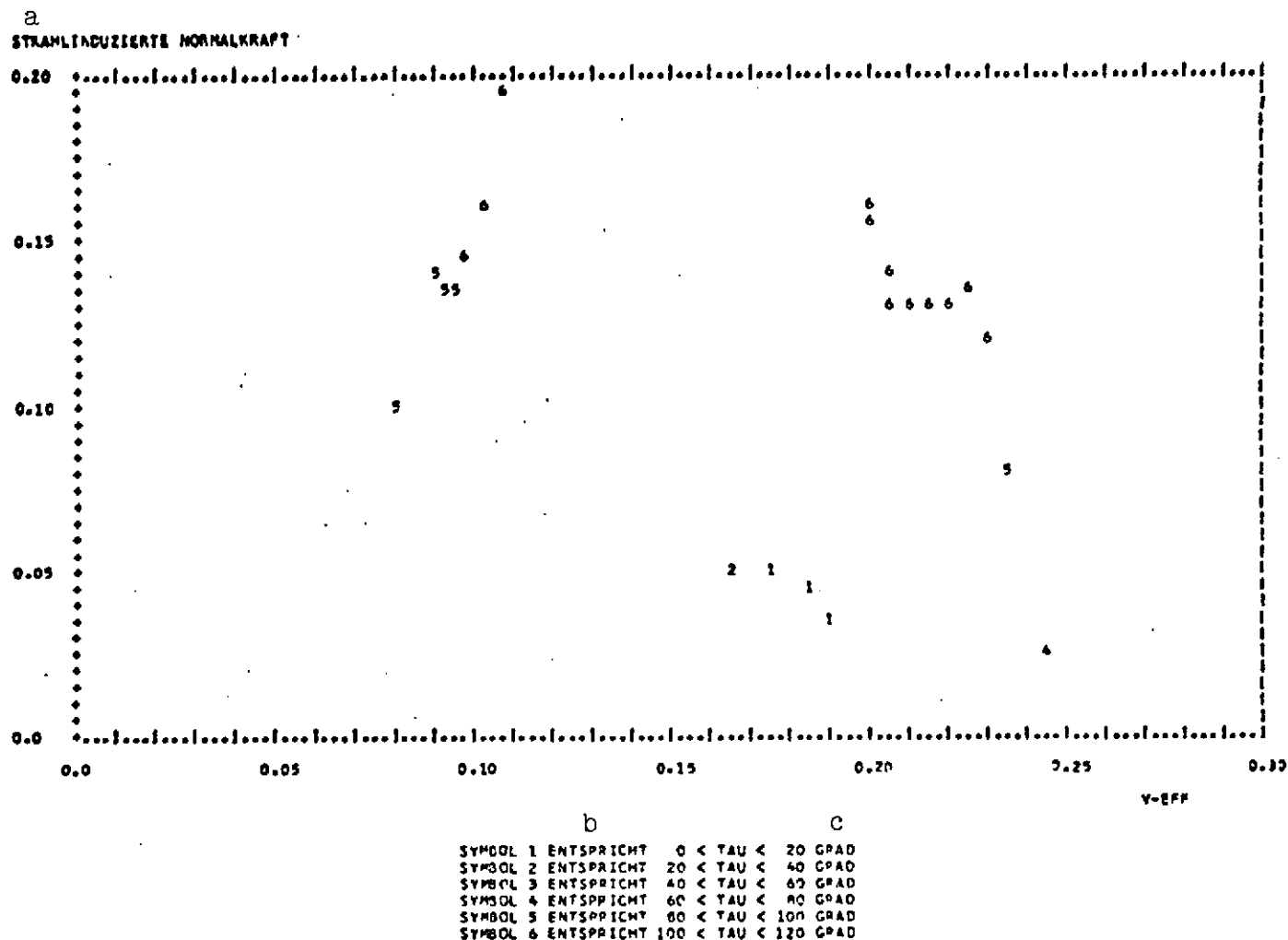


Fig. 3.1.b. Jet-induced normal force, Do 31 E3, trial 247. Thrust ratio S_H/S_M of 1.400 to 2.100, without ground effect ($H/b > 0.8$).

Key: a. Jet-induced normal force
 b. Corresponds to
 c. Degrees

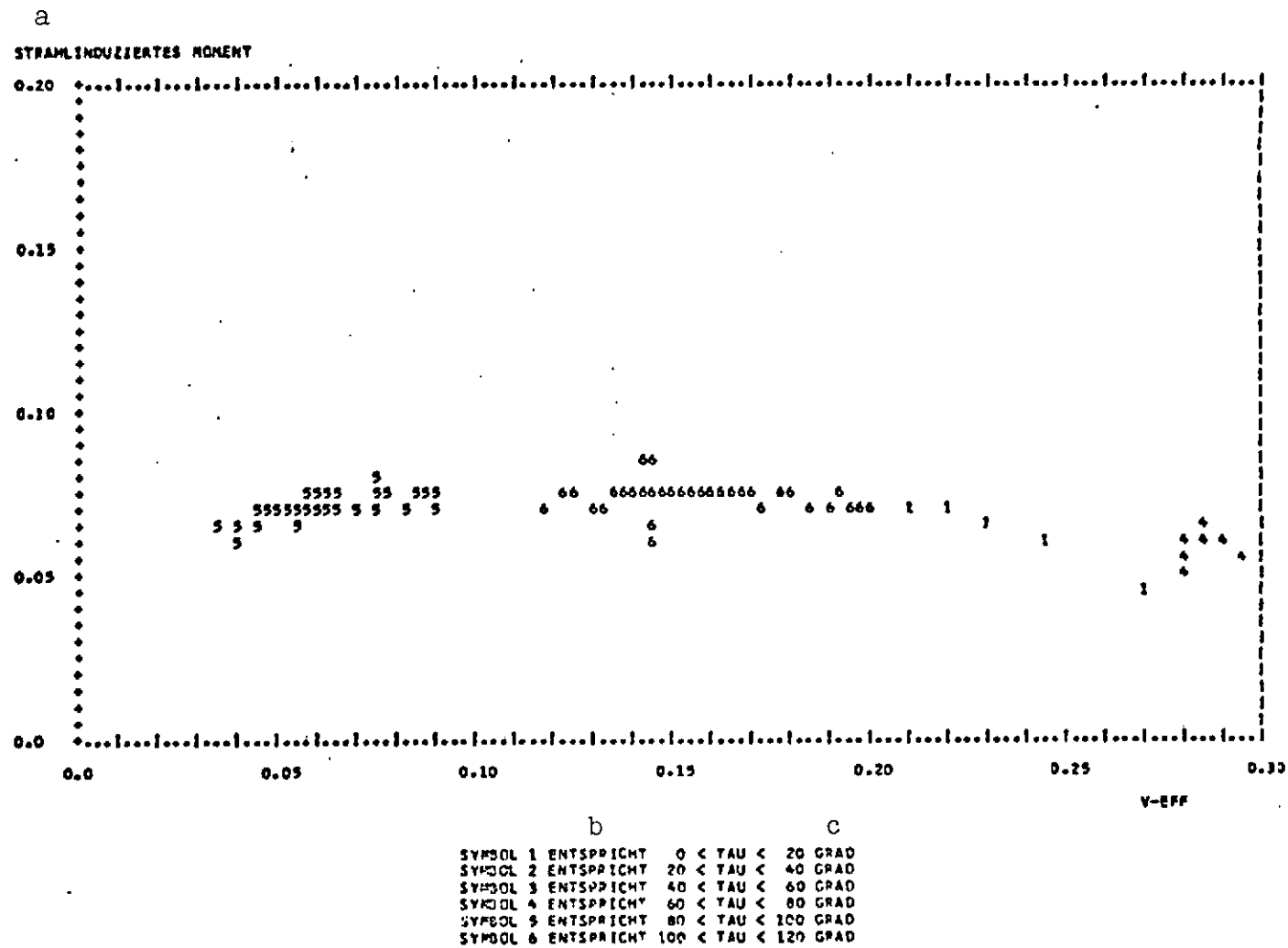


Fig. 3.2.a. Jet-induced torque. Do 31 E3, trial 247. Thrust ratio S_H/S_M of 1.000 to 1.400, without ground effect ($H/b > 0.8$).

Key: a. Jet-induced torque
 b. Corresponds to
 c. Degrees

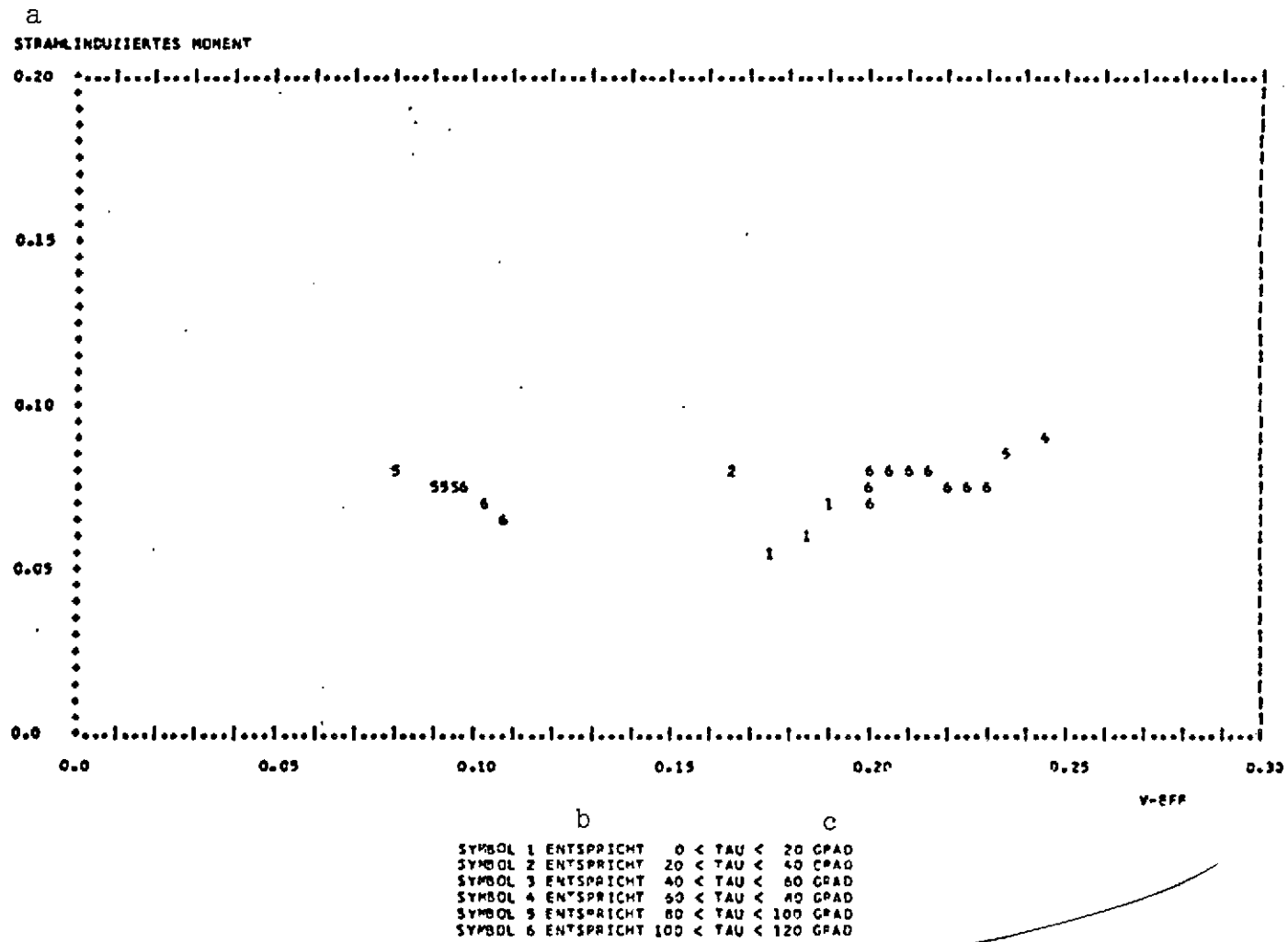


Fig. 3.2.b. Jet-induced torque. Do 31, E3, trial 247. Thrust ratio S_H/S_M of 1.400 to 2.100, without ground effect ($H/b > 0.8$).

Key: a. Jet-induced torque
 b. Corresponds to
 c. Degrees

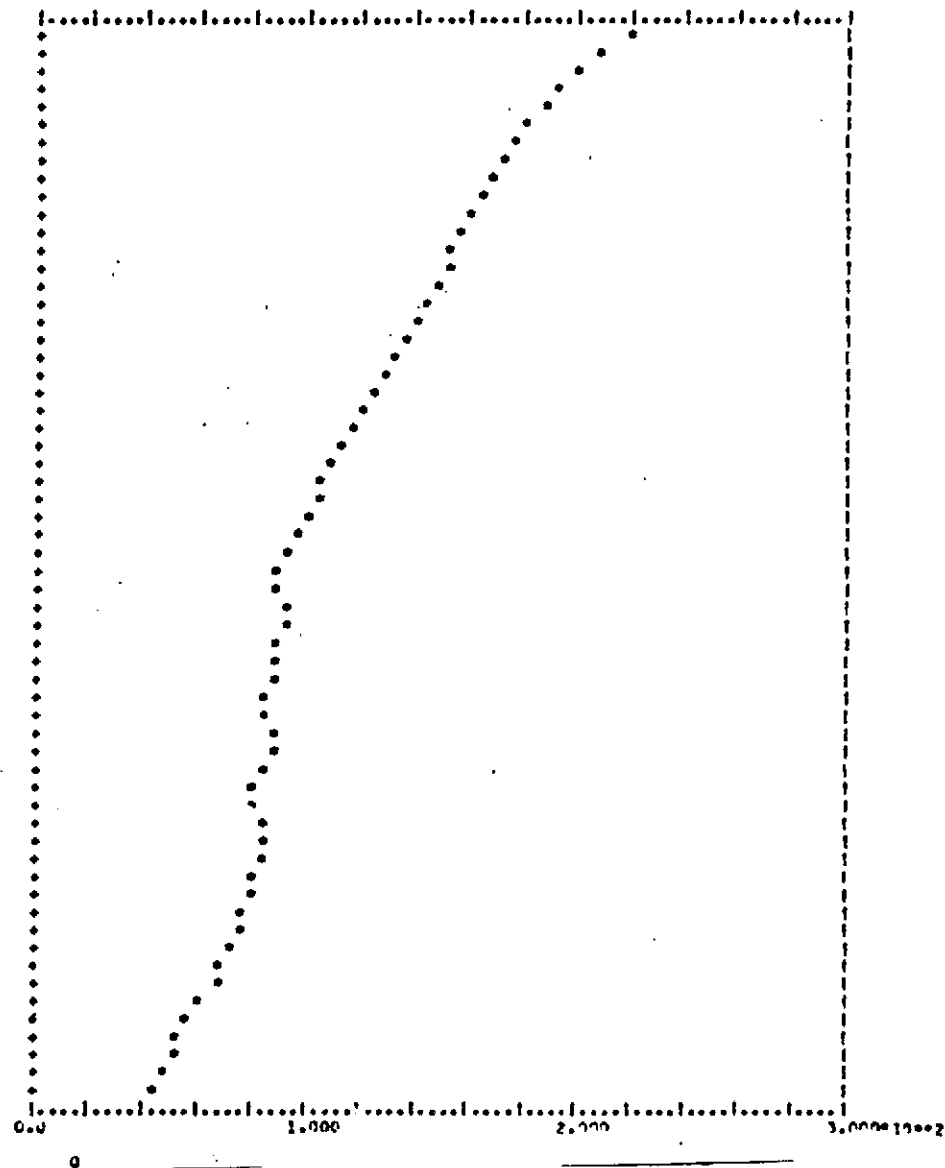
a

E3-VERS.247

OKL1, KM3b

b Zeit
Sek

92381.02
 92382.02
 92383.02
 92384.02
 92385.02
 92386.02
 92387.02
 92388.02
 92389.02
 92390.02
 92391.02
 92392.02
 92393.02
 92394.02
 92395.02
 92396.02
 92397.02
 92398.02
 92399.02
 92400.02
 92401.02
 92402.02
 92403.02
 92404.02
 92405.02
 92406.02
 92407.02
 92408.02
 92409.02
 92410.02
 92411.02
 92412.02
 92413.02
 92414.02
 92415.02
 92416.02
 92417.02
 92418.02
 92419.02
 92420.02
 92421.02
 92422.02
 92423.02
 92424.02
 92425.02
 92426.02
 92427.02
 92428.02
 92429.02
 92430.02
 92431.02
 92432.02
 92433.02
 92434.02
 92435.02
 92436.02
 92437.02
 92438.02
 92439.02
 92440.02



/77

Fig. 3.3.a. Dynamic pressure q kp/m^2 , Do 31 E3 trial 247, landing phase.

Key: a. E3 trial 246; b. Time, sec

a

E3-VEF 3-247

K11, RM3

b
Zeit
Sek

52381.02
 52382.02
 52383.02
 52384.02
 52385.02
 52386.02
 52387.02
 52388.02
 52389.02
 52390.02
 52391.02
 52392.02
 52393.02
 52394.02
 52395.02
 52396.02
 52397.02
 52398.02
 52399.02
 52400.02
 52401.02
 52402.02
 52403.02
 52404.02
 52405.02
 52406.02
 52407.02
 52408.02
 52409.02
 52410.02
 52411.02
 52412.02
 52413.02
 52414.02
 52415.02
 52416.02
 52417.02
 52418.02
 52419.02
 52420.02
 52421.02
 52422.02
 52423.02
 52424.02
 52425.02
 52426.02
 52427.02
 52428.02
 52429.02
 52430.02
 52431.02
 52432.02
 52433.02
 52434.02
 52435.02
 52436.02
 52437.02
 52438.02
 52439.02
 52440.02

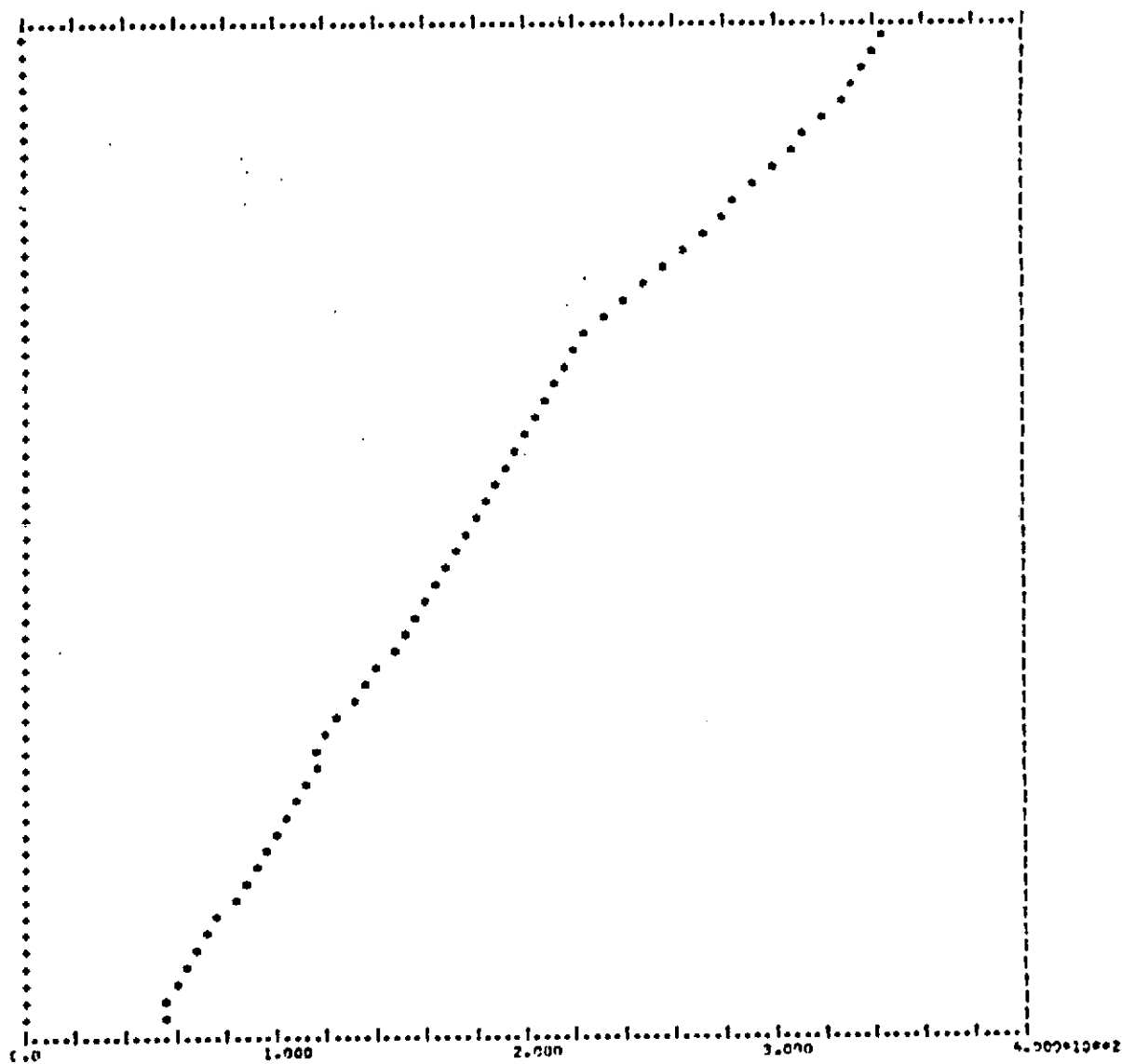


Fig. 3.3.b. Altitude H m.

Key: a. E3 Trial No. 247
 b. Time, sec

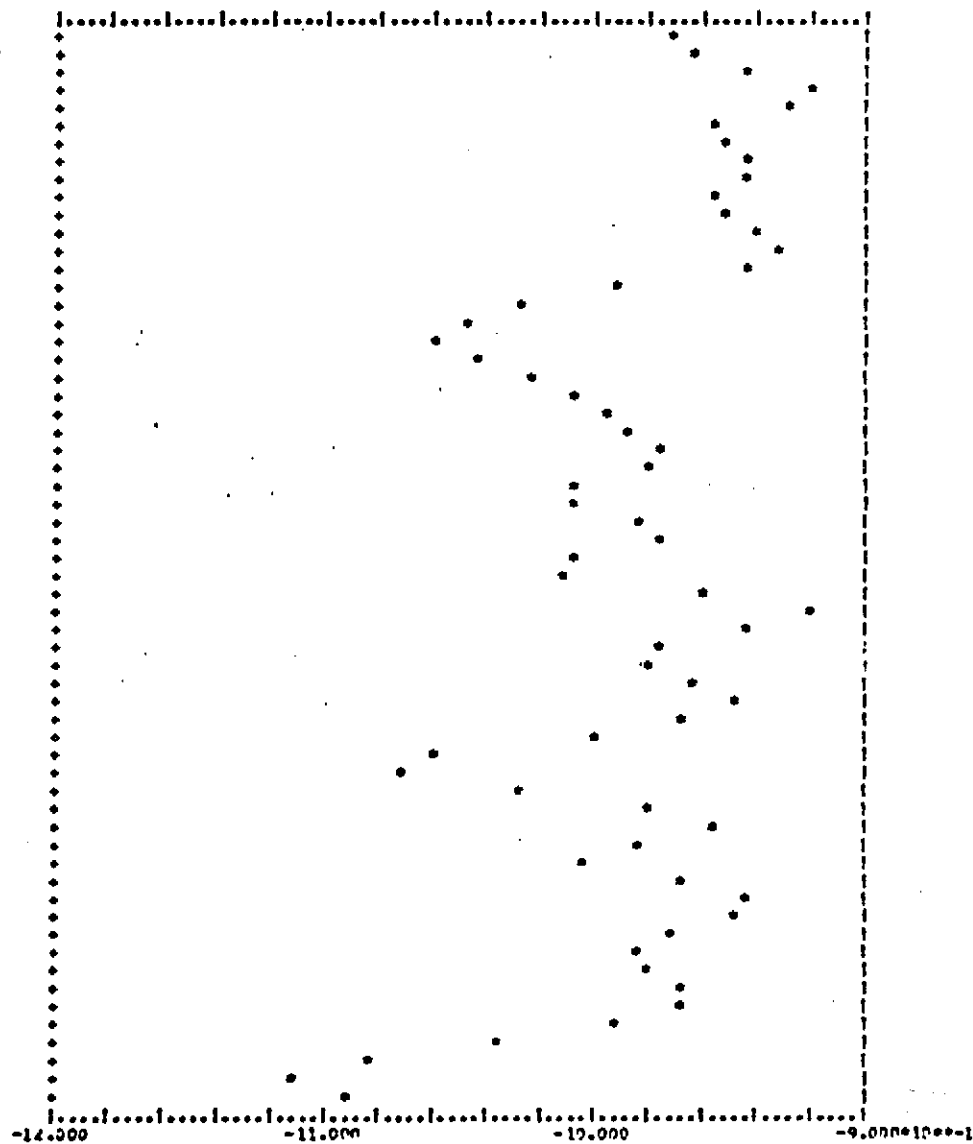
a

E3-VEP5.247

KL1,KH3

b Zeit
Sek

52381.02
 52382.02
 52383.02
 52384.02
 52385.02
 52386.02
 52387.02
 52388.02
 52389.02
 52390.02
 52391.02
 52392.02
 52393.02
 52394.02
 52395.02
 52396.02
 52397.02
 52398.02
 52399.02
 52400.02
 52401.02
 52402.02
 52403.02
 52404.02
 52405.02
 52406.02
 52407.02
 52408.02
 52409.02
 52410.02
 52411.02
 52412.02
 52413.02
 52414.02
 52415.02
 52416.02
 52417.02
 52418.02
 52419.02
 52420.02
 52421.02
 52422.02
 52423.02
 52424.02
 52425.02
 52426.02
 52427.02
 52428.02
 52429.02
 52430.02
 52431.02
 52432.02
 52433.02
 52434.02
 52435.02
 52436.02
 52437.02
 52438.02
 52439.02
 52440.02



/79

Fig. 3.3.c. Normal acceleration BZ m/s².

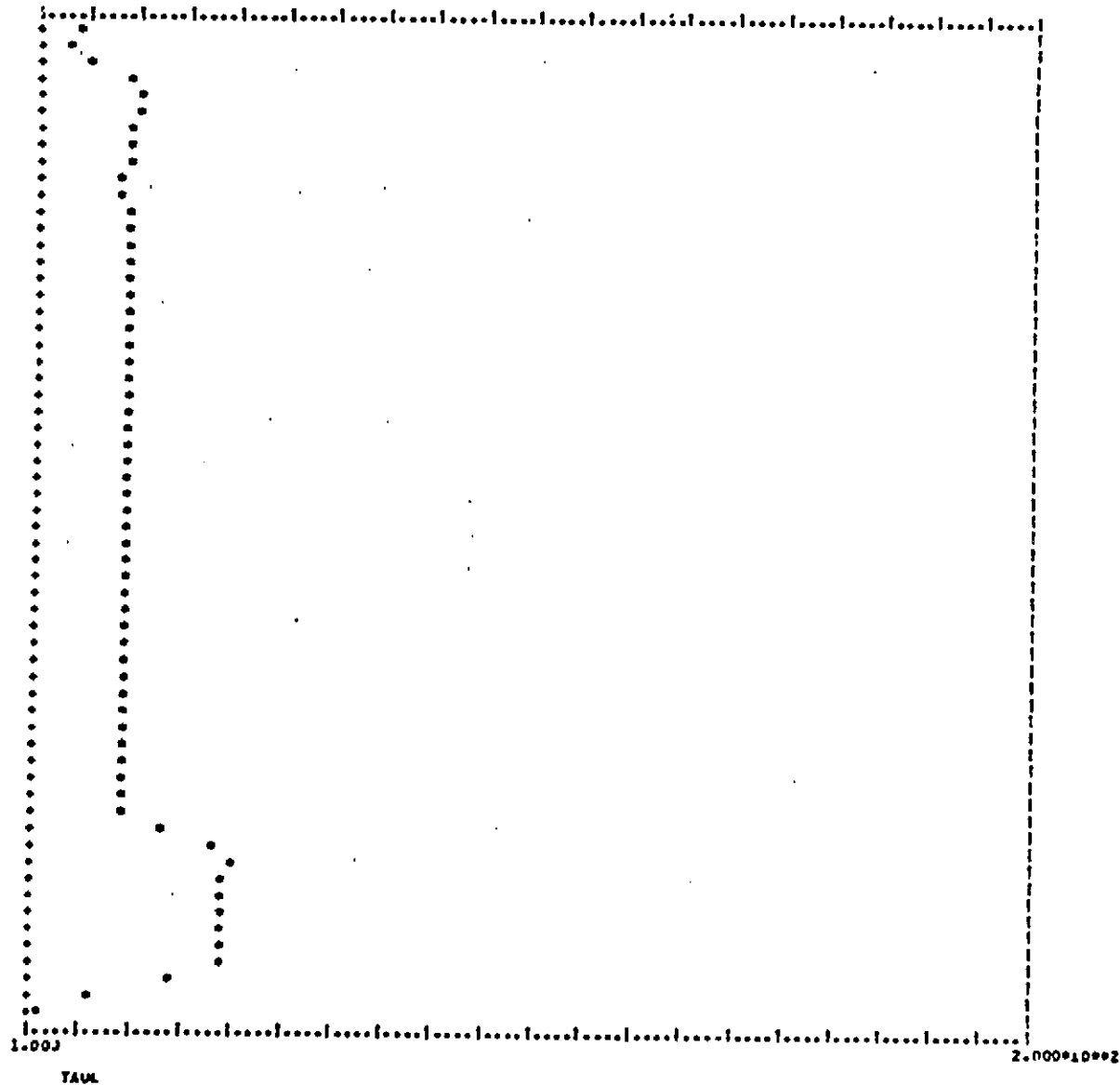
Key: a. E3 trial No. 247; b. Time, sec

a E3-VEFS.247

OKL1,XM30

b Zeit
Sek

92381.02
 92382.02
 92383.02
 92384.02
 92385.02
 92386.02
 92387.02
 92388.02
 92389.02
 92390.02
 92391.02
 92392.02
 92393.02
 92394.02
 92395.02
 92396.02
 92397.02
 92398.02
 92399.02
 92400.02
 92401.02
 92402.02
 92403.02
 92404.02
 92405.02
 92406.02
 92407.02
 92408.02
 92409.02
 92410.02
 92411.02
 92412.02
 92413.02
 92414.02
 92415.02
 92416.02
 92417.02
 92418.02
 92419.02
 92420.02
 92421.02
 92422.02
 92423.02
 92424.02
 92425.02
 92426.02
 92427.02
 92428.02
 92429.02
 92430.02
 92431.02
 92432.02
 92433.02
 92434.02
 92435.02
 92436.02
 92437.02
 92438.02
 92439.02
 92440.02

Fig. 3.3.d. Angle of nozzle rotation τ .

Key: a. E3 trial no. 247; b. Time, sec

a

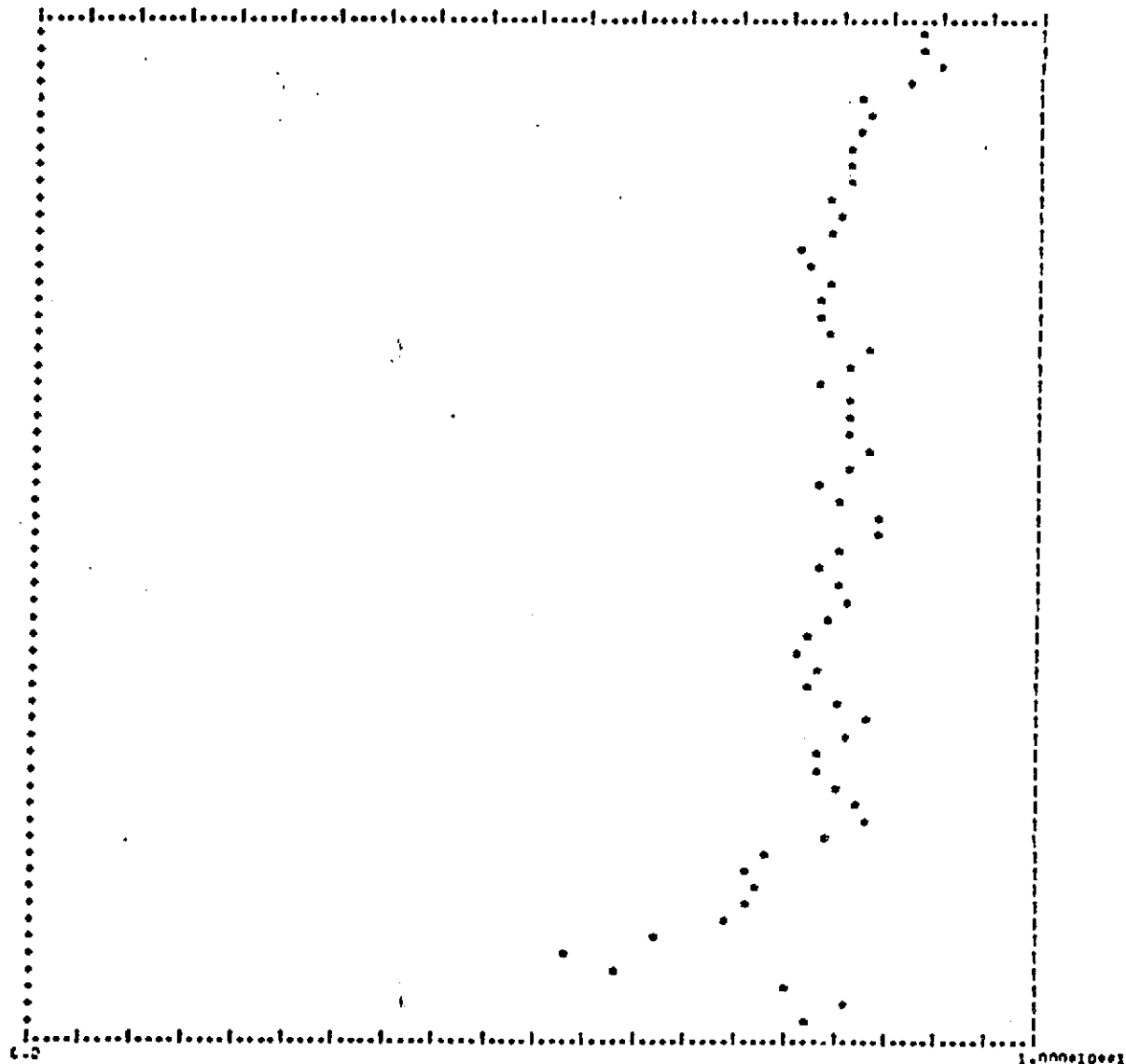
E3-VEPS.247

MK11, KM30

b

Zeit
Sek

52381.02
 52382.02
 52383.02
 52384.02
 52385.02
 52386.02
 52387.02
 52388.02
 52389.02
 52390.02
 52391.02
 52392.02
 52393.02
 52394.02
 52395.02
 52396.02
 52397.02
 52398.02
 52399.02
 52400.02
 52401.02
 52402.02
 52403.02
 52404.02
 52405.02
 52406.02
 52407.02
 52408.02
 52409.02
 52410.02
 52411.02
 52412.02
 52413.02
 52414.02
 52415.02
 52416.02
 52417.02
 52418.02
 52419.02
 52420.02
 52421.02
 52422.02
 52423.02
 52424.02
 52425.02
 52426.02
 52427.02
 52428.02
 52429.02
 52430.02
 52431.02
 52432.02
 52433.02
 52434.02
 52435.02
 52436.02
 52437.02
 52438.02
 52439.02
 52440.02



ATAN

Fig. 3.3.e. Elevator angle η .

Key: a. E3 trial No. 247; b. Time, sec

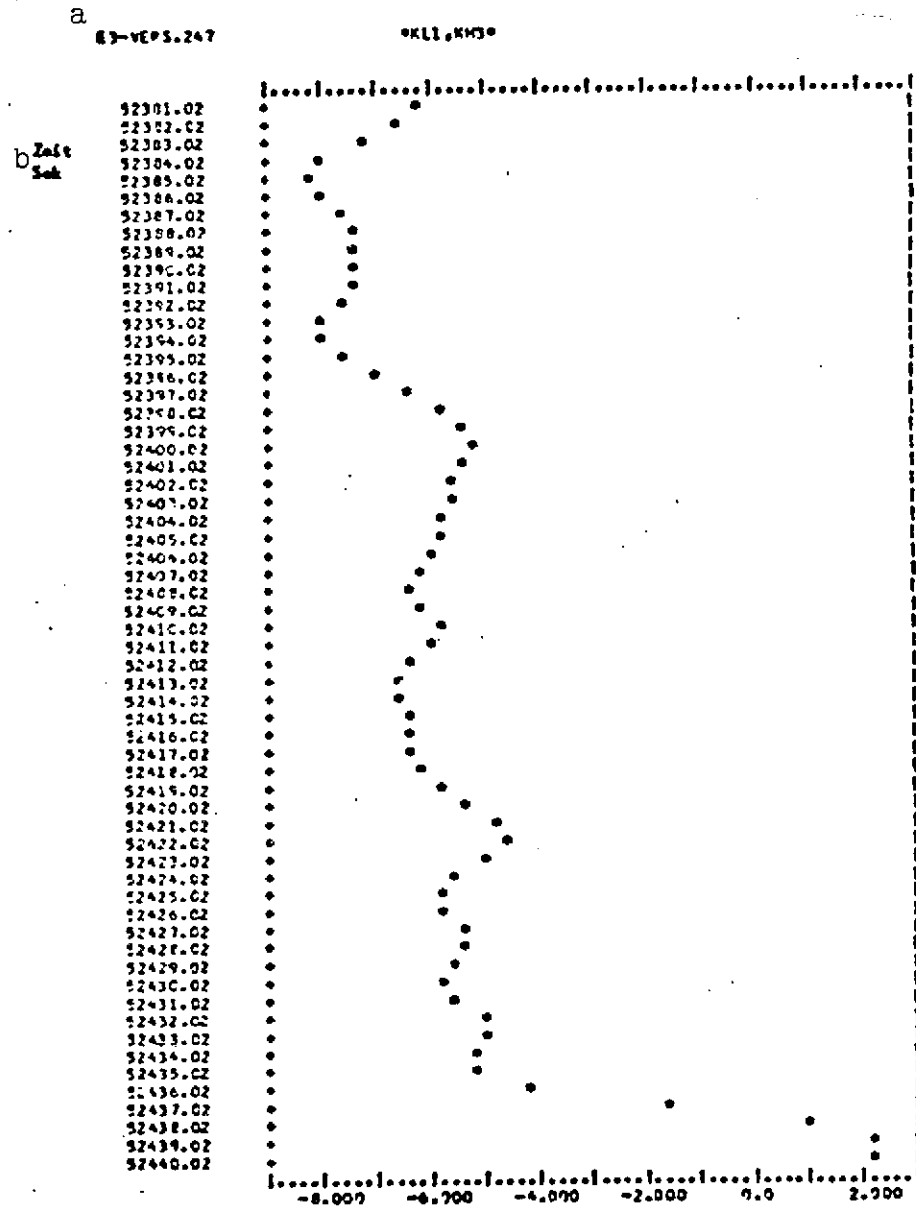


Fig. 3.3.f. Angle of pitch θ .

Key: a. E3 trial no. 247; b. Time, sec

a E3-VEPS.247

WELL, WY30

b Zeit
Sek

92381.02
92382.02
92383.02
92384.02
92385.02
92386.02
92387.02
92388.02
92389.02
92390.02
92391.02
92392.02
92393.02
92394.02
92395.02
92396.02
92397.02
92398.02
92399.02
92400.02
92401.02
92402.02
92403.02
92404.02
92405.02
92406.02
92407.02
92408.02
92409.02
92410.02
92411.02
92412.02
92413.02
92414.02
92415.02
92416.02
92417.02
92418.02
92419.02
92420.02
92421.02
92422.02
92423.02
92424.02
92425.02
92426.02
92427.02
92428.02
92429.02
92430.02
92431.02
92432.02
92433.02
92434.02
92435.02
92436.02
92437.02
92438.02
92439.02
92440.02

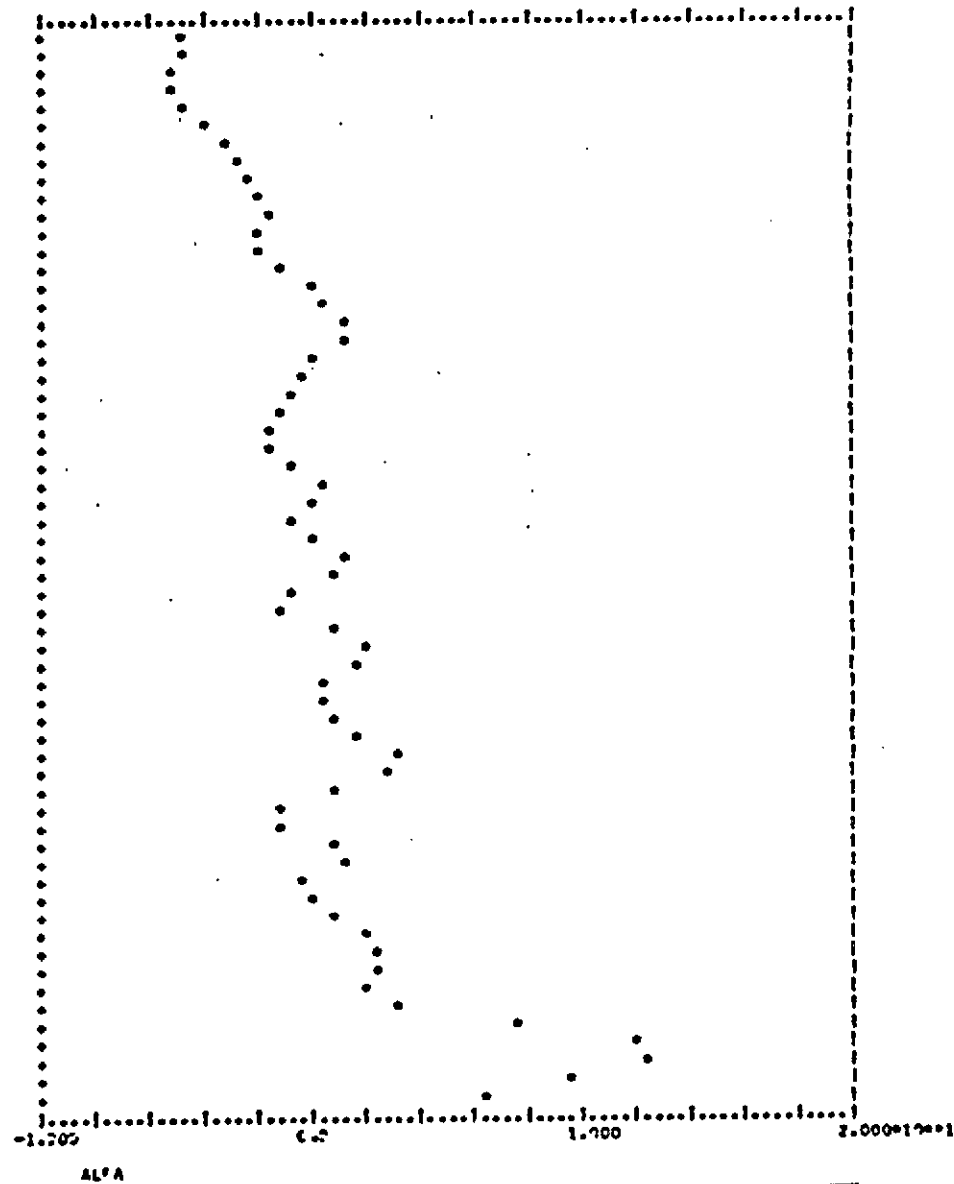


Fig. 3.3.g. Angle of attack α .

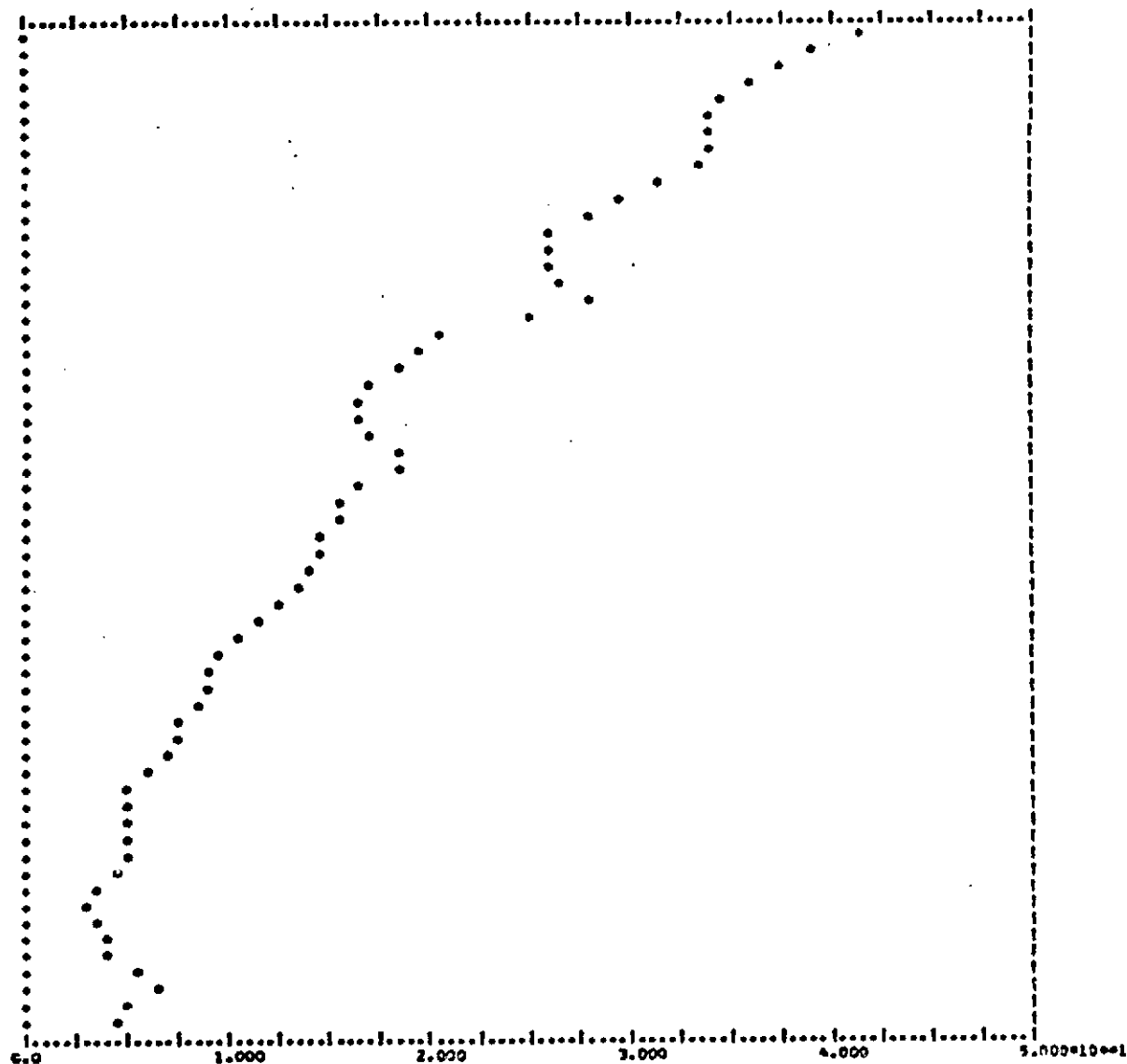
Key: a. E3 trial no. 247; b. Time, sec

a E3-247

0.11, 0.070

b Zeit
Sek

92441.02
 92442.02
 92443.02
 92444.02
 92445.02
 92446.02
 92447.02
 92448.02
 92449.02
 92450.02
 92451.02
 92452.02
 92453.02
 92454.02
 92455.02
 92456.02
 92457.02
 92458.02
 92459.02
 92460.02
 92461.02
 92462.02
 92463.02
 92464.02
 92465.02
 92466.02
 92467.02
 92468.02
 92469.02
 92470.02
 92471.02
 92472.02
 92473.02
 92474.02
 92475.02
 92476.02
 92477.02
 92478.02
 92479.02
 92480.02
 92481.02
 92482.02
 92483.02
 92484.02
 92485.02
 92486.02
 92487.02
 92488.02
 92489.02
 92490.02
 92491.02
 92492.02
 92493.02
 92494.02
 92495.02
 92496.02
 92497.02
 92498.02
 92499.02
 92500.02



/84

Fig. 3.3.h. Dynamic pressure q kp/m^2 .
 Key: a. E3 trial no. 247; b. Time, sec

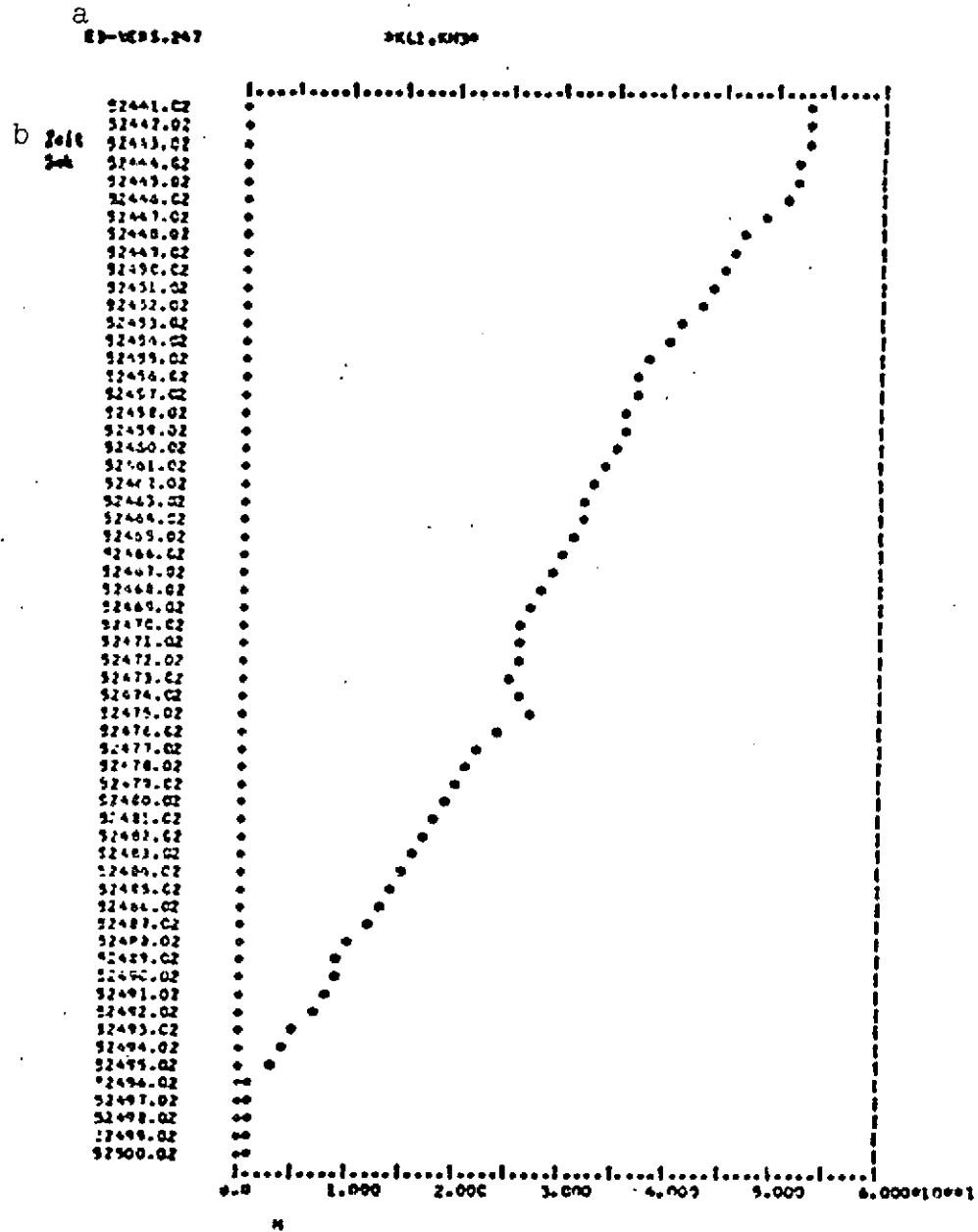
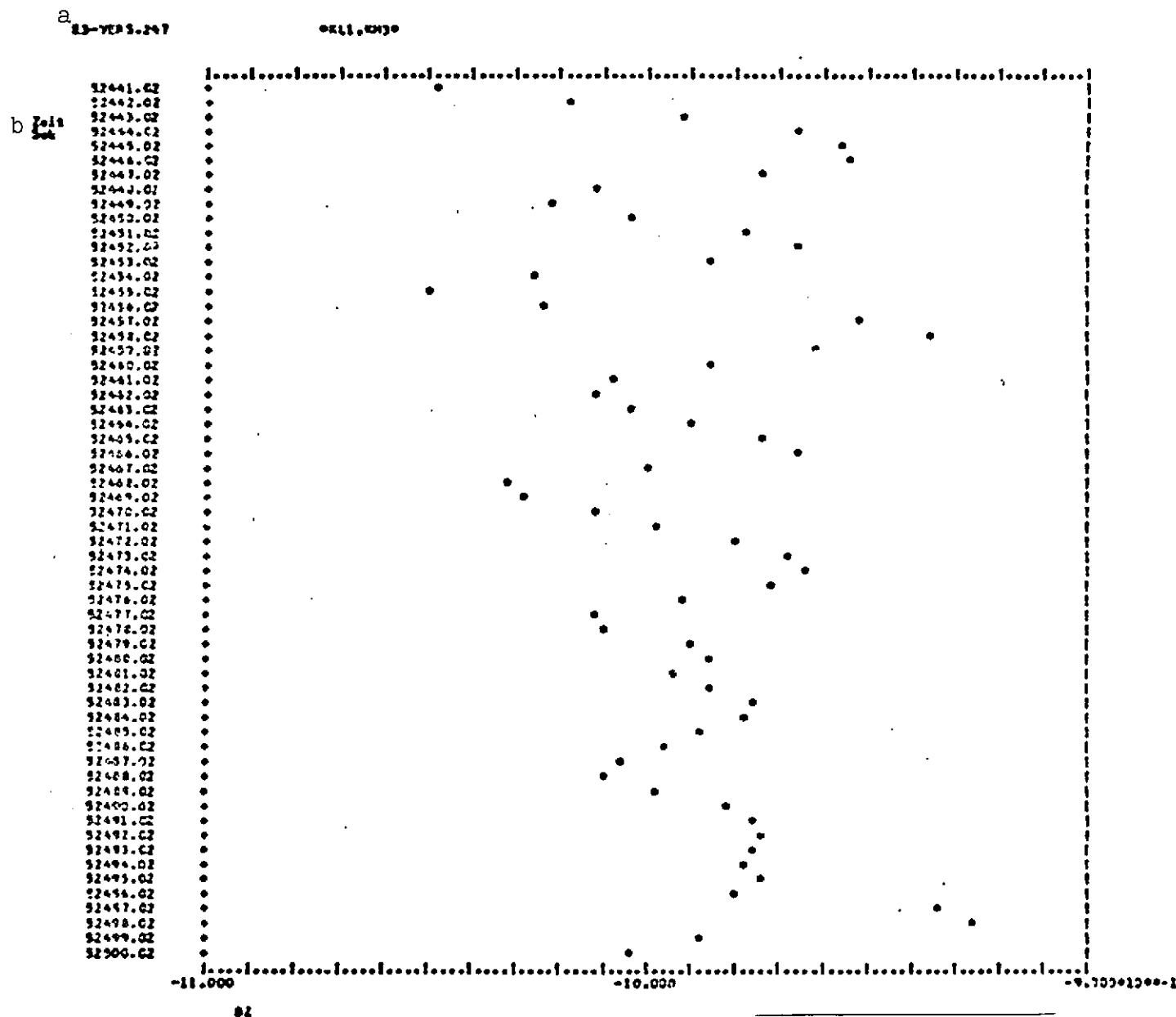


Fig. 3.3.1. Altitude H m.

Key: a. E3 trial no. 247; b. Time, sec



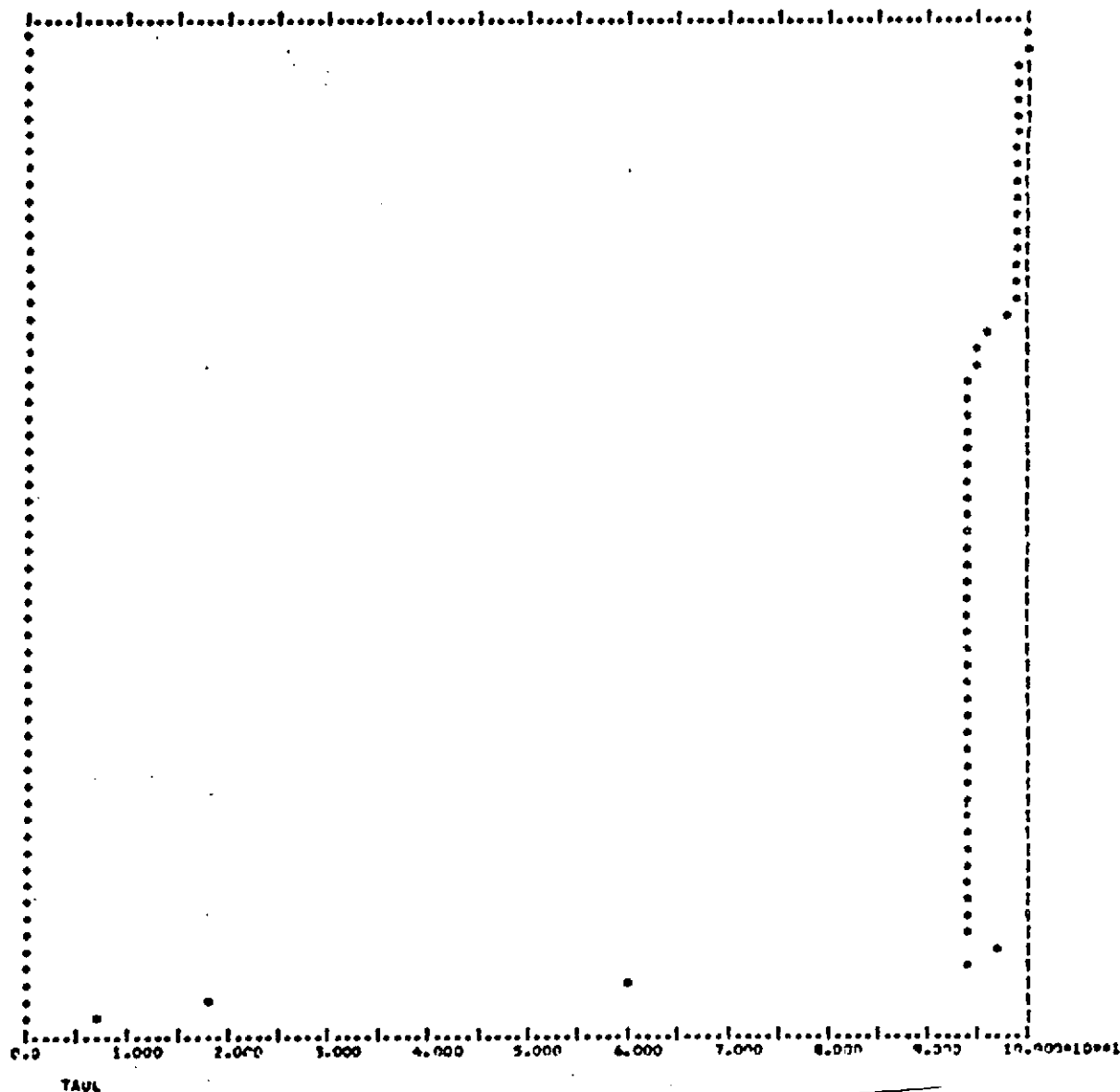
a

E3-VEPS-247

0011,0030

b Zeit
Zeit

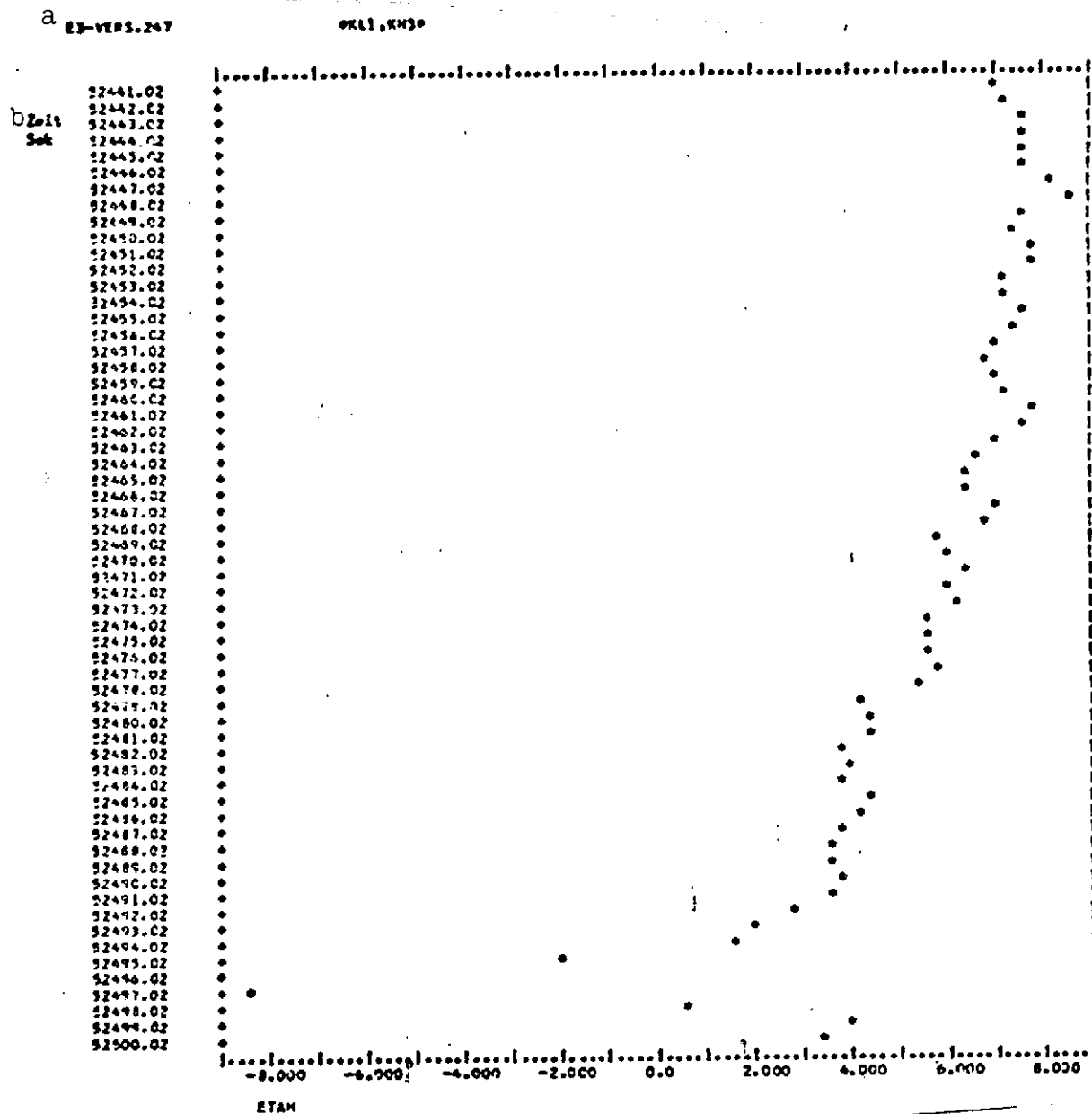
92441.02
 92442.02
 92443.02
 92444.02
 92445.02
 92446.02
 92447.02
 92448.02
 92449.02
 92450.02
 92451.02
 92452.02
 92453.02
 92454.02
 92455.02
 92456.02
 92457.02
 92458.02
 92459.02
 92460.02
 92461.02
 92462.02
 92463.02
 92464.02
 92465.02
 92466.02
 92467.02
 92468.02
 92469.02
 92470.02
 92471.02
 92472.02
 92473.02
 92474.02
 92475.02
 92476.02
 92477.02
 92478.02
 92479.02
 92480.02
 92481.02
 92482.02
 92483.02
 92484.02
 92485.02
 92486.02
 92487.02
 92488.02
 92489.02
 92490.02
 92491.02
 92492.02
 92493.02
 92494.02
 92495.02
 92496.02
 92497.02
 92498.02
 92499.02
 92500.02



/87

Fig. 3.3.1. Angle of nozzle rotation τ .

Key: a. E3 trial no. 247; b. Time, sec

Fig. 3.3.m. Elevator angle η .

Key: a. E3 trial no. 247; b. Time, sec

a

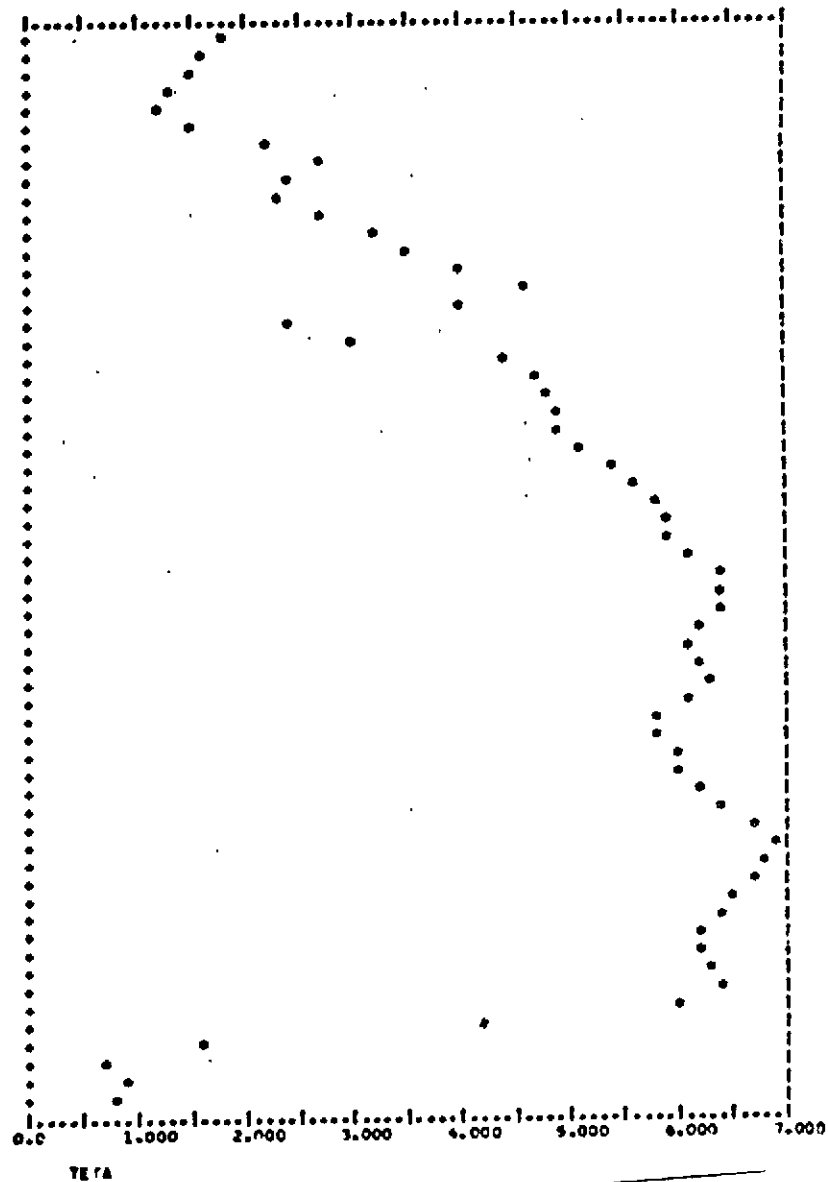
E3-VERB.247

0811, RM30

/89

b Zeit
Sek

92441.02
 92442.02
 92443.02
 92444.02
 92445.02
 92446.02
 92447.02
 92448.02
 92449.02
 92450.02
 92451.02
 92452.02
 92453.02
 92454.02
 92455.02
 92456.02
 92457.02
 92458.02
 92459.02
 92460.02
 92461.02
 92462.02
 92463.02
 92464.02
 92465.02
 92466.02
 92467.02
 92468.02
 92469.02
 92470.02
 92471.02
 92472.02
 92473.02
 92474.02
 92475.02
 92476.02
 92477.02
 92478.02
 92479.02
 92480.02
 92481.02
 92482.02
 92483.02
 92484.02
 92485.02
 92486.02
 92487.02
 92488.02
 92489.02
 92490.02
 92491.02
 92492.02
 92493.02
 92494.02
 92495.02
 92496.02
 92497.02
 92498.02
 92499.02
 92500.02

Fig. 3.3.n. Angle of pitch θ .

Key: a. E3 trial no. 247; b. Time, sec

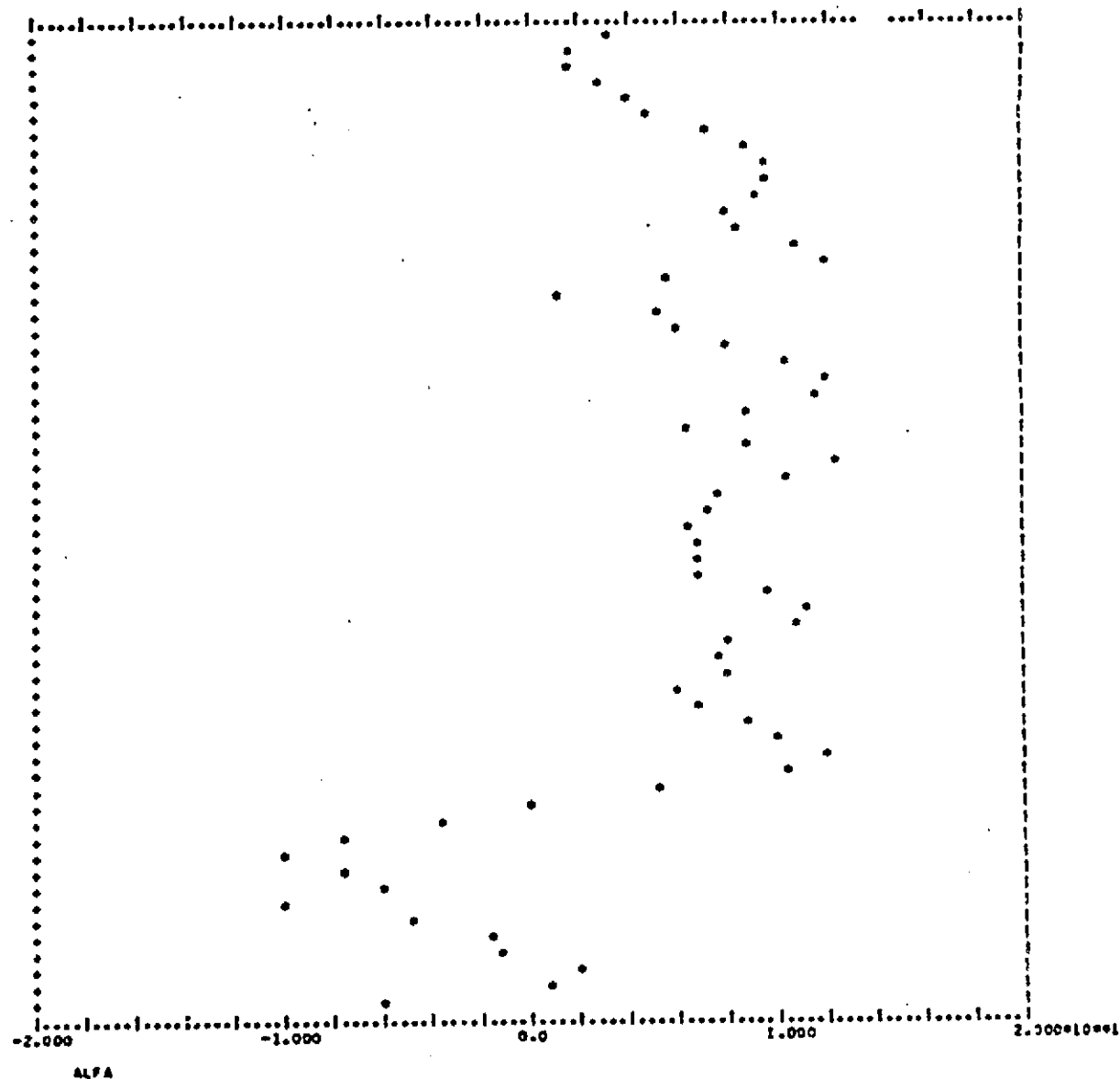
a
E3-VEPS.247

OKL1, KM30

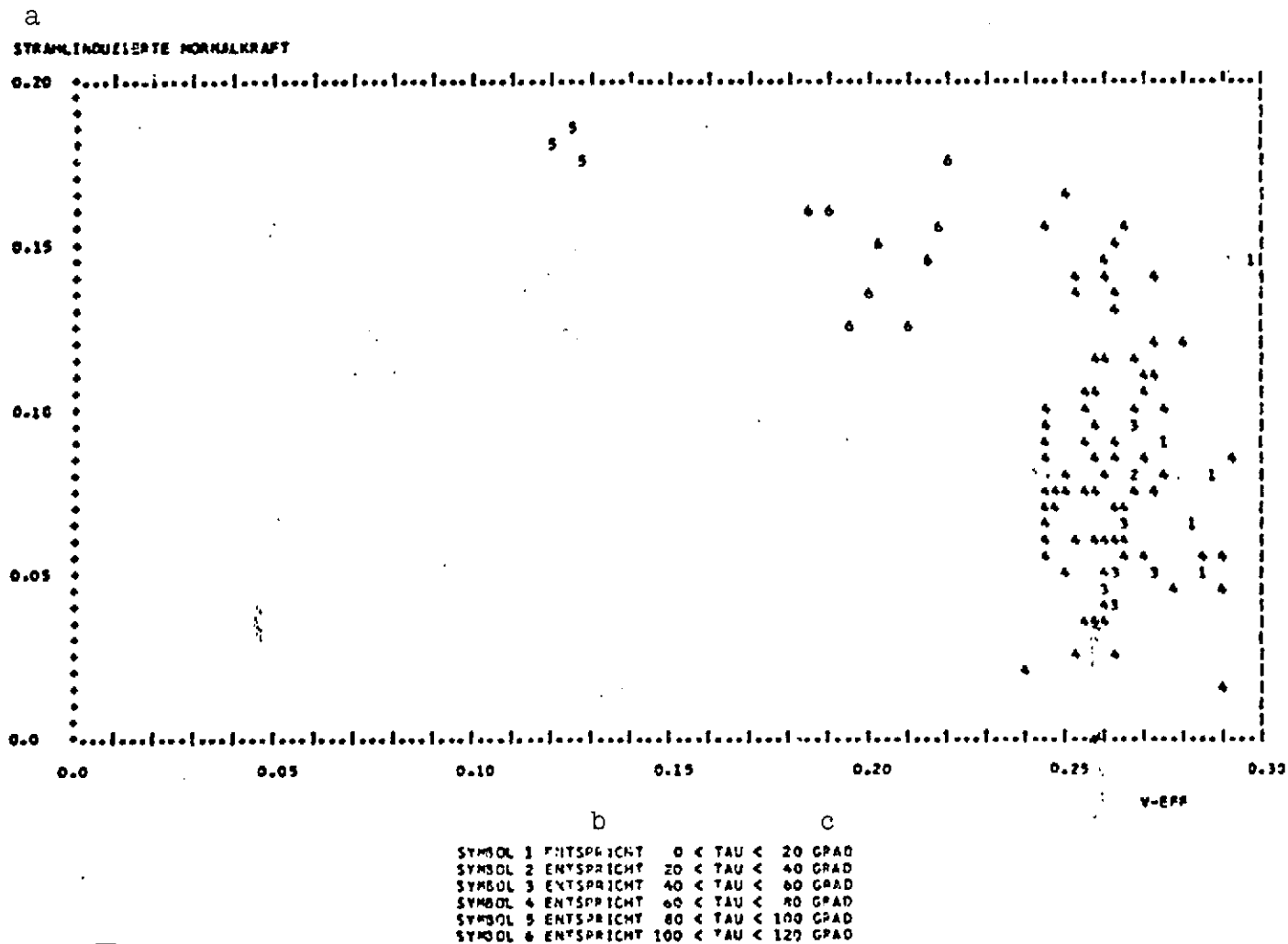
/90

bZeit
Sek

52441.02
 52442.02
 52443.02
 52444.02
 52445.02
 52446.02
 52447.02
 52448.02
 52449.02
 52450.02
 52451.02
 52452.02
 52453.02
 52454.02
 52455.02
 52456.02
 52457.02
 52458.02
 52459.02
 52460.02
 52461.02
 52462.02
 52463.02
 52464.02
 52465.02
 52466.02
 52467.02
 52468.02
 52469.02
 52470.02
 52471.02
 52472.02
 52473.02
 52474.02
 52475.02
 52476.02
 52477.02
 52478.02
 52479.02
 52480.02
 52481.02
 52482.02
 52483.02
 52484.02
 52485.02
 52486.02
 52487.02
 52488.02
 52489.02
 52490.02
 52491.02
 52492.02
 52493.02
 52494.02
 52495.02
 52496.02
 52497.02
 52498.02
 52499.02
 52500.02

Fig. 3.3.o. Angle of attack α .

Key: a. E3 trial no. 247; b. Time, sec



/91

Fig. 3.4.a. Jet-induced normal force, Do 31 E3, all flights listed in Table 3.1. Thrust ratio S_H/S_M of 0.725 to 1.000, without ground effect ($H/b > 0.8$).

Key: a. Jet-induced normal force
 b. Corresponds to
 c. Degrees

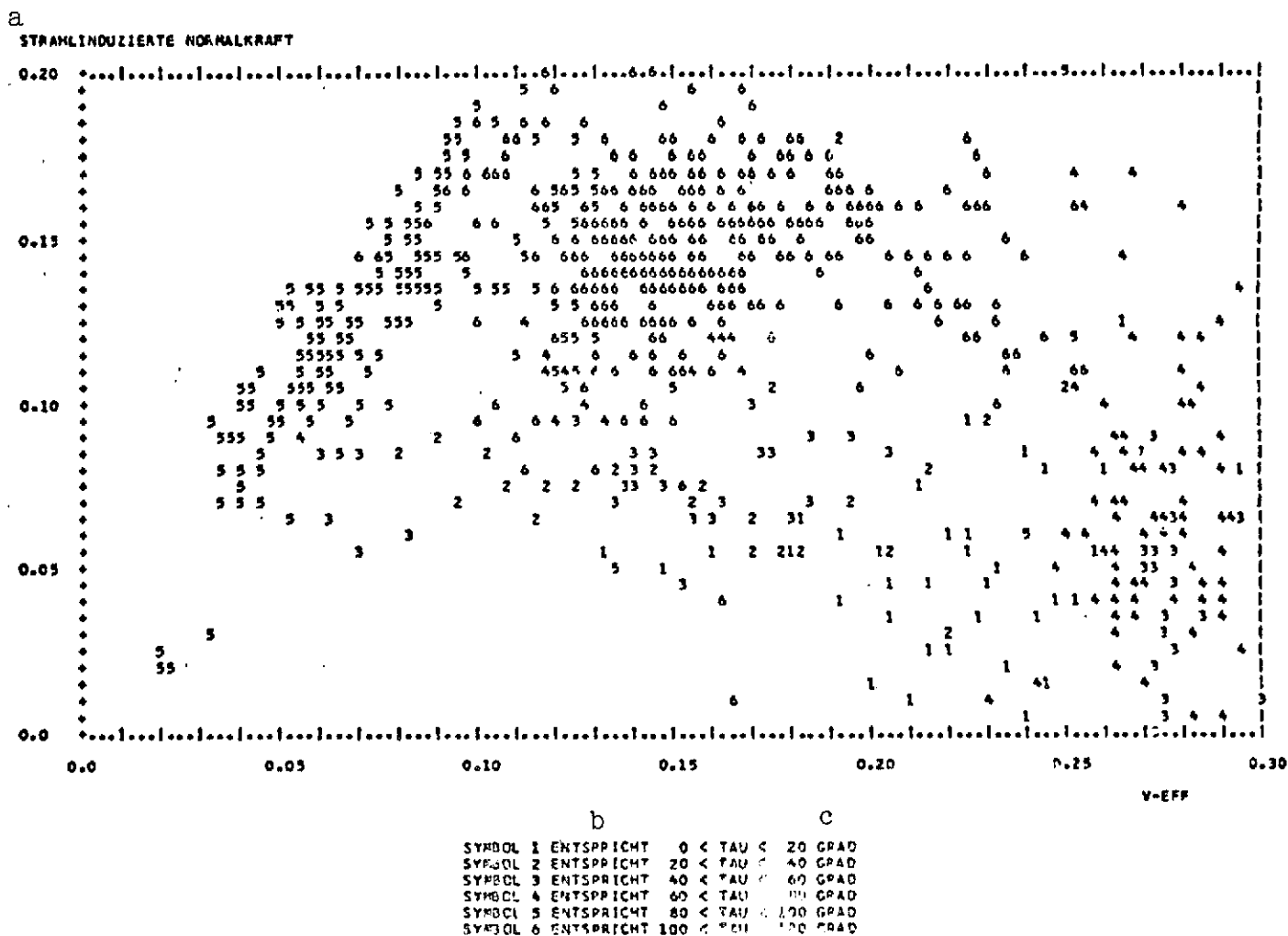


Fig. 3.4.b. Jet-induced normal force, Do 31 E3. Thrust ratio S_H/S_M of 1.000 to 1.400, without ground effect ($H/b > 0.8$).

Key: a. Jet-induced normal force
 b. Corresponds to
 c. Degrees

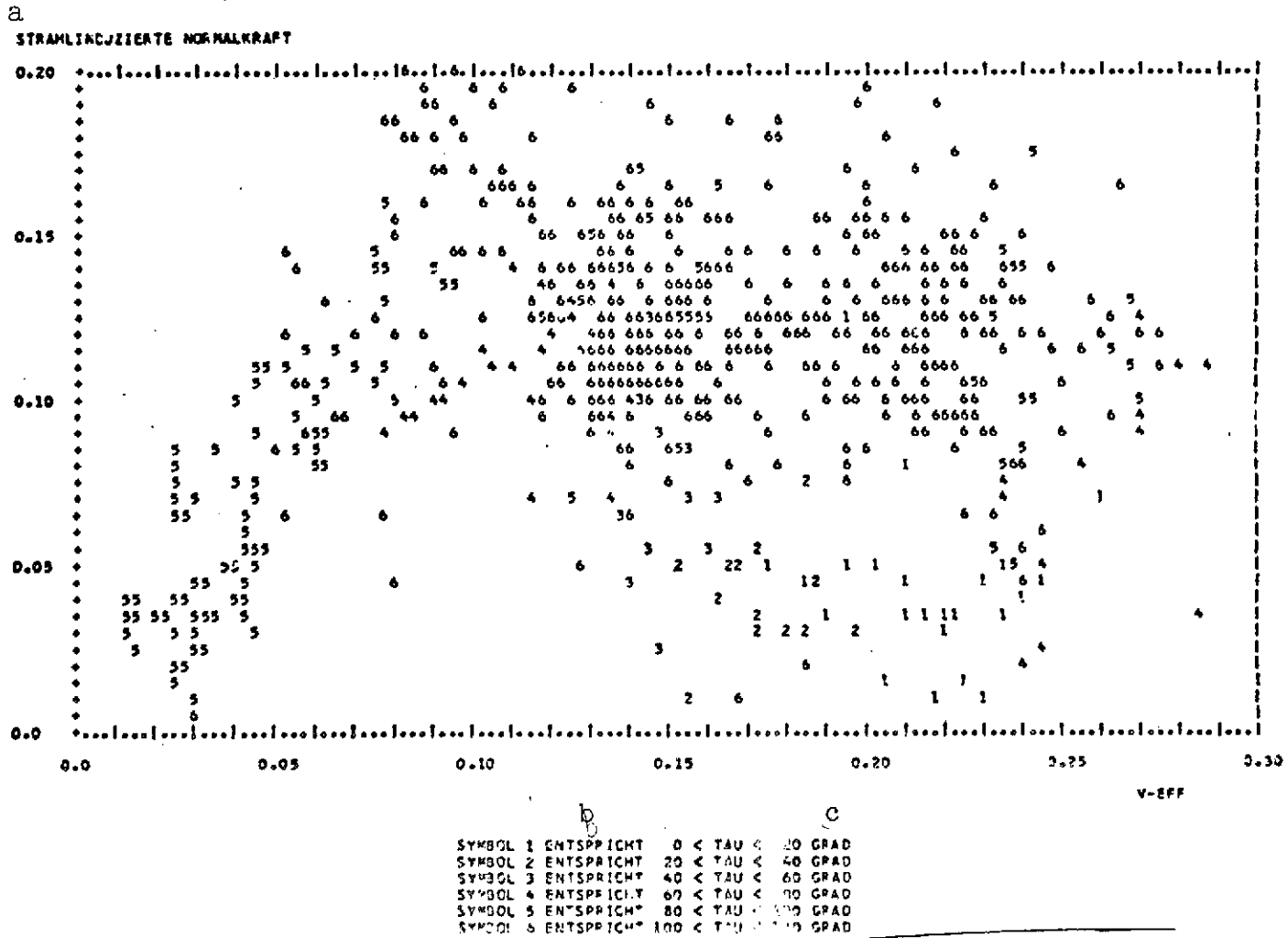


Fig. 3.4.c. Jet-induced normal force, Do 31 E3. Thrust ratio S_H/S_M of 1.400 to 2.100, without ground effect ($H/b > 0.8$).

Key: a. Jet-induced normal forces
 b. Corresponds to
 c. Degrees

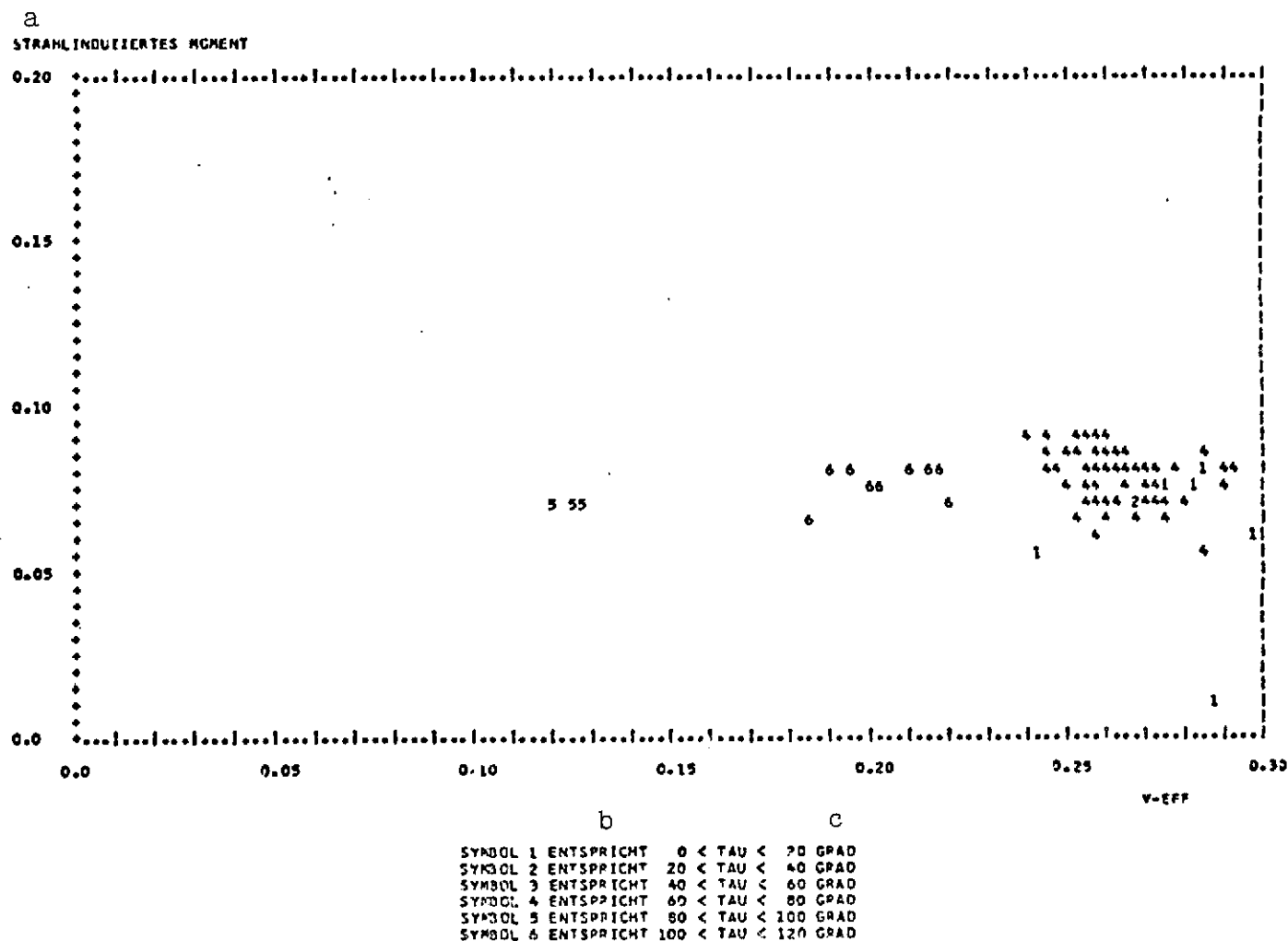


Fig. 3.5.a. Jet-induced torque, Do 31 E3. Thrust ratio S_H/S_M of 0.725 to 1.000, without ground effect ($H/b > 0.8$).

Key: a. Jet-induced torque
 b. Corresponds to
 c. Degrees

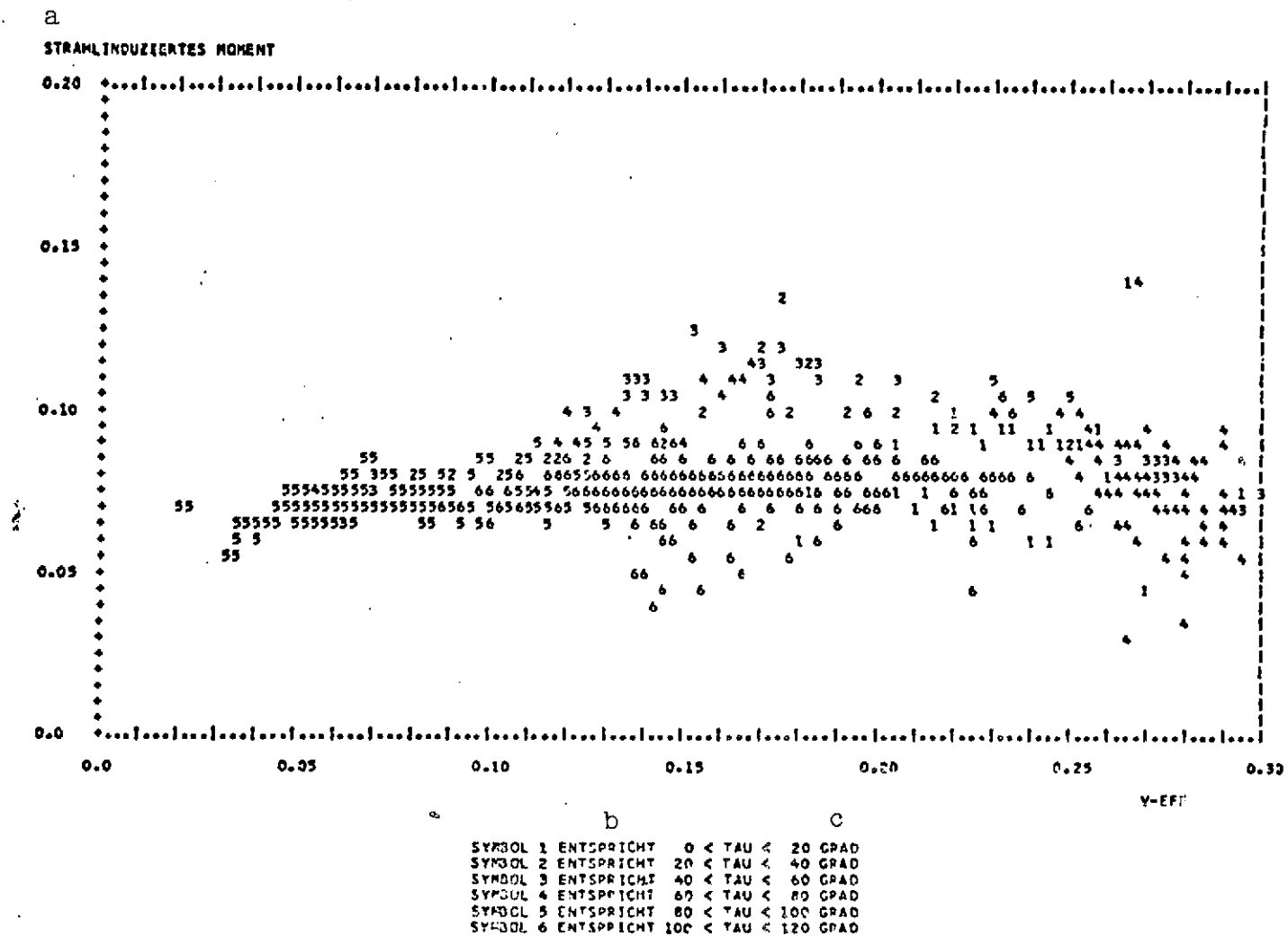


Fig. 3.5.b. Jet-induced torque, Do 31 E3. Thrust ratio S_H/S_M of 1.000 to 1.400, without ground effect ($H/b > 0.8$).

Key: a. Jet-induced torque
 b. Corresponds to
 c. Degrees

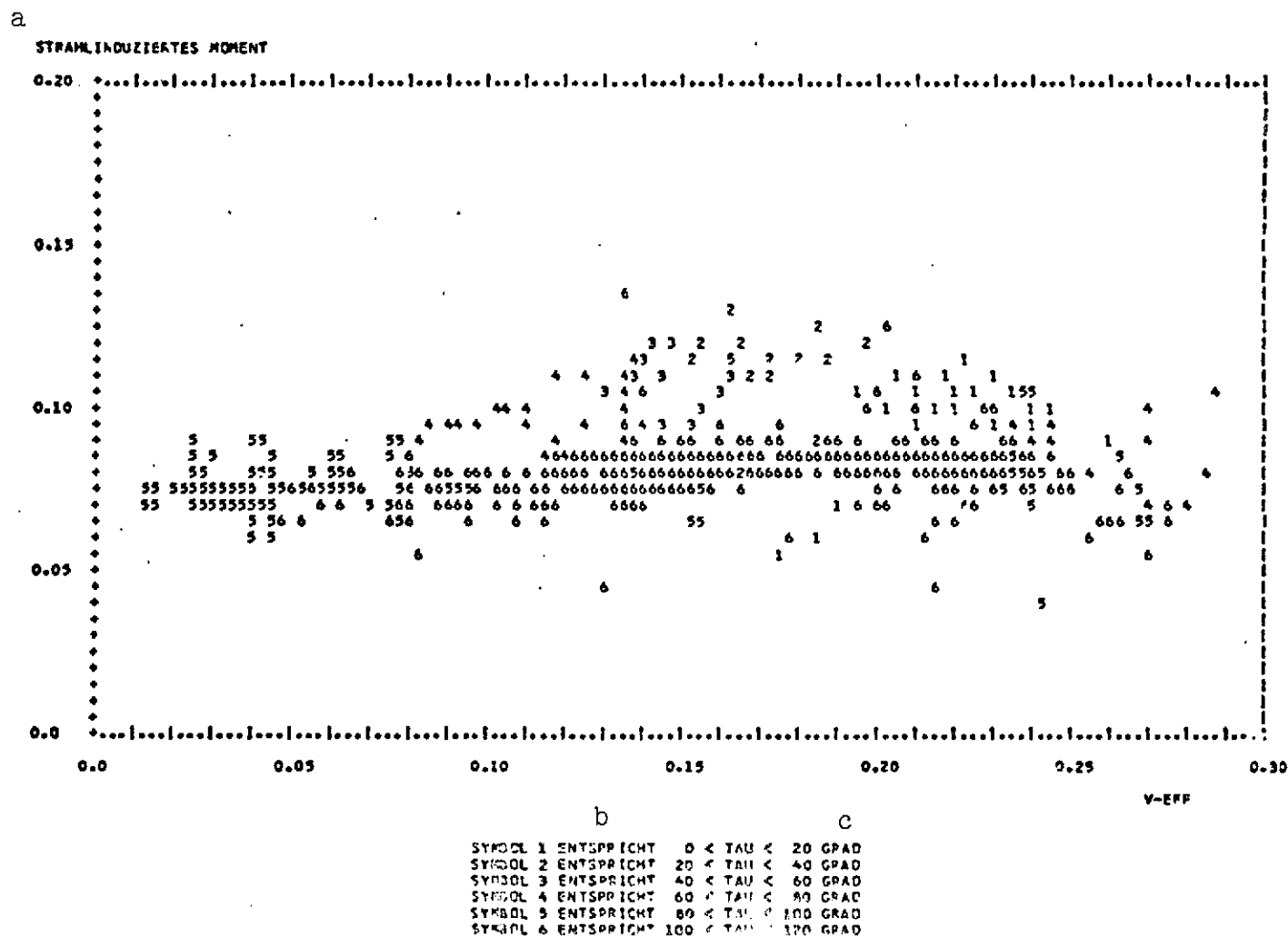


Fig. 3.5.c. Jet-induced torque, Do 31 E3. Thrust ratio S_H/S_M of 1.400 to 2.100, without ground effect ($H/b > 0.8$).

Key: a. Jet-induced torque
 b. Corresponds to
 c. Degrees

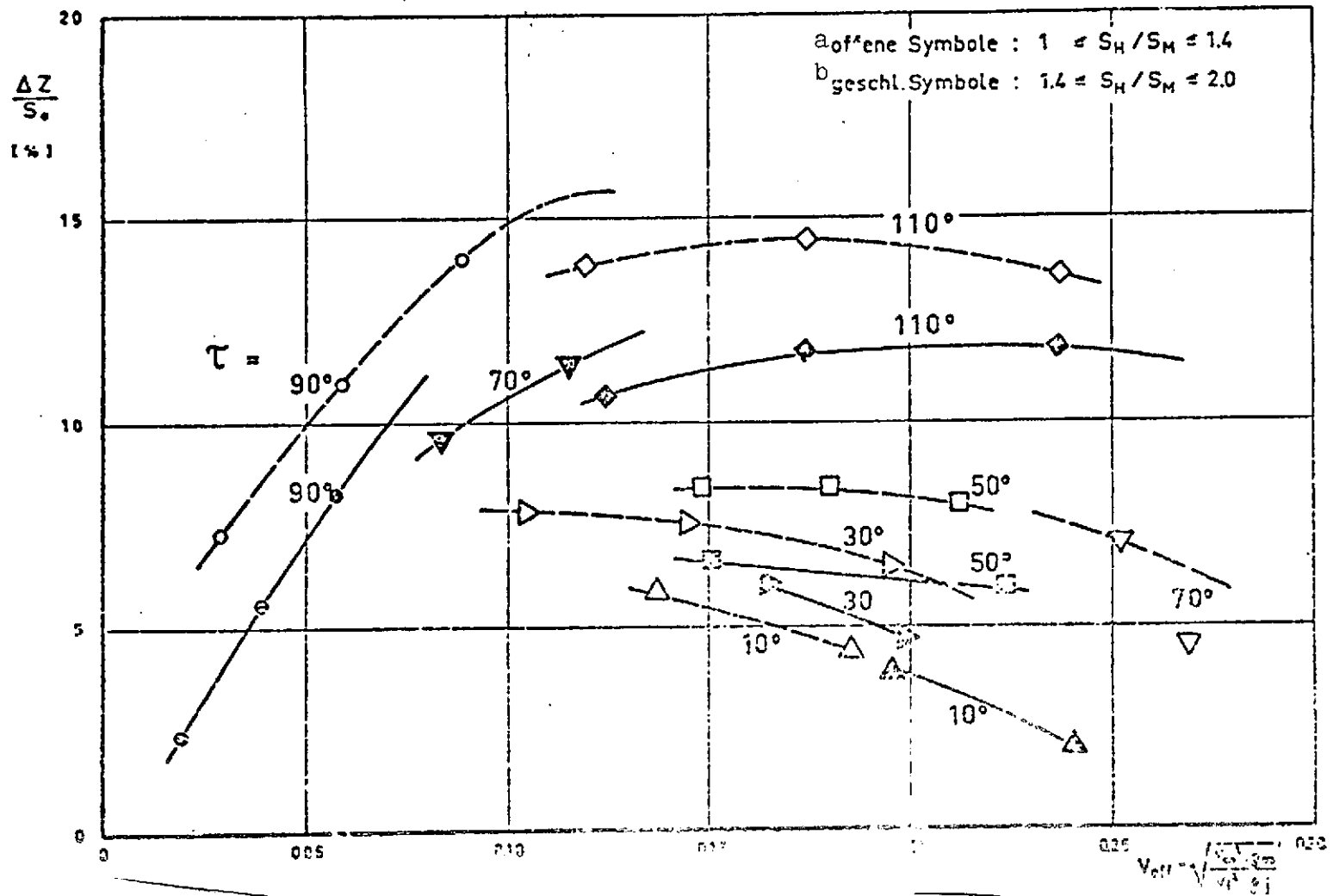


Fig. 3.6. Do 31 E3 flights, mean jet-induced normal force from Fig. 3.4.

Key: a. Open symbols
b. Solid symbols

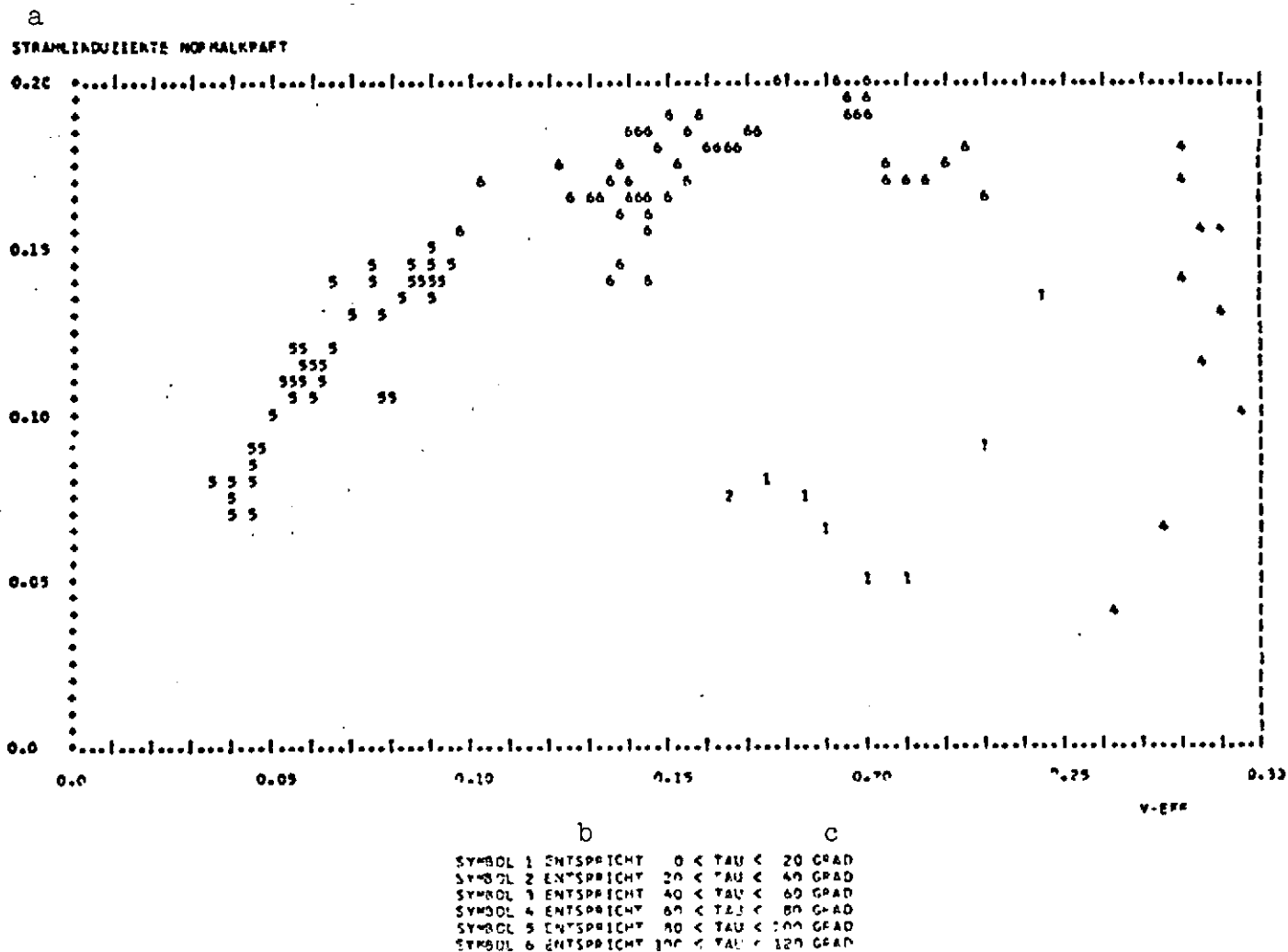


Fig. 3.7. Jet-induced normal force, Do 31 E3 trial 247 with α_0 correction. Thrust ratio S_H/S_M from 1.100 to 1.550, without ground effect ($H/b > 0.8$).

Key: a. Jet-induced normal force
 b. Corresponds to
 c. Degrees

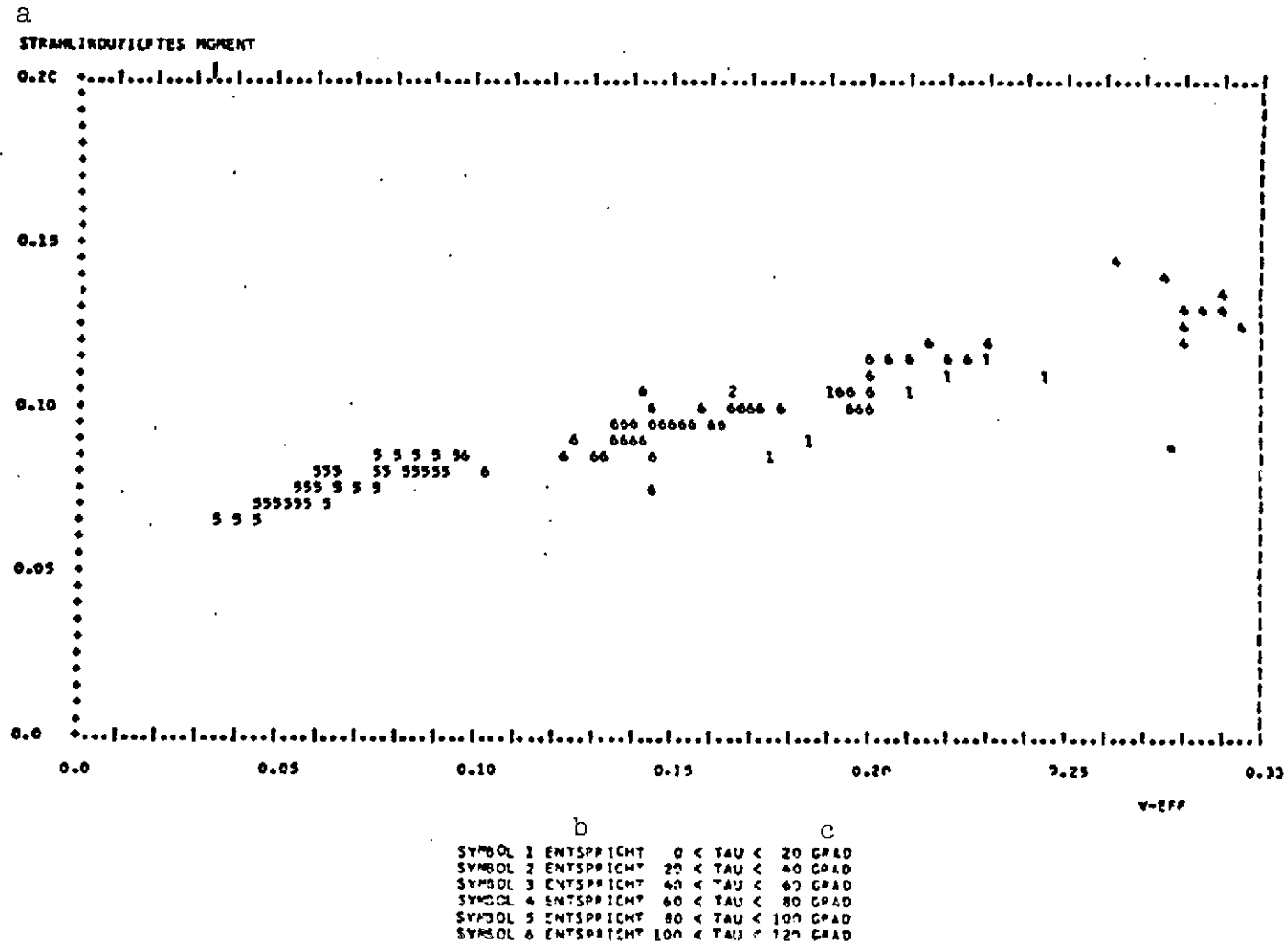


Fig. 3.8. Jet-induced torque, Do 31 E3 trial 247, with M_0 and α_0 correction. Thrust ratio S_H/S_M from 1.100 to 1.550, without ground effect ($H/b > 0.8$).

Key: a. Jet-induced torque
b. Corresponds to
c. Degrees

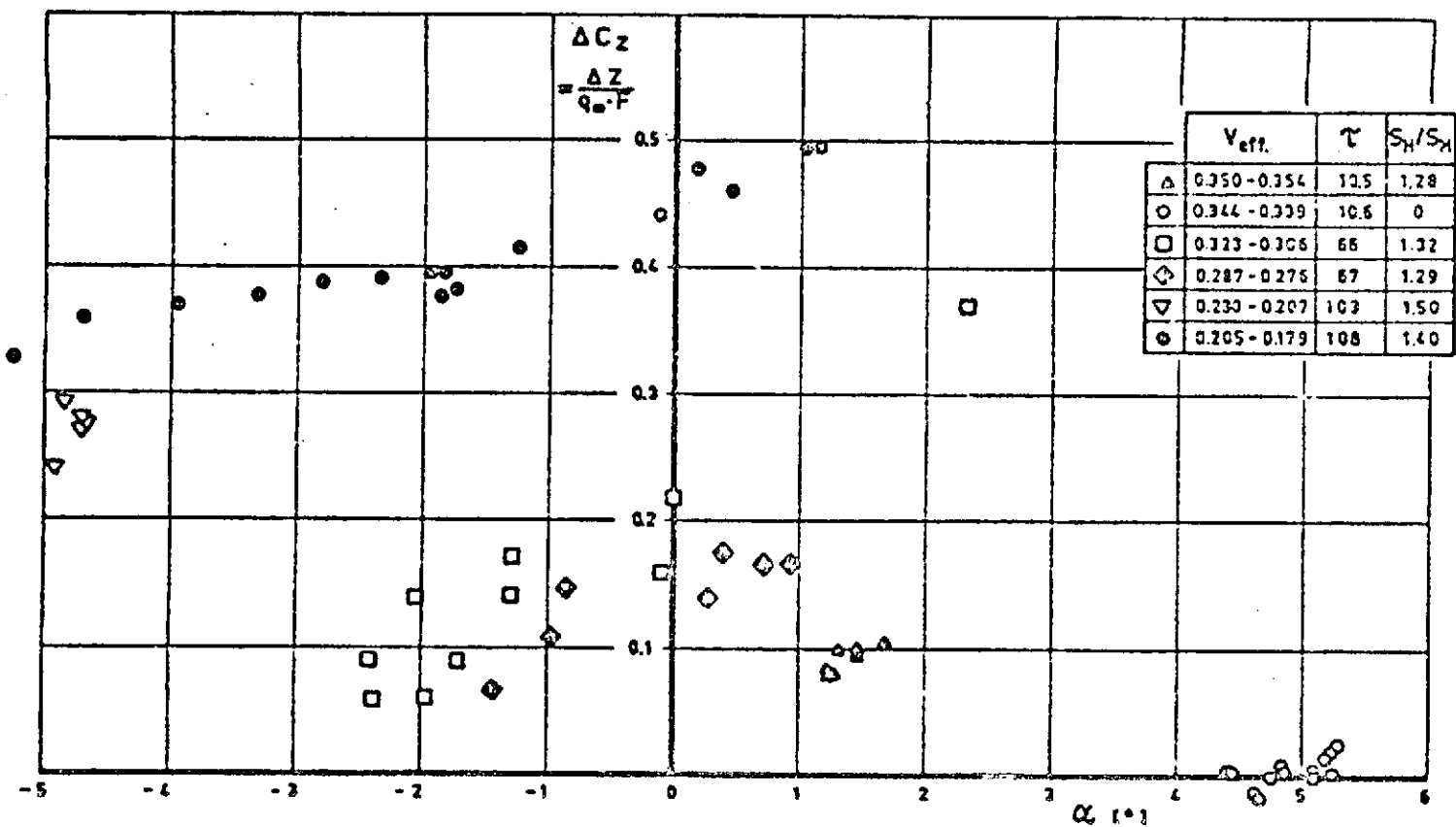
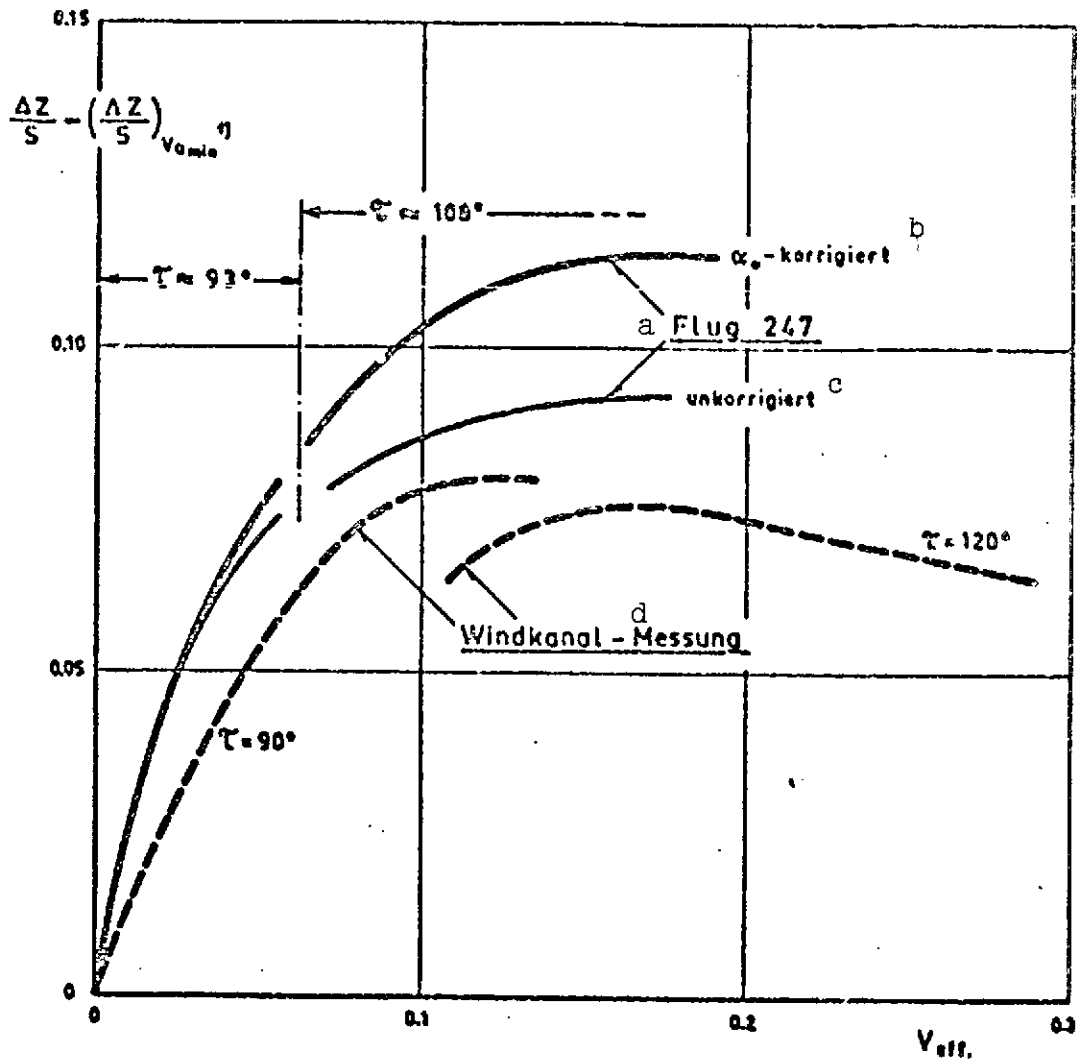


Fig. 3.9. Do 31 E3 trial 247: jet-induced normal force coefficient versus angle of attack.



1) $V_{0 min}$ = indicated velocity at $H/b = 0.8$.

Fig. 3.10. Do 31: jet-induced normal force during vertical landing. Comparison between wind tunnel and flight test.

Key: a. Flight
 b. Corrected
 c. Uncorrected
 d. Wind tunnel measurements

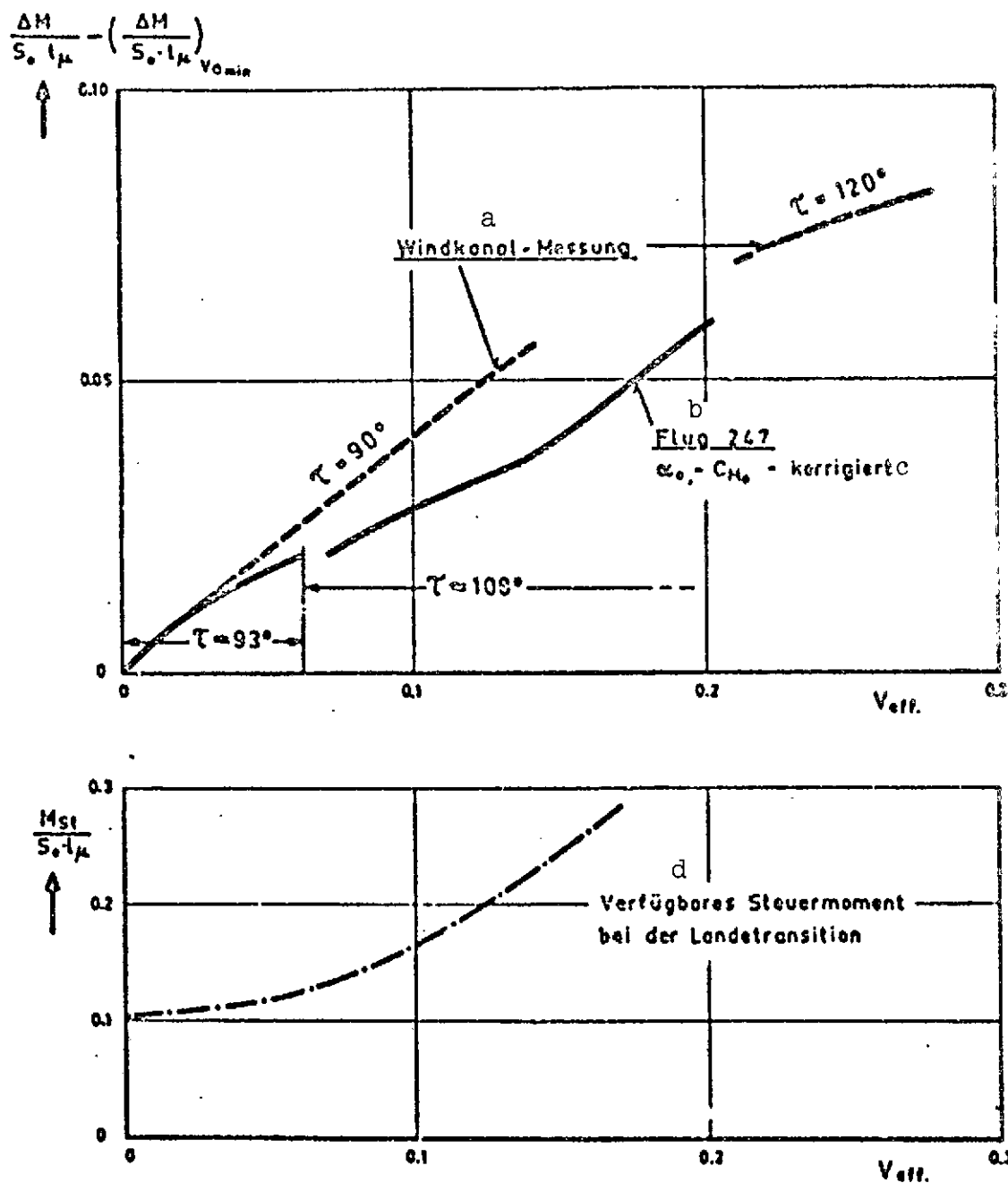


Fig. 3.11. Do 31: jet-induced pitch torque during vertical landing. Comparison between wind tunnel and flight test.

- Key:
- a. Wind tunnel measurements
 - b. Flight
 - c. Corrected
 - d. Available control torque during landing transition

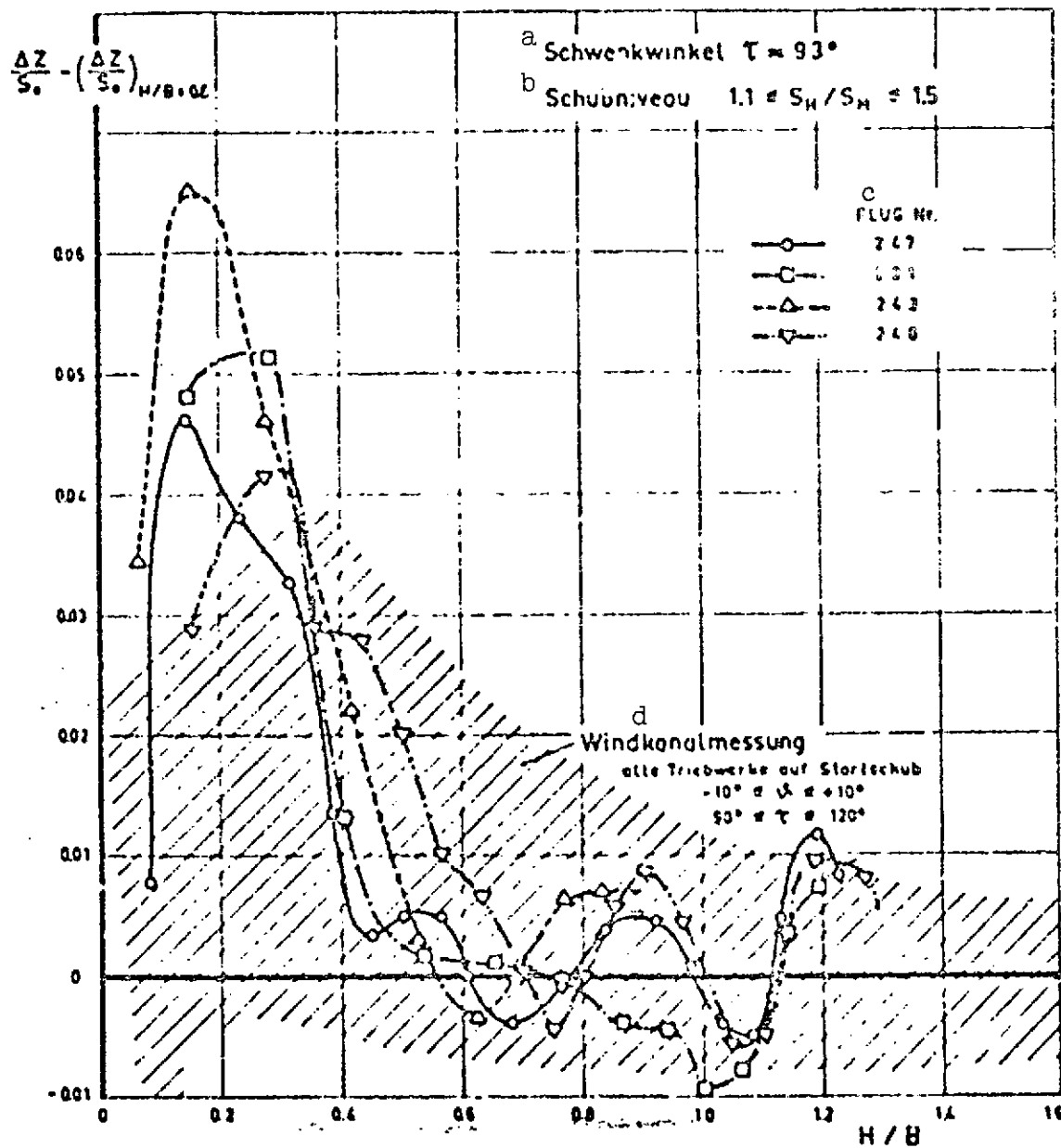


Fig. 3.12. Do 31: jet-induced normal force due to ground effect during four vertical landings.

Key: a. Angle of nozzle rotation
b. Level of thrust
c. Flight number
d. Wind tunnel measurements: all power plants on takeoff thrust

- a Schwenkwinkel $\tau \approx 93^\circ$
 b Schubniveau $1.1 \leq S_H / S_M \leq 1.5$

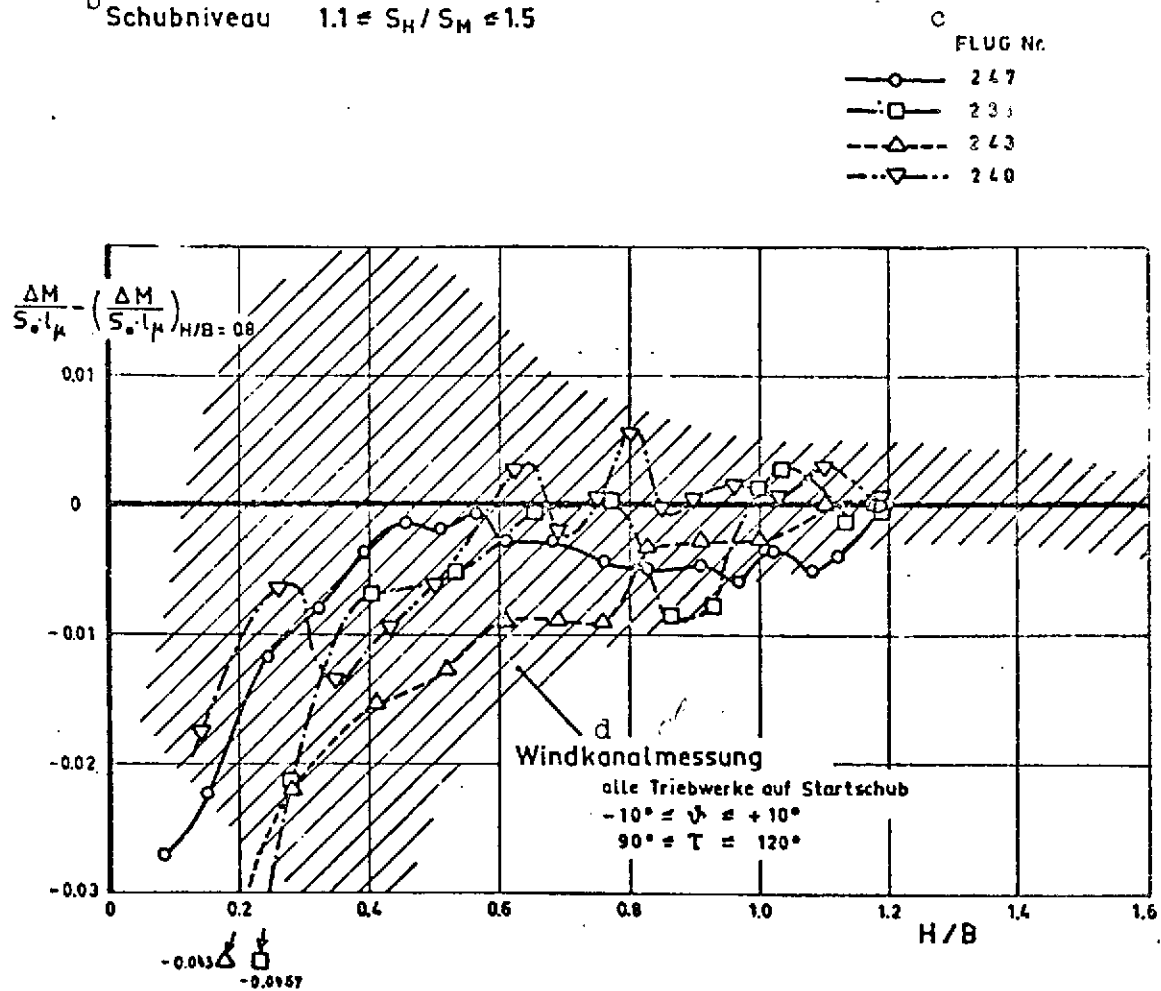


Fig. 3.13. Do 31: jet-induced pitch torque due to ground effect during four vertical landings.

- Key:
- a. Angle of nozzle rotation
 - b. Level of thrust
 - c. Flight number
 - d. Wind tunnel measurements: all power plants on takeoff thrust

Overview of Contents

- 4.1. Introduction [not included with German document]
- 4.2. Notation
- 4.3. Principles Pertaining to Models
- 4.4. Test Method
- 4.5. References

Figures

- 4.1. Jet-induced pressure distribution on the underside of a panel with a central jet. Mach number effect.
- 4.2. Effect of jet Mach number on jet-induced force in Do 131 hover close to ground.
- 4.3. Effect of jet Mach number on jet-induced pitch torque in Do 31 hover close to ground. /106
- 4.4. Do 31 interference measurements. Effect of air feed lines on the aerodynamic coefficients.
- 4.5. Interference from inlet and outlet flows on a partial wing/fuselage model.
- 4.6. Effect of nozzle position, in the longitudinal direction, upon pressure distribution on the wing.
- 4.7. Compilation of practical methods for power plant simulation in model tests.

4.1. Introduction

[Section 4.1 not included with German document.]

4.2. Notation

/108

ΔA	Change in lift due to jet interference
b	Wing span
C_A, C_M, C_W	Aerodynamic coefficients of lift, torque and drag, respectively
C_p	Pressure coefficient
D_j	Diameter of thrust nozzle
H	Ground distance
l_μ	Mean aerodynamic chord depth
ΔM	Change in pitch torque due to jet interference
Ma	Mach number of thrust jet
P_o	Total pressure in thrust jet
p_∞	Ambient pressure
S_o, S_{MTW}	Gross thrust
v_∞	Aircraft speed
v_E	Power plant inlet velocity
v_j	Power plant jet velocity
ΔZ	Change in lift thrust due to jet interference
α	Angle of attack
ρ	Density

4.3. Principles Pertaining to Models

/109

4.3.1. Inlet Flow

The simulation of inlet flow with a model must be done in such a manner that the flow conditions associated with the full-scale version are set up, both in the power plant inlet and in the region surrounding it. Certain conditions with regard to pressure drop, dynamic pressure recovery and uniformity of flow must be satisfied at the inlet for efficient and disturbance-free operation of the power plants. Maintaining the same ratio V_∞/V_E between free stream velocity and inlet velocity can be considered the most important principle pertaining to models. Since separation phenomena at the lip of the inlet or at the hub are a function of Re number, approximately similar conditions to those associated

with the full-scale version must be created by artificial transitional means if the ratio is not maintained with the model. Mach number effects are not so important, in contrast, since the usual mean inlet velocities do not exceed 150 m/s.

The external flow field of the inlet flow is governed by the sink effect, which, if compressibility effects are neglected, is determined only by maintenance of the kinematic flow condition in the form of velocity ratio V_∞/V_E .

4.3.2. Power Plant Jet

The model principles which apply to jet simulation are governed by the principles of free jet propagation in quiescent or moving air surrounding the jet. The most important similarity parameter is the ratio of the momentum densities of the oncoming flow and the jet ($\rho_\infty v_\infty^2 / \rho_j v_j^2$). From this is derived the so-called effective velocity ratio

$$\frac{v_\infty}{v_j} e = \sqrt{\frac{\rho_\infty v_\infty^2}{\rho_j v_j^2}} \quad \underline{/110}$$

which has generally been adopted as a useful characteristic quantity in jet interference processes. Temperature effects can thereby be neglected for all cases encountered in practice. Mach number plays a certain role in free jet propagation; the drop in dynamic pressure along the axis of the jet takes place more slowly at high Mach number than at low Mach number.

Measurements in [4], Fig. 4.1, show the corresponding effect upon the jet-induced pressure distribution on a panel with a central jet. Measurements with the 1:20 model of the Do 131 in hover close to the ground likewise show that jet-induced force decreases slightly with increasing Mach number, Fig. 4.2. The Mach number effect will probably become insignificant for future V/STOL aircraft with fan power plants of relatively low jet Mach number.

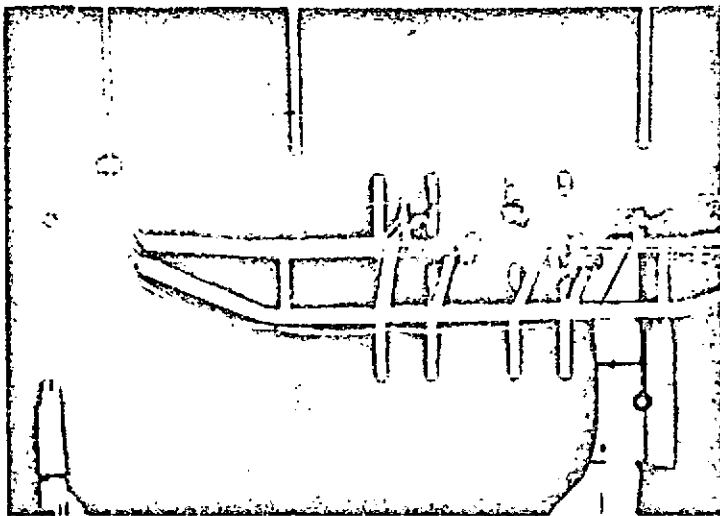
The effect of the Re number of both the free stream and the jet can be neglected. However, initial conditions in the nozzle outlet have a considerable effect on free jet propagation. They include the distribution of static pressure and total pressure, as well as the degree of turbulence. The latter was not taken into consideration in those jet interference studies known to us. Its importance will increase, however, as more is done in the future in the way of measures aimed at the rapid decay of the jet due to noise and erosion considerations. For fan power plants, too,

it is necessary to attend to this point, since attention must be devoted to blockage by the relatively large hub and to a residual spin in the jet.

4.4. Test Method

/111

The decisive point for a reliable V/STOL test method is power plant simulation. The first generation of V/STOL aircraft, including the Do 31, for example, was equipped with single-stage power plants which were installed in engine pods on the wings.



Due to the location at which they were installed, and because the inlet momentum of these lift power plants amounted to only about 20-25% of jet momentum, the interference forces associated with inlet flow are negligibly small, and only the pure momentum components in drag and in pitch torque need be considered. Thus the simplest method of power plant simulation could be applied to jet interference measurements in the wind tunnel, namely the discharging of compressed air. An addition-

al advantage of this setup was that the entire discharge system was suspended separately from the model and wind tunnel balance, on a system which follows the angle of attack. Power plant thrust and aerodynamic forces on the aircraft were thus measured separately, allowing very precise measurements of the interference forces. The design of the wind tunnel model and the test setup have already been shown in Section 1, Figs. 1.5 and 1.6, with the Do 31 serving as an example. A color photograph of the 1:20 jet interference model of the Do 31 in the Dornier wind tunnel is shown above.

The colors show the following:

/112

Red: 1:20 model, suspended on the wind tunnel balance.

Blue: Air-line and follower system, mounted on the turntable independently of the model

Yellow: Support column for the point of rotation of the compressed air follower system.

The effect of the air feed lines on the aerodynamic coefficients was determined from two comparative measurements with and without pipeline. The effect on drag is considerable, that on lift is negligible, and zero torque must be corrected by $\Delta c_M = +0.02$; see Fig. 4.4. As was shown in Sections 1 and 3, the Do 31 interference measurements yielded good results.

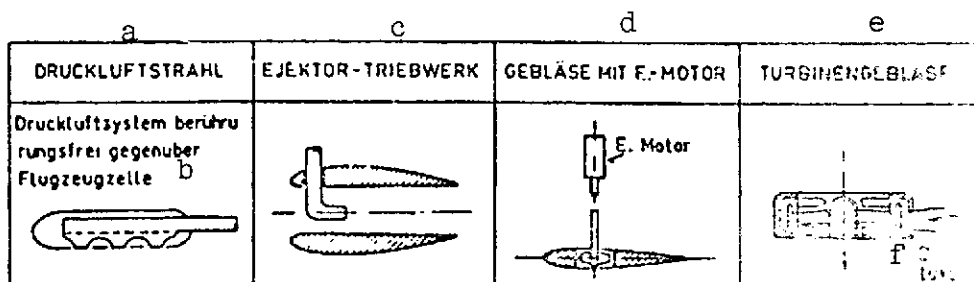
For future V/STOL aircraft with fan power plants or two-stage power plants of high bypass ratio, inlet momentum is almost as high as outlet momentum. The contribution of inlet flow to interference is thus on the same order of magnitude as that of the jet. Fig. 4.5, taken from [6], is an extreme example of this. The force in the lift direction induced by inlet flow far exceeds the lift induced by the jet. Inlet flow induces a considerable tail-heavy torque.

Although the larger component of the force induced by the jet is operant on the underside of the wing, the effect on the pressure distribution at the upper surface of the wing is not inconsiderable, as Fig. 4.6 from [5] shows. Now if the power plant inlet is located close to or on the upper surface of the wing, an interaction of jet and inlet flows occurs.

The necessity of simultaneously simulating inlet and outlet flows in future V/STOL model tests can be seen just from these two examples.

/113

The figure shown below provides an overview of the power plant simulation methods which are available, and Fig. 4.7 gives a compilation of practical methods for power plant simulation in model tests.



Possible methods for power plant simulation in model tests.

- Key:
- a. Jet of compressed air
 - b. Compressed air system makes not contact with airframe
 - c. Ejector power plant
 - d. Blower with electric motor
 - e. Turbine blower
 - f. Compressed air

The discharge of a compressed air jet at the location of the power plant nozzle is the simplest type of power plant simulation. Inlet flow is not simulated. As already mentioned, this method was applied successfully to the Do 31. The list in Fig. 4.7 also shows that a relatively large number of jet interference studies were performed in England and at NASA with this technique. However, these always involved VTOL configurations with jet power plants of high momentum density or measurements in hover with the ground effect, in which cases inlet flow is unimportant.

In the case of the ejector power plant, the high-energy primary jet sucks air from the inlet by turbulent jet mixing, and a multiple of the quantity of air which was blown in is discharged at the outlet. A relatively long mixing length is necessary for this, however (at least five mixing duct diameters). Structural length can be considerably reduced through the use of multiple nozzles for the primary jet, so that approximately the size ratios /114 associated with bypass power plants can be realized, as can be seen from the list in Fig. 4.7. This method has recently been successfully applied by Dornier for recirculation measurements, to simulate lift fans whose height is smaller than their diameter. No empirical information is available for jet interference measurements.

Blowers driven by electric motors to simulate lift fans have been used by the RAE and AVA (see Fig. 4.7) in several jet interference studies on VTOL components. Depending upon space conditions, the electric motor was connected with the blower via a short shaft, an angular drive system or an extension shaft. Guide vanes eliminate rotation, so outlet flow is quite similar to the large-scale version. Inlet measurements are also possible at the same time, and the measurement of power and torque provide information concerning the fan characteristics in transition flight. In the case of blowers driven by extension shafts, vibration problems must be expected. The effect of extension shaft blockage upon flow about the model is highly dependent upon the aircraft's configuration. This point is not considered to be critical. The AVA Göttingen provides a tested series of high-speed three-phase motors, with blower rotors.

The blowers with blade-tip drive used to simulate lift fans are in some cases still under development (AVA), or they are already available as complete units. Although no prices are available, it is estimated that the price is to be a multiple of that for the blower with electric motor, to say nothing of maintenance expense and maintenance requirements.

In summary, the following recommendations can be made concerning the test method to be selected for future V/STOL aircraft with lift jets:

1. The interference effect of power plant jets (jet power plants with or without bypass and fan) in hover, with and without ground effect, can be measured with sufficient accuracy in model tests using the simple method of compressed air discharge. /115

2. Interference between cell and power plant in transition flight can be determined reliably only through the simultaneous simulation of inlet and outlet flows in the case of V/STOL configurations with lift fans. At present, wind tunnel models with blowers driven by electric motors are best suited for this purpose.

4.5. REFERENCES

1. Trebble, W.J.G., "The aerodynamics of V/STOL aircraft. /116
Part G: Techniques for the aerodynamic testing of V/STOL models," Von Karman Institute for Fluid Dynamics, Lecture Series 9, May 13-17, 1968.
2. Melzer, E. and Wulf, R., "Possibilities for jet simulation in the 3 m wind tunnel of the DFVLR-AVA Göttingen," DGLR Paper No. 70-047.
3. Thiel, E., "V/STOL jet interference: study of suitable measurement methods for future V/STOL transport aircraft development," Dornier Test Report VW 630-B1, 1969.
4. Genty, C. L. and Margason, R. J., "Jet-induced lift losses on VTOL configurations hovering in and out of ground effect," NASA TN D-3166, 1966.
5. Carter, A. W., "Effects of jet-exhaust location on the longitudinal aerodynamic characteristics of a jet V/STOL model," NASA TN D-5333, 1969.
6. Williams, J., "The aerodynamics of V/STOL aircraft. Part E: Turbojet/turbofan aircraft," Von Karman Institute for Fluid Dynamics, Lecture Series 9, May 13-17, 1968.

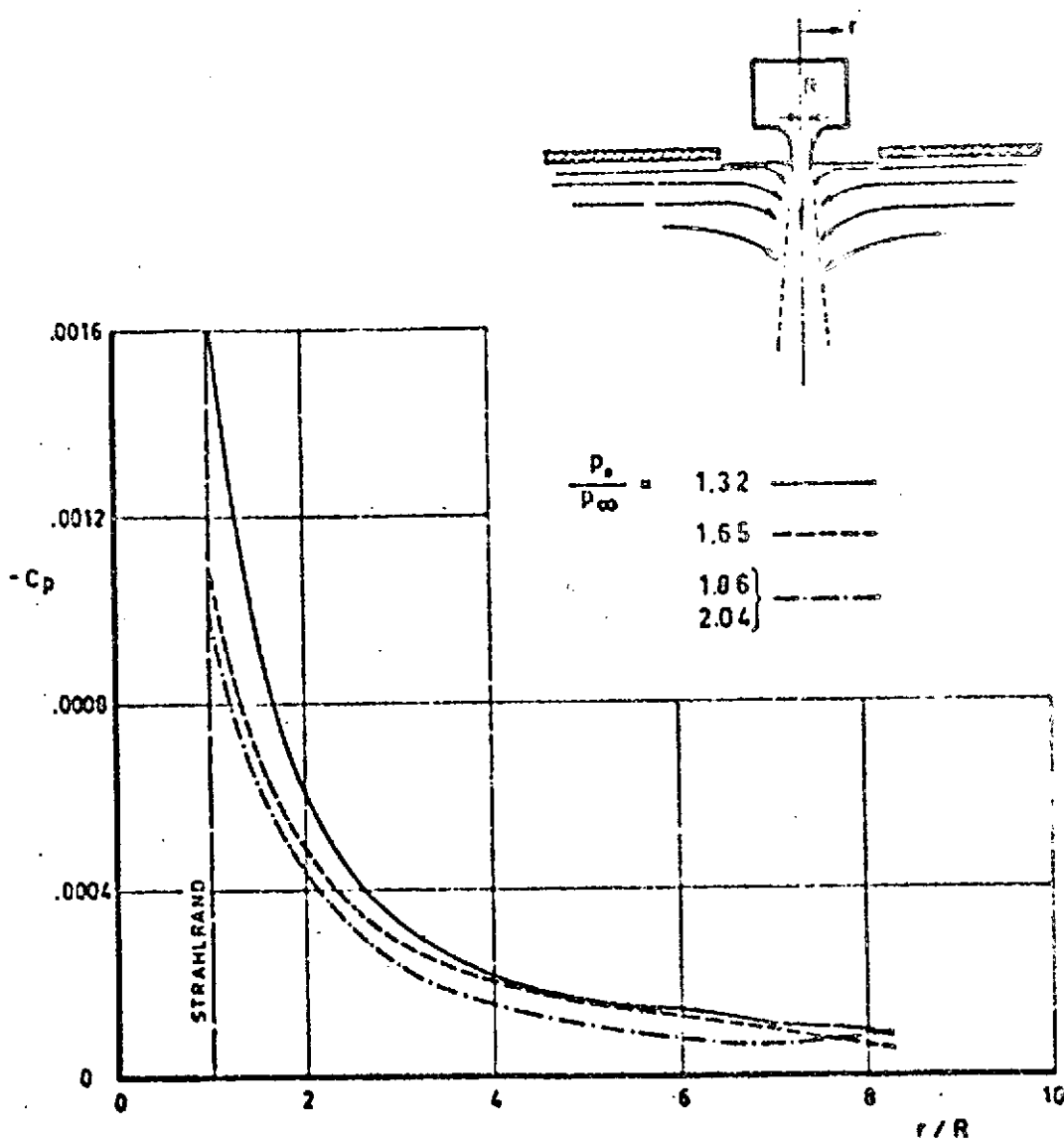


Fig. 4.1. Jet-induced pressure distribution on the underside of a panel with a central jet. Mach number effect.

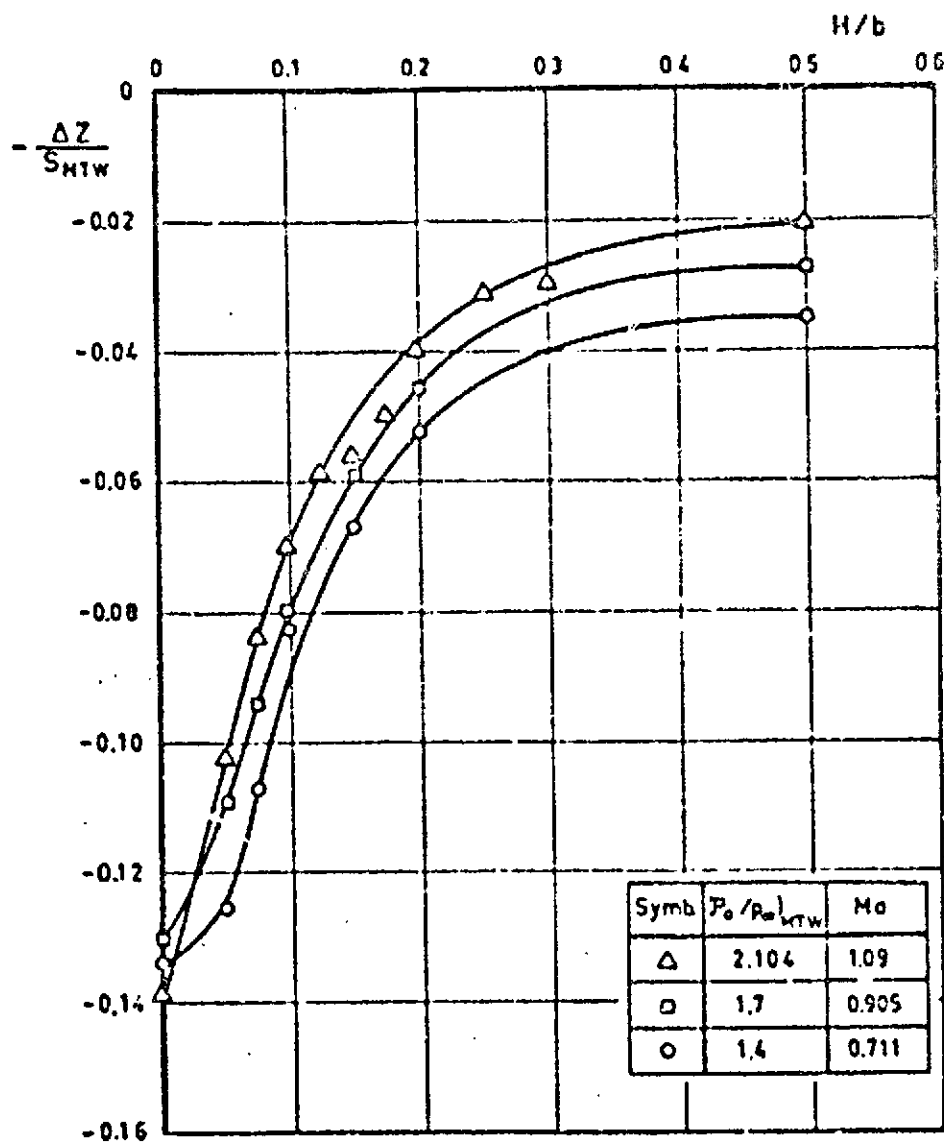


Fig. 4.2. Effect of jet Mach number on jet-induced force in Do 131 hover close to ground.

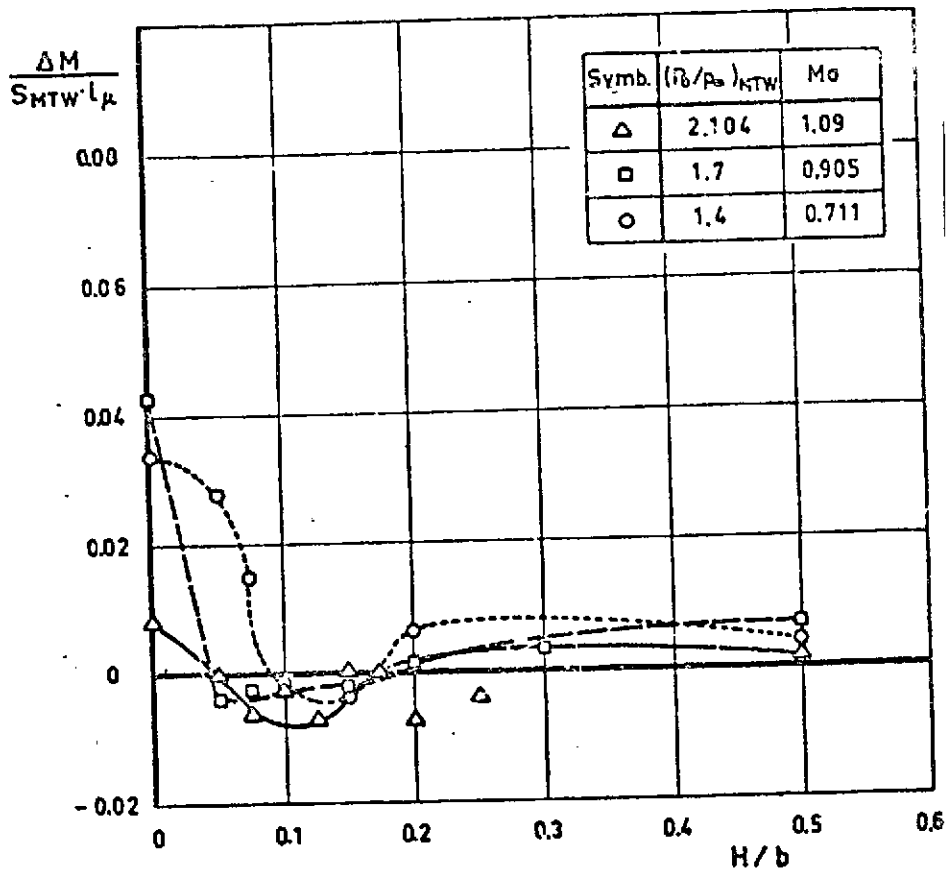


Fig. 4.3. Effect of jet Mach number on jet-induced pitch torque in Do 131 hover close to ground.

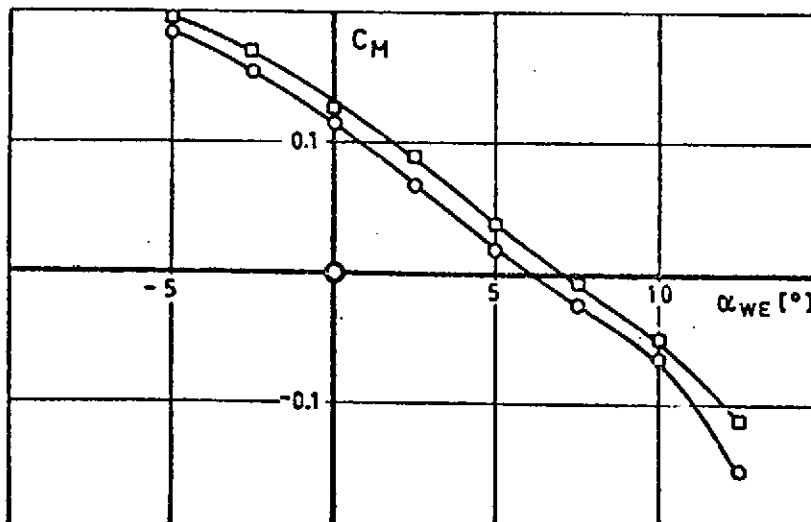
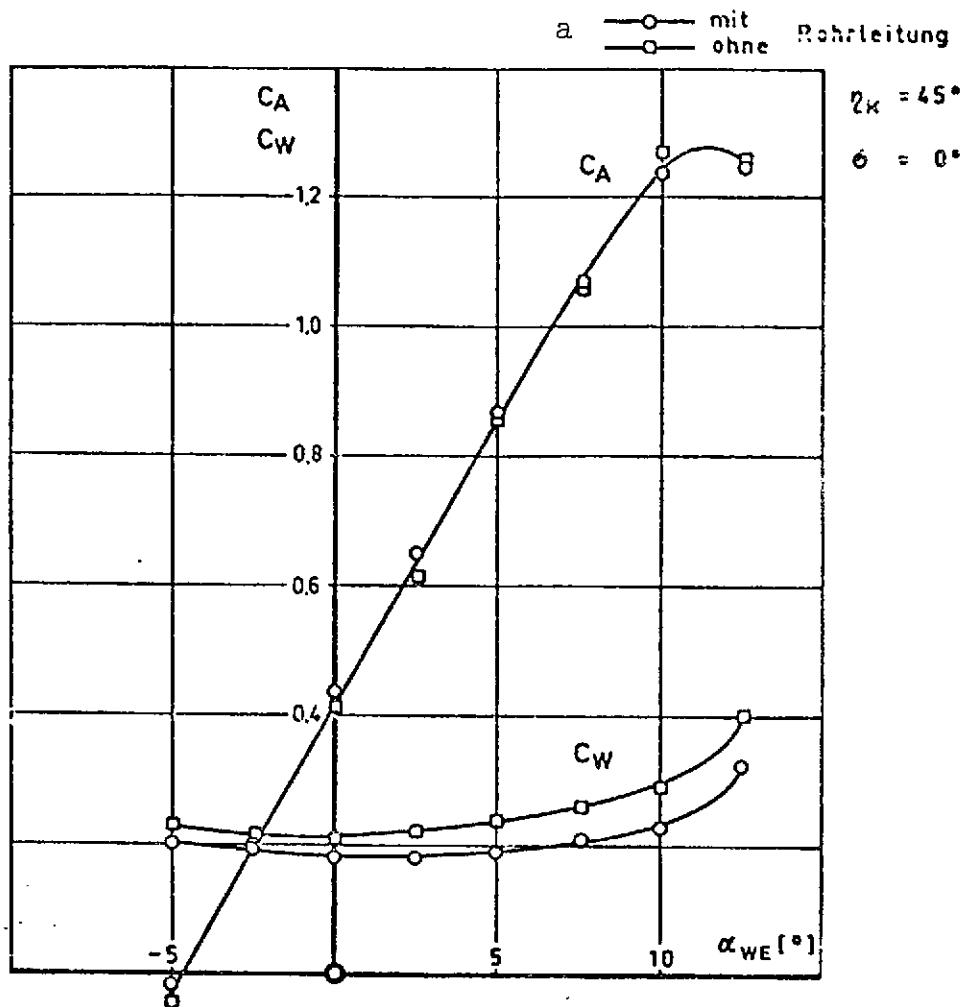


Fig. 4.4. Do 31 interference measurements.
 Effect of air feed lines on the aerodynamic
 coefficients.

Key: a. With, without pipeline
 WE = horizontal plane
 η_K = flap angle

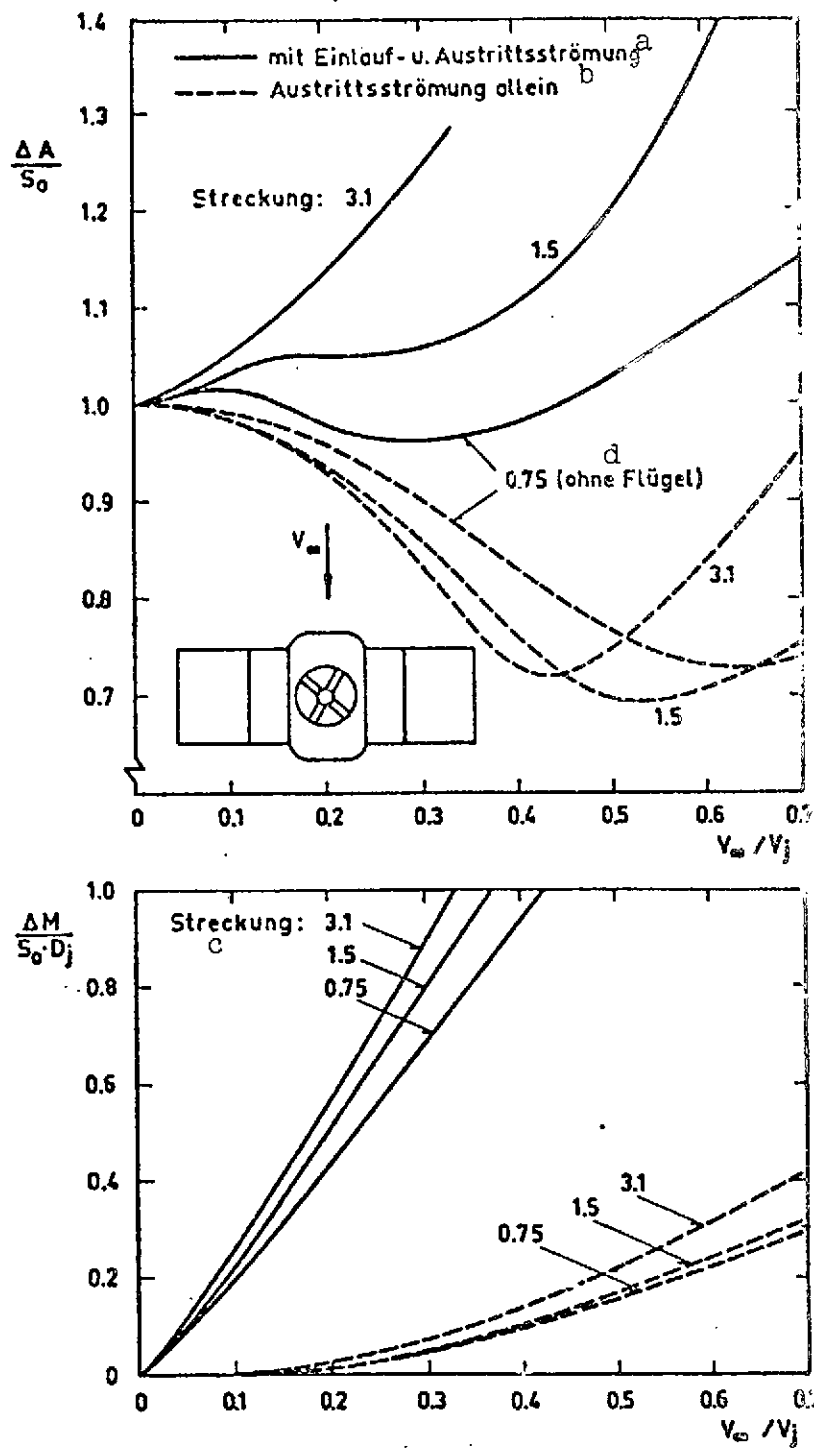


Fig. 4.5. Interference from inlet and outlet flows on a partial wing/fuselage model.

- Key:
- a. With inlet and outlet flow
 - b. Outlet flow only
 - c. Aspect ratio
 - d. Without wings

a Klappenausschlag 40°
 Strahlaustrittswinkel 90°
 Düsenhochlage $z/l = -0.64$

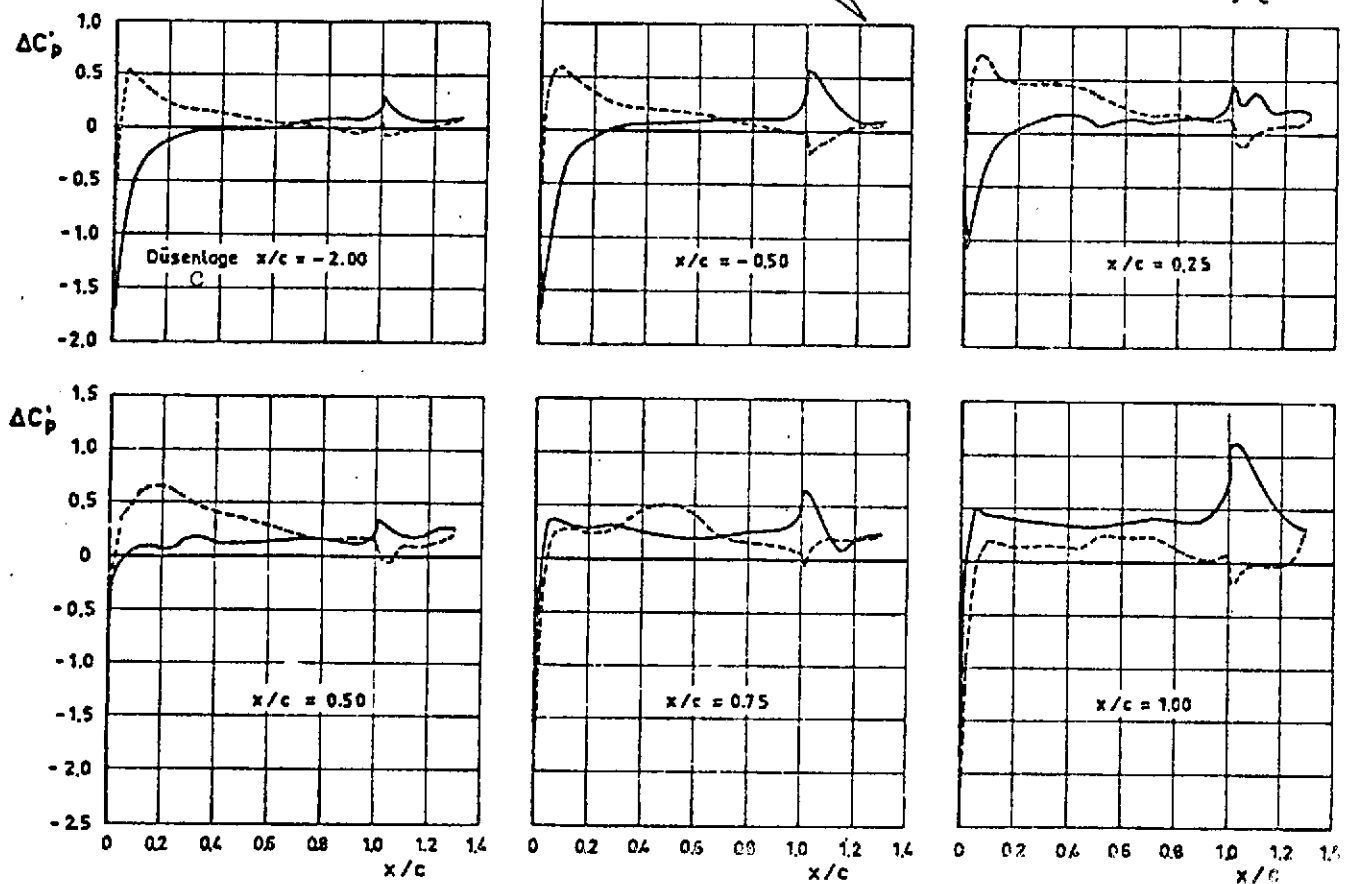


Fig. 4.6. Effect of nozzle position, in the longitudinal direction, upon pressure distribution on the wing.

Key: a. Flap angle, jet exhaust angle, nozzle position (height)
 b. Upper surface, lower surface
 c. Nozzle position

Fig. 4.7. Compilation of practical methods for power plant simulation in model tests.

/123

Firm/Institute	Project	Literature reference
<u>1. Compressed air jet</u>		
Dornier	Do 31 V/STOL transport aircraft with jet lift and lift/thrust power plants	VW 537
Hawker Siddeley Av.	P1127 VTOL combat aircraft with jet lift/thrust power plants	ZfW 15/7
NASA	VTOL configuration model with jet lift power plants	NASA TN D-3166 NASA CR-1297 NASA TN D-2380 NASA TN D-3213 NASA TN D-1400
RAE	VTOL component model with jet lift power plants	RAE TN AERO 2971 ARC CP 718
DFVLR	V/STOL transport aircraft, principal model with jet lift/thrust power plants	DFVLR Report 70-28

2. Injector power plant

/124

NASA	VTOL configuration model with jet lift and lift/thrust power plants	NASA TN D-4812 NASA TN D-5727 NASA TM X-1758
AVA	Airbus with bypass power plants	DLR Report 70-28
MBB	VTOL combat aircraft with lift and lift/thrust bypass power plants	DLR Report 70-28

3. Blower with electric motor

Dornier	Do 31 V/STOL transport aircraft	VW 313
AVA	VTOL half-model with lift fans	DLR Report 70-28

Fig. 4.7. (continued)

Firm/Institute	Project	Literature reference
----------------------	---------------	-------------------------------

3. Blower with electric motor

RAE	Wing with lift fans	RAE TR 67302 RAE TN AERO 2643
RAE	VTOL component model with lift fans	ARC CP 597

4. Blower with blade-tip drive

/125

NASA	V/STOL transport aircraft model with six lift fans in wing	NASA TN D-5695
AVA	Project for a turbine blower	DLR Report 70-28
Dowty-Rotol	Blower with blade-tip drive	[1]
Tech. Development Inc., Ohio	Blower with blade-tip drive	Manufacturer's prospectus
Douglas Aircraft Co.	DC 10	<u>J. Aircraft</u> 8(7)

5. Basic Material for Estimating Jet Interference in Hover and in Transition for Future V/STOL Aircraft

/126

Overview of Contents

- 5.1. Introduction
- 5.2. Notation
- 5.3. Jet Interference in Hover Outside Ground Effect
- 5.4. Jet Interference in Hover Close to the Ground
- 5.5. Jet Interference in Transition for V/STOL Transport Aircraft with Jet Power Plants
- 5.6. References

Figures

- 5.1. Alternative models for treatment of change in lift in Do 31 hover with cruising power plants only.
- 5.2. Decrease in dynamic pressure along axis of jet. Measurements taken from [2].
- 5.3. Change in thrust close to ground as a function of ratio of rectangular panel area to nozzle area. /127
- 5.4. Change in lift close to ground, based on suction effect measurements.
- 5.5. Jet interference measurements on a medium-range V/STOL airliner in hover close to ground, taken from [10].
- 5.6. Change in thrust close to ground, fountain effect predominating. Model measurements.
- 5.7. Dropoff in max. velocity of upward flow between a pair of nozzles, from measurements taken from [7].
- 5.8. Change in lift close to ground. Do 31 and Do 131 model measurements. Suction and fountain effects superimposed.
- 5.9. Do 31: change in thrust in hover as a function of ground distance. All power plants on takeoff thrust.
- 5.10. Stagnation points and stagnation lines in ground flow field during Do 31 vertical takeoff.
- 5.11. BAC models and Do 31 models with lift and lift/thrust power plants in transition.

- 5.12. Jet interference for a rectangular wing, from measurements taken from [1] and [2].
- 5.13. Jet interference for a rectangular wing, from measurements in [1].
- 5.14. Do 31 jet interference with cruising + thrust power plants. Comparison between measured and calculated values.

5.1. Introduction

/128

So far, it is not yet possible to determine the jet-induced forces and torques of an aircraft configuration in closed form by theoretical means, due to the complex flow processes.

Usable computational methods are available only for the simplest cases such as a panel with a central jet in hover in and out of ground effect, as well as formulations for solving the problem in oncoming flow. In addition, a large number of measurements, primarily wind tunnel measurements, exist for a great variety of aircraft configurations and also for simplified basic models. To be sure, the available measurement results are far from adequate for setting up empirical relations by means of which jet interference in hover and in flight, in and out of ground effect, can be determined for any aircraft configuration.

Estimating jet interference for a new aircraft project amounts to extrapolation on the basis of more or less well-known influencing factors, starting with a similar aircraft for which measurements have been taken.

With a view toward future V/STOL transport aircraft, an attempt is made in the following to indicate the most important influencing factors on the basis of experience gained during Do 31 development and through the evaluation of outside work, and to give the project engineer points of reference for estimating the jet interference effect.

Unfortunately, studies could not be performed systematically enough during Do 31 development that all influencing factors are known quantitatively. Suitable wind tunnel measurements cannot be dispensed with in a new project.

5.2. Notation

/129

A	Aerodynamic effect
B, b	Wing span
C_p	Pressure coefficient
D_j	Diameter of thrust nozzle
D_e, D_{ie}	Equivalent nozzle diameter
F	Area of aircraft planform
F_j	Area of thrust nozzle
H, h	Ground distance
h_{FW}	Distance between landing gear and ground

P_0	Total pressure in thrust nozzle
p_∞	Ambient pressure
q	Dynamic pressure in thrust jet
S_0	Nozzle thrust
v_∞	Aircraft speed
v_j	Initial velocity of jet
X	Coordinate in direction of power plant axis
ρ_j	Jet density

5.3. Jet Interference in Hover Outside Ground Effect

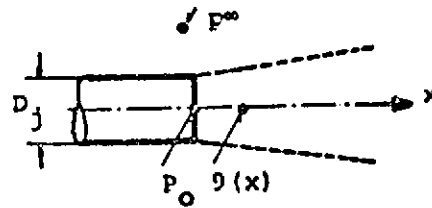
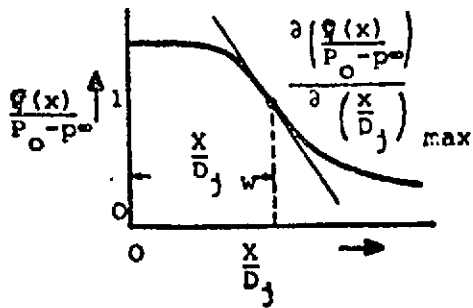
/130

A power plant jet exhausting from the underside of an airframe causes a loss in lift. The lift loss is caused by the underpressure on the underside of the aircraft, which in turn is produced by mixing of the turbulent power plant jet with the surrounding air. Close to the ground, the jet interference effect can change both in magnitude and in sign, depending upon ground distance and aircraft configuration. The ground effect is treated below in Section 5.4.

There have so far been a few dozen studies on the jet interference effect on certain aircraft configurations. Systematic studies to determine the parameters are known only from [1] and [2], however; these, too, possess no general validity, since only fighter configurations are covered. In purely empirical terms, a relationship is found between lift loss, on the one hand, and, on the other, the ratio of the aircraft surface area F surrounding the jet(s) to jet area F_j , the drop in dynamic pressure along the axis of the jet, and the static pressure of the jet:

$$\frac{-\Delta S}{S_0} = K \sqrt{\frac{F}{F_j}} \sqrt{\frac{\frac{\partial q(x)}{\partial \left(\frac{X}{D_j}\right)} \cdot \frac{1}{\left(\frac{X}{D_j}\right)_w}}{\frac{P_0 - P_\infty}{P_0}}}} \cdot \left(\frac{P_0}{P_\infty}\right)^{-0,64} \quad (1)$$

The significance of the second square root expression is made clear by the following diagram:



For a fighter configuration with lift power plants mounted in /131 the center section of the fuselage, model measurements in [1] yielded the following for approximately critical discharge:

$$K \cdot \left(\frac{P_c}{P_\infty} \right)^{-0.64} = 0.009$$

A conspicuous feature in (1) is that the static pressure ratio for the jet appears as a parameter. If we look at the extensive studies in [9] on free jet propagation, for example, the effect of Mach number on jet propagation becomes clear.

The constant K in (1) is by no means universally applicable. It is valid only if the configuration does not deviate too much from the arrangement under discussion.

Considerable differences in the magnitude of K can occur between central and peripheral arrangements of jets. In particular, power plant pods with a series of lift power plants, which are often mounted outboard on the wings of VTOL transport aircraft, can result in a considerable reduction in jet-induced lift loss, since a relatively small wing area is located in the immediate vicinity of the jets. Thus in the case of the Do 31, the four power plants installed in a pod at the wing tip caused about 2.22% lift loss, whereas the four nozzles of the Pegasus cruising power plants located inboard under the wing produced 3.6% lift loss (referred to inherent thrust). In both cases, jet area was approximately the same and jet propagation from each set of four nozzles was probably likewise about the same.

The effect of the distribution of the area surrounding the jet will be covered in the following discussion. The force exerted on the underside of the aircraft is expressed as follows:

$$\frac{\Delta S}{S_0} = - \int \frac{dF \cdot \Delta p}{F_j \cdot \rho_j \cdot v_j^2} = - \frac{1}{2} \int \frac{dF}{F_j} \cdot c_p$$

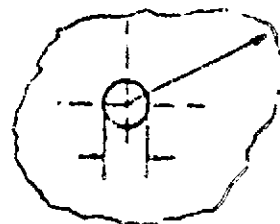
where C_p is the local pressure coefficient on the underside of the aircraft. It is now assumed that C_p decreases linearly with the reciprocal dimensionless distance from the center of the jet, /132

$$C_p = \frac{K_1}{r/D_j} ,$$

an assumption which proves to be reasonable, as will be shown below.

For lift loss we thus obtain

$$\begin{aligned} \frac{\Delta S}{S_0} &= -\frac{1}{2} \int \frac{dF}{F_j} \cdot \frac{K_1}{D_j} = -\frac{1}{2} K_1 \frac{D_j}{F_j} \int_{D_j/2}^r \int_{0_1=0}^{0_2=2\pi} dr d\theta \\ &= -\frac{K_1}{2} \frac{D_j}{F_j} \int_{2\pi}^{2\pi} [r(\theta) - D_j/2] d\theta \\ &= -2 K_1 \frac{\int_0^{2\pi} [r(\theta) - D_j/2] d\theta}{\pi D_j} . \end{aligned}$$



If we set $\frac{1}{\pi} \int_0^{2\pi} [r(\theta) - D_j/2] d\theta = \bar{D}$

(2)

then $\frac{\Delta S}{S_0} = -2K_1 \frac{\bar{D}}{D_j}$

(2)

Here, D_j is nozzle diameter, and \bar{D} can be conceived of as the equivalent diameter of the aircraft's planform.

For the special case of the round panel with a central jet, we can integrate and obtain

$$\frac{\Delta S}{S_0} = - 2 K_1 \frac{D}{D_j}$$

where D is panel diameter.

Converted to the ratio of areas, this becomes

/133

$$\frac{\Delta S}{S_0} = - 2 K_1 \cdot \sqrt{\frac{F}{F_j}} \quad (3)$$

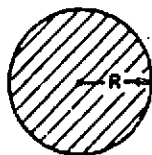
The same relation exists in (1) and (3) between lift loss and area ratio, thus indicating the assumption regarding the dependence of C_p to be reasonable. The constant K_1 is a function only of jet characteristics, and these are taken into consideration in relation (1). Relation (1), expanded to cover any aircraft configuration, thus reads as follows:

$$-\frac{\Delta z}{S_0} = K \cdot \frac{D}{D_j} \sqrt{\left[\frac{\frac{\partial q(x)}{\partial x}}{\frac{P_0 - P_\infty}{D_j}} \right]_{\max} \cdot \frac{1}{\left(\frac{x}{D_j}\right)_W}} \cdot \left(\frac{P_0}{P_\infty}\right)^{-0,64} \quad (4)$$

Like (1), relation (4) can only be used to convert lift loss from a known configuration to one which is somewhat similar, since the constant K does not possess general validity.

The progress which (4) represents over (1) consists of the fact that deviations in the planform of the aircraft and in the arrangement of power plants can be covered. Example:

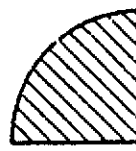
Circular panel



$$F = \pi R^2$$

$$\int_0^{2\pi} r \, d\theta = 2 \pi R$$

Quarter-circle



$$F = \pi R^2$$

$$\int_0^{2\pi} r \, d\theta = \pi R$$

The circular panel and the quarter-circle of the same surface area F differ in size

/134

$$\int_0^{2\pi} r \, d\theta$$

by a factor of two. The same lift loss would be obtained from (1) for the two cases, whereas on the basis of (4), lift loss for the circular panel would be twice as large as that for the quarter-circle, which is reasonable.

Unfortunately, no systematic measurements are available to demonstrate the usability of relation (4). An attempt will be made, however, to calculate lift loss with (1) and (4) in the example of the Do 31 lift power plants and the cruising power plants, oriented vertically in the downward direction, and to compare it with wind tunnel measurements. Although the configuration of the Do 31 differs considerably from that studied in [1], we shall adopt the value $K \times (P_0/P_\infty)^{-0.64} = 0.009$.

The four Do 31 lift power plants, arranged in a line, and the four cruising power plant nozzles, arranged in a square, can be treated in relations (1) and (4) on the basis of three different model representations; Fig. 5.1 provides an overview.

Model I

The four individual nozzles are treated as one normal nozzle of equivalent diameter, with the dynamic pressure drop of a normal nozzle.

Model II

The four individual nozzles are treated as a quadruple mixing nozzle of equivalent diameter with the dynamic pressure drop of a mixing nozzle.

Model III

The four individual nozzles are treated in isolation, each nozzle being surrounded by the entire aircraft surface and possessing the dynamic pressure drop of the individual nozzle. The overall effect is obtained by linear superposition.

All three models are treated both with relation (1) and with (4). /135

Unfortunately, values for maximum dynamic pressure drop in the jet are not available for Do 31 model measurements. Measurement results from (1) [sic] are used here; these are plotted in Fig. 5.2. They are from measurements performed on a group of four which are arranged much like the Do 31 cruising power plants. In the case of the single nozzle, D_j represents the diameter of the single nozzle, whereas for the group of four, D_j corresponds to the equivalent diameter.

The results for changes in lift determined in this manner are given in Fig. 5.1 and are repeated in the table below.

CRUISING POWER PLANTS: $-\Delta S/S_0$ IN %

	Model representation		
	I	II	III
Relation (1)	1.97	3.94	3.94
(4)	1.68	3.36	3.36

As already mentioned, the lift loss measured in the wind tunnel for the cruising power plants is $-\Delta S/S_0 = 3.6\%$.

The same approach was applied to the lift power plants. The table below shows the results of computation.

LIFT POWER PLANTS: $-\Delta S/S_0$ IN %

	Model representation		
	I	II	III
Relation (1)	1.98	3.96	3.96
(4)	1.2	2.4	2.4

The lift loss measured in the wind tunnel for the lift power plants is $-\Delta S/S_0 = 2.22\%$. Since the parameter K_S for the dynamic pressure drop in this case is exactly twice as large as for the individual nozzle, lift loss as indicated by equation (4) will be exactly identical in cases II and III and exactly half as large in case I. /136

Model representations II and III yield good agreement with the wind tunnel measurements for the cruising power plants, as determined both with relation (1) and with (4), whereas only (4) yields good agreement for the lift power plants. This is reasonable, since the lift power plants have an extremely outboard position, where the considerations which led to relation (4) are quite applicable. Relation (4) can be recommended on the basis of these positive results. That model representation I greatly underestimates lift loss is clear and reasonable, since the equivalent individual nozzle in I has completely different jet propagation from that associated with a group of four.

Thus the use of model representation II or III can be recommended for groups of nozzles. If the behavior of the dynamic pressure drop is known, II is probably to be preferred, since the superposition principle used with III has not been validated.

5.4. Jet Interference in Hover Close to the Ground

In hover close to the ground, other changes in force and torque besides jet-induced secondary forces of free hover act upon the airframe.

A single jet directed perpendicularly or obliquely at the ground, or a line of jets, is deflected at the ground and flows off in the form of a wall jet. Like the free jet, the wall jet draws air from the surroundings and generates an underpressure on the underside of a panel perpendicular to the ground. When a pair of jets or pair of rows of jets is aimed at the ground, an upward current (fountain) develops between the pair which generates an overpressure on the underside of the panel.

In an aircraft configuration with a particular power plant arrangement, both effects, namely the suction effect and fountain effect, are superimposed on one another and affect each other. A theoretical solution is not yet possible for this complex process. We will first determine the approximate flow pattern, particularly stagnation points and lines of flow, from information on the individual effects and also on the basis of personal experience, and then attempt to also obtain quantitative information regarding secondary forces and torques by superimposing the individual effects.

/137

As a basis for this approach, an attempt will be made below to analyze the individual effects; this is followed by the analysis of a complex configuration, using the example of the Do 31.

5.4.1. Analysis of Jet Interference Close to the Ground

The process of jet interference close to the ground can be analyzed in simplified form as shown below and broken down into several basic configurations.

a KONFIGURATION		b Ursache für Sekundärkraft	c Geschwindigkeitsabnahme auf der Wandstromlinie bzw im Aufstrom	d SCHUBÄNDERUNG H: BODENNAHE	e Analyt. Beziehung	f Qualitativer Verlauf
Einzelstrahl, von Platte umgeben g		k Saugeffekt	$\frac{U_{max}}{U_i} = \frac{K}{r/D_j}$		$\frac{S}{S_0} = \frac{S_{H=0}}{S_0} - 0,012 \left(\frac{H/D_j}{0,994(F/F_i)^{1/2} - 1} \right)^{2,2}$	
Strahlreihe od. Strahlschlitz von Platte umgeben h		l Saugeffekt	$\frac{U_{max}}{U_i} = \frac{K}{(z/D_j)^{1/2}}$ (zweidimensional) m			
Strahlreihen-Paar mit dazwischenliegender Platte i		l Fontänen-effekt	Hypothese: n $\frac{U_{max}}{U_i} = \frac{K}{(z/D_j)^{1/2}}$ (zweidimensional) m	Hypothese: n	$\frac{\Delta S}{S_{H=0}} = \frac{K}{h/D_j}$ (zweidimensional) m	
Strahl-Paar mit dazwischenliegender Platte j		Saugeffekt u. Fontänen-effekt k + l				

Reproduced from best available copy.

- Key:
- a. Configuration
 - b. Cause of secondary force
 - c. Velocity drop along wall flow line or in upward flow
 - d. Change in thrust close to ground
 - e. Analytical relation
 - f. Qualitative curve(s)
 - g. Individual jet, surrounded by panel
 - h. Row of jets or slotted jet surrounded by panel
 - i. Two rows of jets with panel between them
 - j. Two jets with panel between them
 - k. Section effect
 - l. Fountain effect
 - m. Two-dimensional
 - n. Hypothesis

- a) Individual jet exhausting normally from a panel and oriented normally with respect to the ground

/138

A jet exhausting from a nozzle is propagated in accordance with the known empirical principles governing free jet propagation and, after deflection at the ground, in accordance with those governing wall jet propagation. The region close to the stagnation point, with a radius of about one nozzle diameter, is excluded here. The drop in the characteristic velocity of the free or wall jet occurs linearly with distance from the nozzle or stagnation point, respectively. The decrease in maximum velocity in the wall jet is governed by the propagation law

$$\frac{v_{\max}}{v_j} = \frac{K}{r/D_j},$$

in which the nozzle's distance from the ground does not appear. The constant K has various values in the literature. The reason for this lies primarily in the different initial conditions in the nozzle.

The natural flow toward the free or wall jet is obstructed in the case of a jet exhausting from a panel parallel to the ground. The surrounding air is sucked in along the underside from the margin of the panel and produces an underpressure. If the panel is very large or the distance between nozzle and ground is very small ($H/D_j < 1$), this flow pattern no longer applies. This case is of no practical interest, however.

The underpressure on the underside of the panel and thus the total force acting upon the panel can be calculated with the aid of potential theory if assumptions are made regarding the air sucked in by the free and wall jets. In Seibold [10], the jets are represented here by coverage with sinks, the panel by coverage with vortices, and the ground by reflection. The comparison between calculations and measurements is unfortunately shown only to a ground distance of $H/D_j < 0.5$ in [10].

In [11], an empirical relation, obtained from measurements with circular panels of various size, is given between relative thrust loss and ground distance, which is made dimensionless with the difference between panel diameter and nozzle diameter.

$$\frac{s-s_{H=\infty}}{s_0} = 0.012 \left(\frac{H}{D_p - D_j} \right)^{-2.3} \quad (4a)$$

The reference quantity on the right side, which can be conceived of as the equivalent diameter of the panel area surrounding the nozzle, is interesting and is physically meaningful. Panel area and nozzle area are thereby eliminated as independent variables. This relation is also applicable to configurations with fan power plants, for which the ratio of nozzle area to panel area is an order of magnitude larger than in the case of jet configurations. It is suggested that in the case of noncircular panels, panel diameter D_p be replaced with an equivalent diameter \bar{D}_p in analogy to the considerations discussed in Section 5.3.

A likewise empirical relation, almost identical to (4a), is given in [4]:

$$\frac{S}{S_0} = \frac{S_{H=\infty}}{S_0} - 0.012 \left[\frac{H/D_j}{0.994 (F/F_j)^{1/2} - 1} \right]^{-2.3} \quad (4b)$$

Expression (4b) differs from (4a) by a factor of only 0.994 in the case of the circular panel. Relation (4b) is handier for first approximations than (4a) and is shown in Fig. 5.3 as a working graph. A comparison between (4b) and measurements performed on various rectangular panels in Fig. 5.4 shows acceptable agreement for project estimates.

- b) Row of jets or slotted jet, exhausting from a panel and oriented perpendicular to the ground

A notable feature in Fig. 5.4 is that a slot nozzle with an aspect ratio of about 9 generates a smaller secondary force than a round nozzle of equal area. The difference is in the different propagation laws governing the three-dimensional single jet and the quasi-two-dimensional slotted jet /140. As already mentioned, the linear propagation law applies to the round jet for velocity:

$$\frac{v_{\max}}{v_j} = \frac{K}{r/D_j}$$

whereas the square-root law applies to the two-dimensional case:

$$\frac{v_{\max}}{v_j} = \frac{K}{(r/D_j)^{1/2}}$$

It is reasonable to formulate relation (4b) as follows for the two-dimensional case:

$$\frac{S}{S_0} = \frac{S_{H=\infty}}{S_0} - K \left[\frac{H/D_j}{(F/\Gamma_j)^{1/4} - 1} \right] \quad (5)$$

c) Two rows of jets with panel between them

In the case of two rows of jets or two slotted jets oriented perpendicular to the ground, a stagnation line is generated in the plane of symmetry above which the wall jets coming from opposite directions proceed in the form of an upward vertical current. A body lying transverse to this upward current experiences a force in the direction of oncoming flow similar to the drag of the particular body in a free stream.

Now the drag of various bodies differs considerably. An infinitely long circular cylinder has a coefficient of drag of about 0.4 at a Reynolds number greater than $5 \cdot 10^5$, whereas an infinitely long panel in perpendicular oncoming flow has a coefficient of about 2.0. Just this numerical comparison is enough to show how problematic it is to estimate the force acting on the body of an aircraft located in an upward flow with all possible flaps extended for takeoff. /141

Due to the same facts, on the other hand, influence can be exerted by relatively simple means, such as auxiliary flaps. An example of this is provided by the measurements from [10] shown in Fig. 5.5, obtained with a medium-range V/STOL airliner.

In Fig. 5.6, the thrust acting upon the aircraft close to the ground is plotted against ground distance. Reference quantities include operant thrust out of ground effect and the diameter of a single nozzle. The curves came from measurements performed on the Do 31 and its successor, the Do 131. The measurements confirm the predominance of the fountain effect, which is reasonable on the basis of the arrangement of jets and the planform.

It is conspicuous that the curve for the Do 31 lies considerably below that for the Do 131. Various factors play a part here, such as different inclinations of the power plant jets and different fuselage shapes, including extended landing gear doors, and the like. The inflection point for the Do 131 is conspicuous.

For the two rows of jets or two slotted jets oriented perpendicular to the ground, the same propagation laws apply, in qualitative terms, as in the case of the free and wall jets of the corresponding individual configurations up to about the point at

which the wall jets form a stagnation line. In the vicinity of the stagnation line, the wall jets parallel to the ground are deflected into a vertically rising fountain. If secondary factors are neglected, the fountain can be viewed as a continuation of the wall jets. The plane of symmetry takes the place of the wall here. Just as a propagation law which is independent of nozzle height applies to the wall jet, an analogous propagation law which is independent of nozzle height H and nozzle separation A can be derived for the fountain.

$$\frac{v_{\max}}{v_j} = \frac{K}{(z/D_j)^{1/2}} \quad (5) \quad [\text{sic}]$$

In analogy to the linear law governing the drop in velocity, the following would apply to the fountain between a pair of nozzles:

$$\frac{v_{\max}}{v_j} = \frac{K}{z/D_j} \quad (5) \quad [\text{sic}]$$

Measurements of maximum upward flow velocity along the axis of symmetry of a pair of nozzles presented in [7] confirm, to a certain extent, the linear relationship and the subordinate effect of nozzle separation A beyond a ground distance of $z/D_j > 3$ (Fig. 5.7).

The discussion of principles presented here applies only if the distance between the pair of jets is not too small compared to ground distance. In this case, the two free jets merge even before they impinge on the ground and thus obstruct the development of a fountain. S. Harmsen [8] shows this effect very clearly by means of momentum measurements between a pair of nozzles and by means of flow pictures taken by the light section method and finds that no fountain occurs between a pair of nozzles if the distance between them is not at least one or two times the distance between the nozzles and the ground.

The following can be written formally for the aerodynamic force on a body located in the upward flow:

$$\Delta S = c_W \cdot q_m \cdot F$$

or, referred to nozzle thrust,

$$\frac{\Delta S}{S_0} = \frac{1}{2} c_W \cdot \frac{\rho}{\rho_j} \cdot \frac{F}{F_j} \cdot \frac{v_m^2}{v_j^2} \quad (6)$$

where v_m is mean velocity in fountain, c_W is the body's coefficient of drag, F is the aircraft area which is located in the upward flow. The density effect is of subordinate importance in jet propagation and is neglected.

/143

For v_m , we assume $v_m = K \cdot v_{max}$, and we let the distance of the underside of the fuselage from the ground be $Z = h$, whereupon we obtain the following relation with (5) and (6)

$$\frac{\Delta S}{S_0} = c_W \cdot \frac{F}{F_j} \cdot \frac{K}{h/\rho_j} \quad (7)$$

In Fig. 5.6, measured jet-induced force is plotted against ground distance for the Do 31 and Do 131 with the cruising power plants in two rows of nozzles each. The linear relation is valid in terms of trend. The different levels of the curves can be explained by the different shapes and sizes of the fuselage undersides.

d) Two jets with panel between them

The flow pattern in case d) is a mixture of case a) and case b) and is therefore difficult to determine even qualitatively. As in case c), a stagnation line does develop at the ground, in one of the planes of symmetry. A vertical fountain is formed only near the axis of symmetry, however. The fountain flows off to the side over the remainder of the ground stagnation line. Thus the fountain effect is operant only in the vicinity of the axis of symmetry, whereas the suction effect prevails over the rest of the panel. Fig. 5.8 shows model measurements of the change in thrust, close to the ground, on the Do 31 and Do 131 with just the cruising power plants running. The configuration of the Do 131 corresponds roughly to the case under consideration, whereas a fountain effect clearly occurs at low altitude in the case of the Do 31.

5.4.2. Application of the Analysis in 5.4.1 to the Example of the Do 31

The most important features relating to jet interference in hover close to the ground are as follows for the case of the Do 31:

high-wing configuration
lift power plants at wing tips
cruising power plants inboard under wing.

First, the jet interference associated with the different groups of power plants is estimated separately. The lift power plants of the Do 31 contribute little to the change in thrust, due to their peripheral location. The lift loss due to the suction effect outside of the ground effect is only about 1% of overall takeoff thrust. Even close to the ground, no appreciable additional suction effect or fountain effect occurs because of the high-wing configuration and the peripheral location. These statements agree with the model measurements plotted in Fig. 5.9. Only at a landing gear to ground distance of less than $2.4 (h_{FW}/D_j)$ does a weak fountain effect become operant.

The cruising power plants of the Do 31 produce a thrust loss of 2% of overall takeoff thrust outside the ground effect. Close to the ground, the cruising power plants represent a mixture of cases c) and d) as treated in Section 5.3.2, for which reason their jet interference effect can only be estimated quite roughly. The model measurements in Fig. 5.9 show that a slight suction effect exists between values of $H/D_{eMTW} = 7$ and 1.

Next, the ranges of influence of the lift and cruising power plants under takeoff and landing conditions are delimited, for which purpose we estimate the ground stagnation lines. In the case of the Do 31, the ground stagnation lines are available from flow patterns taken in model measurements (Fig. 5.10). It can be seen from the ground stagnation lines that the range of influence of the lift power plants is markedly limited close to the ground. The one appreciable contribution from the lift power plants comes from the stagnation line between the lift and cruising power plants.

This stagnation line causes the deflection of a large portion of the cruising power plant jets in the direction of the fuselage underside. The effects of the cruising power plants are thereby enhanced: instead of 360° , the central angle of jet propagation amounts to only about 220° , so we must expect the effect to be increased by a factor of 1.64. The fountain rising above the ground stagnation line between the lift and cruising power plants is directed against the underside of the wing. Since the distance between ground and underside of the wing is already $10 D_{HTW}$ (individual nozzle) with the aircraft standing on the ground, the fountain effect is neglected. /145

The addition of lift and cruising power plant thrusts outside the ground effect and the 1.64-fold change in cruising power plant thrust close to the ground yields the curve of thrust versus ground distance plotted in Fig. 5.9. The curve, obtained by superposition, lies below the measured value but provides a satisfactory picture of the distribution and order of magnitude of the jet interference effect.

5.5. Jet Interference in Transition for V/STOL Transport Aircraft with Jet Power Plants

For V/STOL aircraft with pure jet power plants or with fan power plants of low bypass ratio (less than 1), the effect on aircraft aerodynamics caused by the power plant jets far exceeds the effect of inlet flow. This applies particularly to lift, while the drag component of inlet flow is known from inlet momentum, and the torque component can likewise be estimated from the momentum vector of inlet flow. But the effect of the jets can be treated separately from that of inlet flow for a first approximation of interference for aircraft configurations. With fan power plants of high bypass ratio, too, so the following statements also apply to these cases.

In hover, jet interference from a nozzle jet is based only on its suction effect due to turbulent mixing of the jet with surrounding air. In transition, an interaction occurs between oncoming flow and the power plant jet, which in turn affects flow about the airframe. The resulting flow field is of a complex nature, and only a few simplifying model representations are known so far for theoretically treating quite simple configurations such as that of a simple jet in a wing, exhausting downward. Calculations and measurements exhibit satisfactory agreement in this case [12-14]. Two nozzle jets positioned behind one another are covered in [15]. These model representations do not apply to jet positions close to the wing forward edge or trailing edge or close to the extended landing flap, under the wing or in the fuselage as they occur in V/STOL transport aircraft, so we must rely entirely upon measurements. /146

The jet interference forces on V/STOL transport aircraft known from the literature and from our own measurements are reported in the following section. An attempt is made in a subsequent section to apply the interferences known from systematic measurements on single nozzles to the Do 31 configuration by superposition and to compare these with our own wind tunnel measurements.

5.5.1. Determination of Jet Interference from Wind Tunnel Measurements

In order to be able to convert from a configuration known from measurements to a new one, we must know the influencing factors. As was already shown in the introduction, no such function is known for the general case. But no exact conversion function is even known for the special case of geometric similarity in the planform and similarity in power plant nozzle position, but with a different ratio of nozzle area to planform area. Williams [16] presents a conversion function:

$$\frac{\Delta A}{S_0} = \text{Function} \left[\left(\frac{F}{F_j} \right)^{1/2} \left(\frac{v_\infty}{v_j} \right)_0^{1/2} \right],$$

which is obtained from a dimensional analysis of the jet propagation process and the long-range effect of the jet deflection process, approximated with a vortex model. Since this simplified model representation no longer applies to complex configurations such as those of V/STOL transport aircraft, as mentioned in the introduction, the conversion function derived from this is likewise very questionable. Since nothing better is known, however, we will still have recourse to this formula in case of need, if jet interference affecting a new configuration must be estimated with the aid of the measured data for representative V/STOL transport aircraft compiled below.

/147

Jet interference measurements performed on V/STOL transport aircraft are quite sparse. Most of the published jet interference measurements cover aircraft which can be classified as combat aircraft on the basis of configuration and arrangement of jets. Williams [16] offers an excellent summary of the most important measured data, including an extensive bibliography. V/STOL jet transport aircraft with such typical characteristics as high-wing configuration, large aspect ratio, large fuselage diameter and a relatively large number of lift power plants (at least eight) arranged in rows or groups of jets have only been studied by the British Aircraft Corporation (BAC) with a simple variation model. Aside from our own measurements with the Do 31 model, we know of no additional measurements.

Fig. 5.11 shows a compilation of the BAC measurements (taken from [16]) and the Dornier measurements, with lift referred to static thrust, plotted over effective velocity ratio.

Configuration A, with the lift power plants mounted outboard on the wings, exhibits the smallest lift loss. Rows of lift power plants on the sides of the fuselage (configuration B) are enough to cause more than 10% loss, and the configuration of the Do 31, with lift power plant pods mounted outboard on the wings and the pivoting nozzles of the cruising power plants located inboard, likewise causes up to 10% lift losses. Very high losses are produced by rows of lift power plants in the central section of the fuselage (configuration C) or inboard on double delta wings (configurations D and E). In an extremely unfavorable case, more than 50% of static thrust can be lost. A comparison of the various configurations lets us state, in qualitative terms, that loss increases with the area surrounding the jets.

In hover, lift loss is proportional to the square root of the area ratio. This simple relationship does not apply in transition, since the aircraft surface area surrounding the jet makes a variable contribution to jet-induced force, depending upon its position relative to the direction of oncoming flow.

/148

Nothing is known from the BAC models regarding momentum change due to the jet effect. The torque curve of the Do 31 was covered in Section 3. Additional information can unfortunately not be provided.

5.5.2. Superposition of Jet Interference from Individual Jets in the Example of the Do 31

Since good results were obtained in Section 5.3 in the determination of jet interference in hover through superposition of the effects of individual nozzles in the example of the Do 31, this principle will be checked in transition flight. For jet-induced force in hover, it was possible to state an empirical relationship to geometric dimensions and the decrease in dynamic pressure along the axis of the jet. As was already established in the introduction, this is not possible for the general case of the individual jet in transition, so we must have recourse to measurements performed on a basic model with a single jet. Such measurements are known from [17] and [18], in which the position of the single nozzle in a rectangular wing was varied systematically.

A prerequisite for fruitful superposition is that geometric conditions be approximately equivalent with regard to the position and size of the jet on the basic model and on the aircraft and that the reciprocal effects of the individual jets remain relatively small. By chance, the first condition is satisfied approximately for the lift and cruising power plants of the Do 31 in [6], while the second condition is probably not adequately satisfied by the nozzle jets, which are located close beside or behind one another in the case of the Do 31 under consideration. Only the results at the end of the following discussion will provide some information.

The jet-induced forces and torques on a rectangular wing with ^{/149} a single nozzle are studied systematically in the wind tunnel in [17] and [18]. In [17], the single nozzle lies in the plane of symmetry of a rectangular wing of aspect ratio 5 at a distance of $z_D/l = -0.25$ under the plane of the wing. The forward or rearward position of the nozzle lies between $-0.5 < x_D/l < +0.75$ (zero point at $1/4 \cdot l$ positive to the rear), the jet exhausting vertically, in the downward direction, among other things. The configuration of the wind tunnel model in [18] consists of a wing/fuselage combination, rectangular wing of aspect ratio 4.6, with a single nozzle under each half of the wing separated by $1/4$ of the span. Among other things, the forward or rearward positions were varied between $-2.25 < x_D/l < +1.0$ for nozzle levels (in terms of height) of $z_D/l = -0.64$ and -0.84 , with the jets exhausting vertically, in the downward direction. The data plotted in Fig. 5.12 are supposed to indicate the effect of the nozzles' forward position upon jet-induced force, with the nozzles' position on the vertical axis and the velocity ratio as parameters.

While the effect is approximately constant for a nozzle location in the forward portion of the wing, the "jet flap effect" occurs if the nozzle is located to the rear, causing a positive component in jet-induced lift due to supercirculation effects. The position of the nozzle along the vertical axis influences both the magnitude of the interference and the rise in the curves due to the jet flap effect. It must be mentioned, however, that the curves for $z_D/\ell = -0.64$ and -0.89 come from [18], in which a wing with a single 30% split flap at an angle of 60° was used. The crossover plot in Fig. 5.12 shows no reasonable trend for the effect of nozzle location along the vertical axis, for which reason the results in [17] are used for the application of superposition to the Do 31. The positions of the cruising and lift power plant nozzles of the Do 31 along the vertical lie in the range $-0.3 < z_D/\ell < -0.4$, whereas $z_D/\ell = -0.25$ in [17]. The ratio of the area of individual cruising power plant nozzles to the area of the half wing lying outside the fuselage is $F_j/F = 1/133$, whereas $F_j/F = 1/145$ in [17]. The ratio of the area of individual cruising power plant nozzles to the area of the outboard wing up to the cruising power plant side wall is $F_j/F = 1/65$. Since the lift power plants at the wing tip of the Do 31 can be assumed to be lying in the plane of symmetry of a rectangular wing, the effective area ratio is $F_j/F = 130$ [sic], and is thus a value which is applicable to [17]. The ratio of diameter to chord is probably just as important as the area ratio. This ratio is $D_j/L = 5.7$ in [17], while in the case of the Do 31, $D_j/\ell = 5.7$ for the lift power plants and $D_j/\ell = 7.7$ for the cruising power plants. /150

Superposition is based on Fig. 5.13, which is an extension of Fig. 5.12 to $V_B/V_j = 0.77$. Superposition was applied only to the cruising power plants in one case and, in another, to the lift and cruising power plants, since comparable wind tunnel measurements were available for this. The results of superposition are shown in Fig. 5.14. The calculations agree satisfactorily with the measurements for low V_∞/V_j , from about 0.1 to 0.15, while the calculated values are almost twice as large as the measurements for large V_∞/V_j .

The mutual interaction or obstruction of the propagation of individual jets in the group of nozzles is probably being manifested here. The superposition of pitch torque is not possible, since the curves in [17] are too discontinuous and contain too few data points.

In summary, it can be said that for complex power plant configurations with rows and groups of jets such as in the Do 31, the principle of superimposing the effects of individual nozzles yields usable values for first approximations only in the case of a small velocity ratio, up to about $V_\infty/V_j = 0.15$. Systematic measurements on basic models with rows and groups of jets are necessary to permit the preparation of generally valid working data for the project engineer.

5.6. REFERENCES

1. Gentry, G. L. and Margason, R. J., "Jet-induced lift losses /151
on VTOL configurations hovering in and out of ground
effect," NASA TN D-3166, 1966.
2. Shumpert, P. K. and Tibbetts, J. G., "Model tests of jet-
induced lift effects on a VTOL aircraft in hover,"
NASA CR-1297, 1969.
3. Vogler, R. D., "Interference effects of single and multiple
round or slotted jets on a VTOL model in transition,"
NASA TN D-2380, 1964.
4. Hall, G. R., "Scaling of VTOL aerodynamic suckdown forces,"
J. Aircraft 4(4) (1967).
5. Esch, P. and Joos, R., "Do 31 2B interference and ground
effect measurements in the DW wind tunnel," Dornier
Report VW 537-B1.
6. Esch, P. and Bartalszky, H., "Do P-362 interference measure-
ments in the DW wind tunnel," Dornier Report VT 483-B1.
7. Höscher et al., "Systematic studies of free jets, ground /152
jets and hot gas fountains for VTOL configurations with
jet power plants, lift fans and propellers," Dornier
Report VT 483-B5, 1969.
8. Harmsen, S., "Experimental studies on the upward flow caused
by two lift jets close to the ground," Engineering
University of Berlin Report on Aircraft Construction 64/8.
9. Warren, W. R., An Analytical and Experimental Study of
Compressible Free Jets, University of Princetown [sic],
New Jersey, 1957.
10. Seibold, W., "Studies on the secondary forces generated by
lift jets on VTOL aircraft," Jahrbuch d. WGLR [Yearbook
of the Scientific Association for Aeronautics and
Astronautics], 1962.
11. Wyatt, L. A., "Static tests of ground effect on planforms
fitted with centrally located round lifting jets,"
ARC CP No. 749, 1964.
12. Bradbury, L.J.S. and Wood, M. N., "The static pressure
distribution around a circular jet exhausting normally
from a plane wall into an airstream," ARC CP 827, 1964.

13. Wooler, P. T., "On the flow past a circular jet exhausting at right angles from a flat plate or wing," J. Roy. Aer. Soc. 71 (March 1967).
14. Wooler, P. T., Burghart, G. H. and Callagher, J. T., "Pressure distribution on a rectangular wing with a jet exhausting normally into an airstream," J. Aircraft 4(6) (1967). /153
15. Ziegler, H. and Wooler, P. T., "Multiple jets exhausting into a crossflow," J. Aircraft 8(6) (1967).
16. Williams, J., "The aerodynamics of V/STOL aircraft. Part E: Turbojet/turbofan aircraft," Von Karman Institute for Fluid Dynamics Lecture Series 9, May 13-17, 1968.
17. Baumert, W. and Harms, L., "Effect of a nozzle jet on the aerodynamic coefficients of wings located above the jet nozzle," DGLR Report 70-28, Report on the Symposium on Aerodynamic Interference Between Aircraft and Power Plant Jet, Düsseldorf, Dec. 3, 1970.
18. Carter, A. W., "Effects of jet-exhaust location on the longitudinal aerodynamic characteristics of a jet V/STOL model," NASA TN D-5333, 1969.

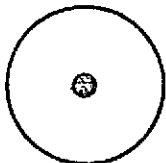
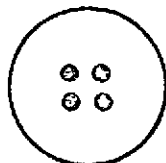
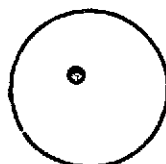
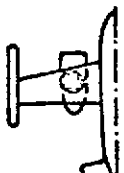
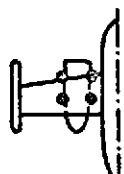

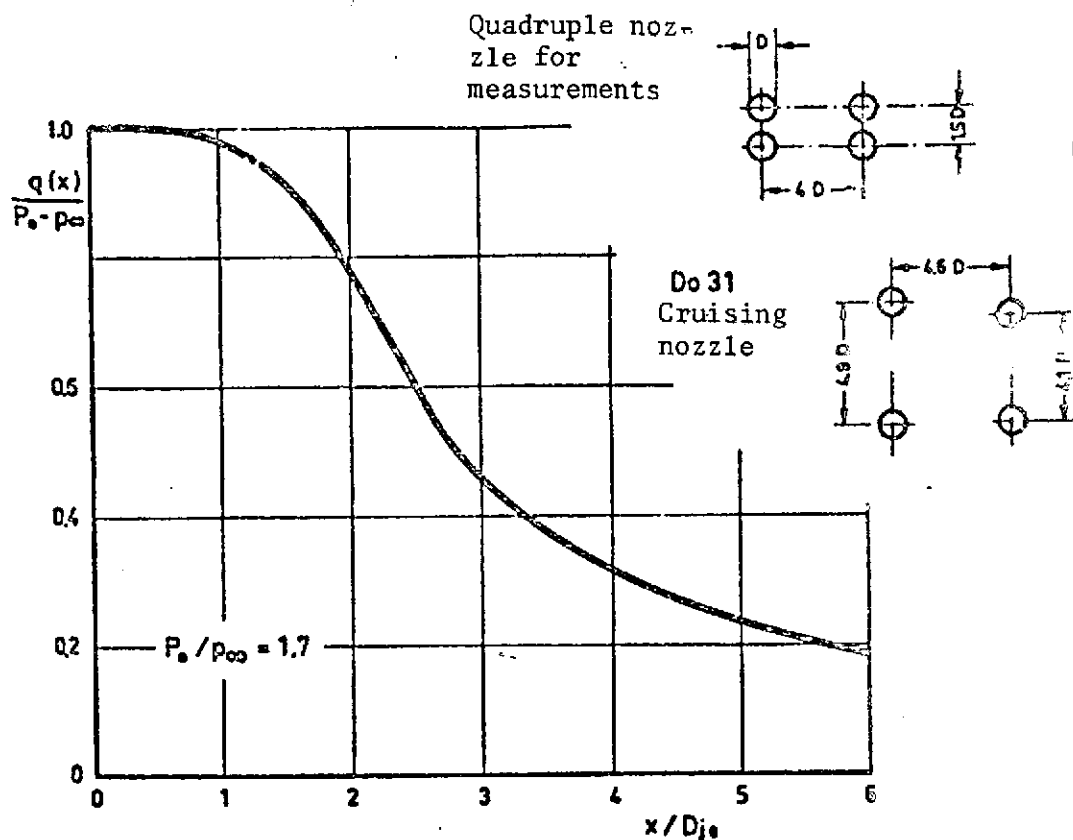
$F/2 = 1630,7 \text{ cm}^2$ $F_j = 3.84 \text{ cm}^2$ Data on wind tunnel model $D_{F/2} = 36.7 \text{ cm}$ $D_j = 2.21 \text{ cm}$				
Case	Model representation	Change in lift ($-\Delta S/S_0$)	K_S	$-\Delta S/S_0$
I		$\frac{0.009}{2} K_{S1} \sqrt{\frac{F/2}{F_j}}$	0.2125	0.0197
II		$\frac{0.009}{2} K_{S4} \sqrt{\frac{F/2}{F_j}}$	0.425	0.0394
III		$0.009 K_{S1} \sqrt{\frac{F/2}{F_j}}$	0.2125	0.0394
IV		$\frac{0.009}{2} K_{S1} \frac{D_{F/2}}{D_j}$	0.2125	0.0168
V		$\frac{0.009}{2} K_{S4} \frac{D_{F/2}}{D_j}$	0.425	0.0336
VI		$0.009 K_{S1} \frac{D_{F/2}}{D_j}$	0.2125	0.0336

Fig. 5.1. Alternative models for treatment of the change in lift in Do 31 hover with cruising power plants only.



Parameters for Jet Propagation:

$$K_S = \sqrt{- \left[\frac{\partial \frac{q(x)}{P_0 - p_\infty}}{\partial (x/D_{je})} \right]_{\max} \cdot \frac{1}{(x/D_{je})_w}}$$

Quadruple nozzle

$$K_{S4} = \sqrt{\frac{1}{2.52} \cdot \frac{1}{2.26}} = 0.425$$

Single nozzle

$$K_{S1} = \frac{1}{2} K_{S4} = 0.2125$$

Fig. 5.2. Decrease in dynamic pressure along axis of jet. Measurements taken from [2].

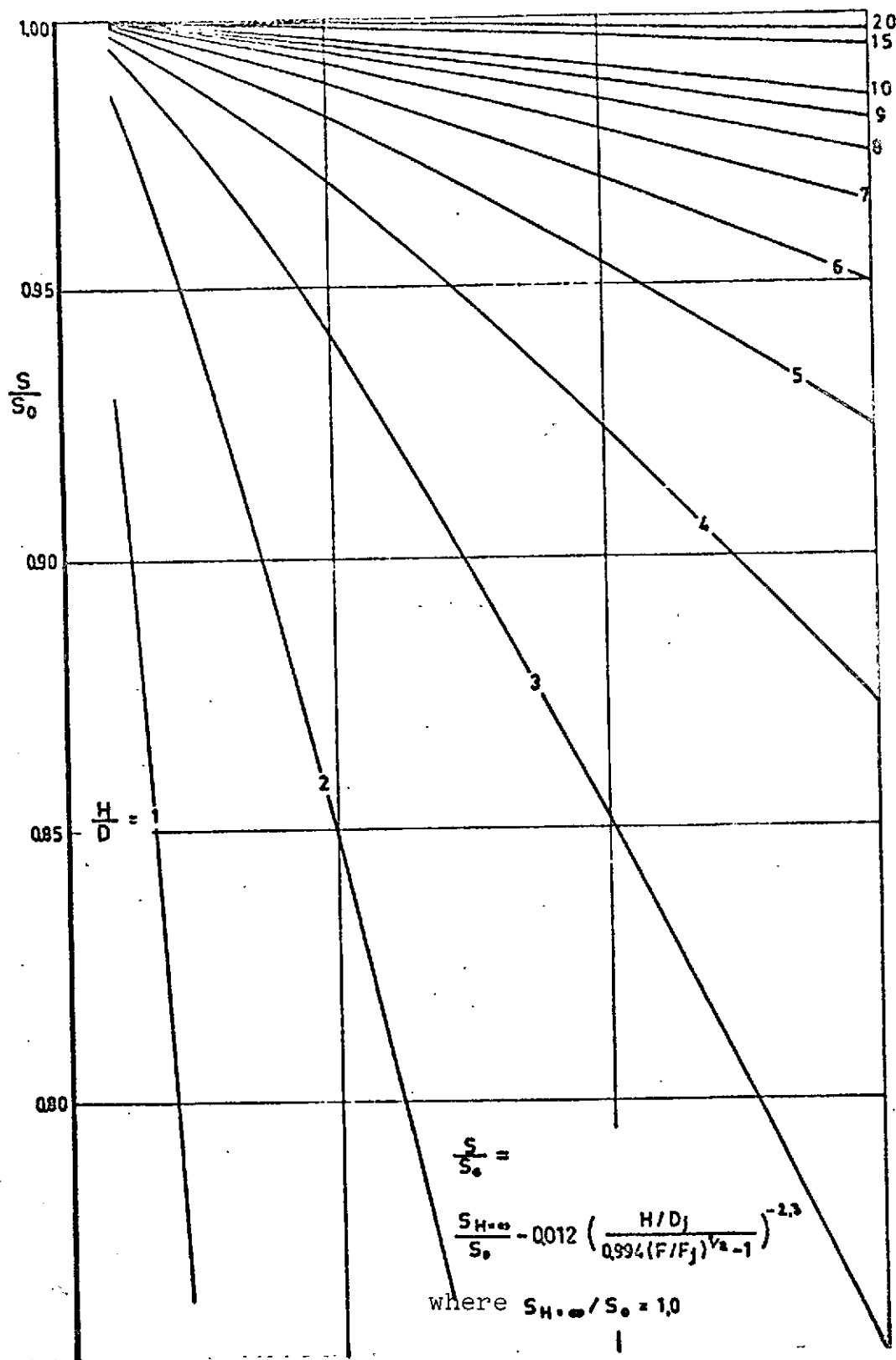


Fig. 5.3. Change in thrust close to ground as a function of ratio of rectangular panel area to nozzle area.

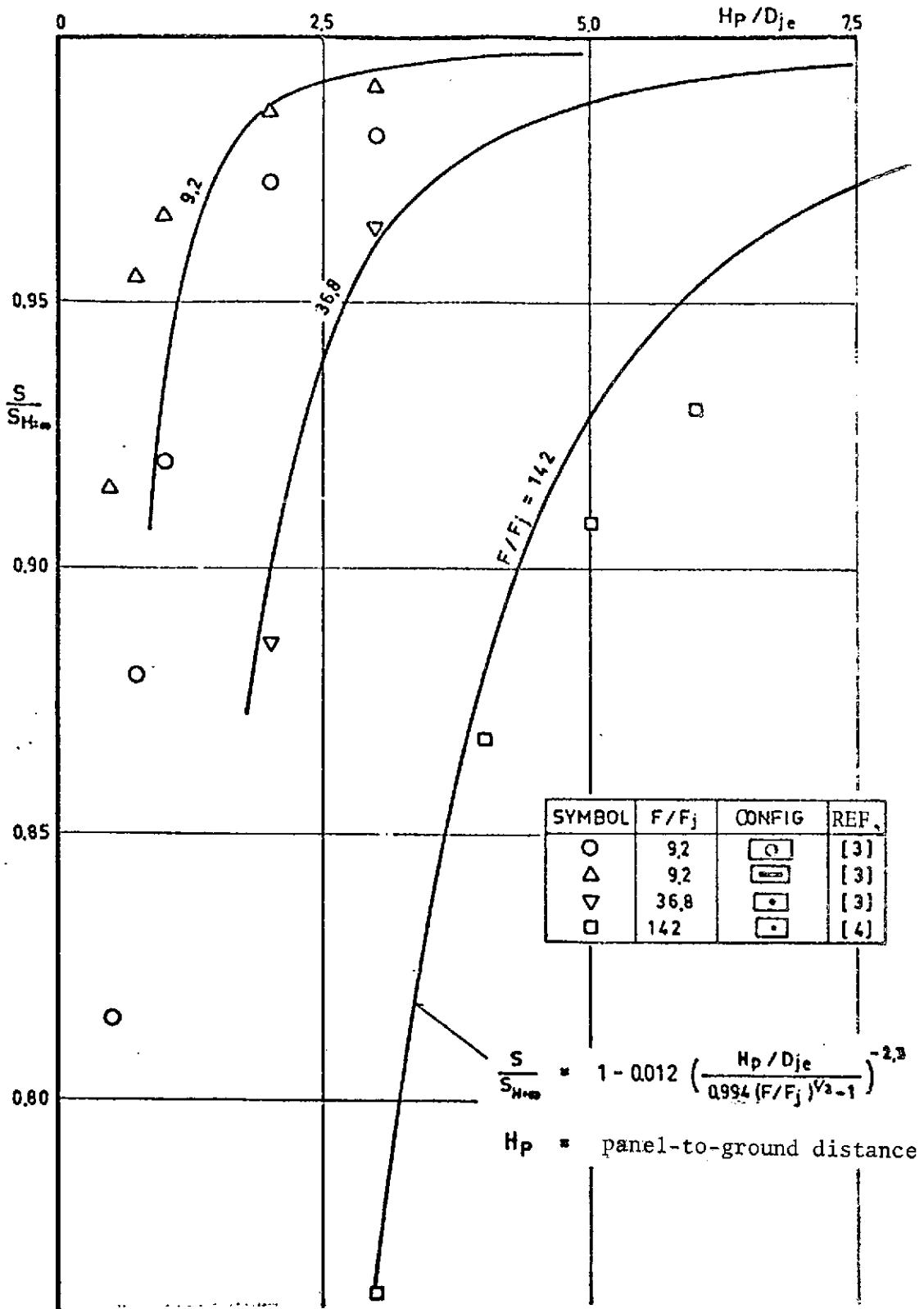
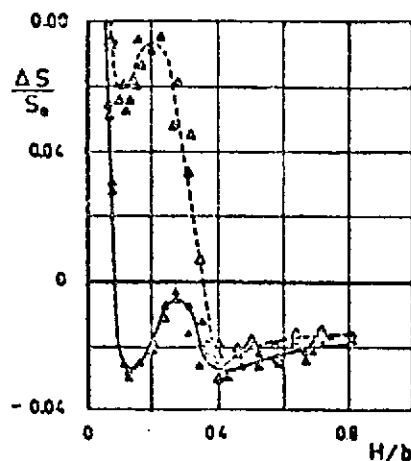
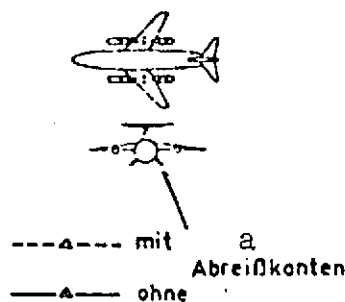


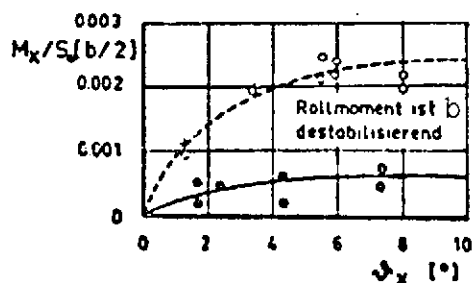
Fig. 5.4. Change in lift close to ground, based on suction effect measurements.



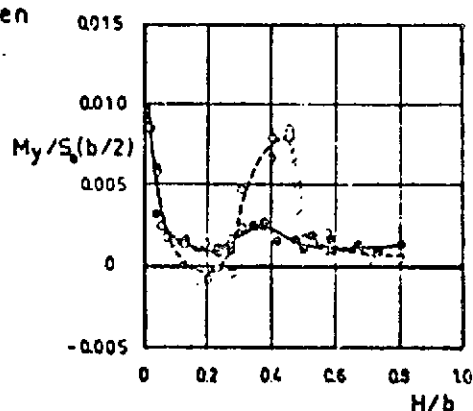
Secondary force ΔS



---○--- mit a
—●— ohne Abreißkonten



Roll torque M_x of aircraft in horizontal hover at altitude $h = 14.4\%$ of span b .



Pitch torque M_y of aircraft in horizontal hover.

Fig. 5.5. Jet interference measurements on a medium-range V/STOL airliner in hover close to ground, taken from [10].

Key: a. With, without spoilers
b. Roll torque is destabilizing

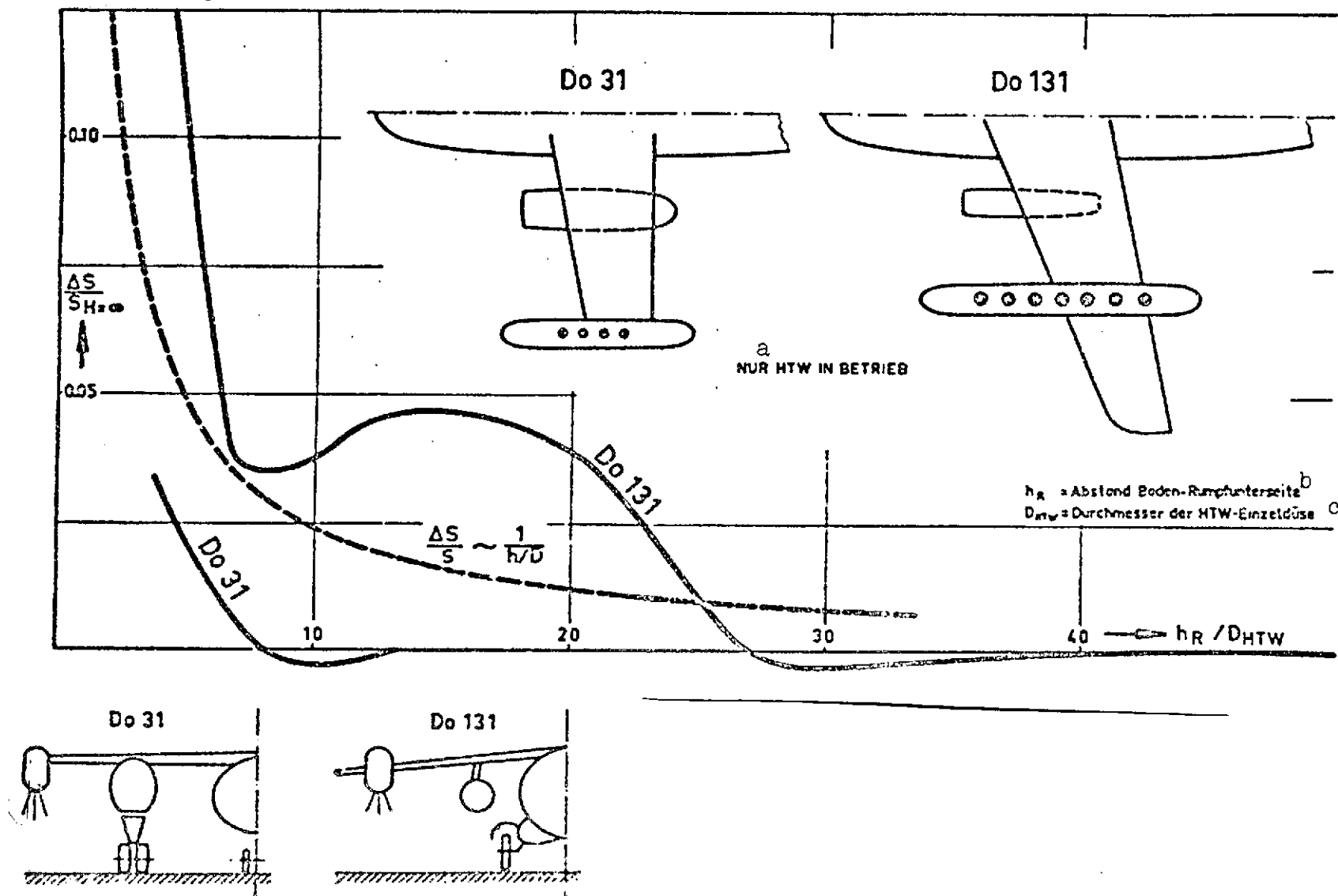


Fig. 5.6. Change in thrust close to ground, fountain effect predominating. Model measurements.

Key: a. Only lift power plants operating; b. Ground ~ to ~ fuselage underside distance; c. Diameter of individual lift power plant nozzle

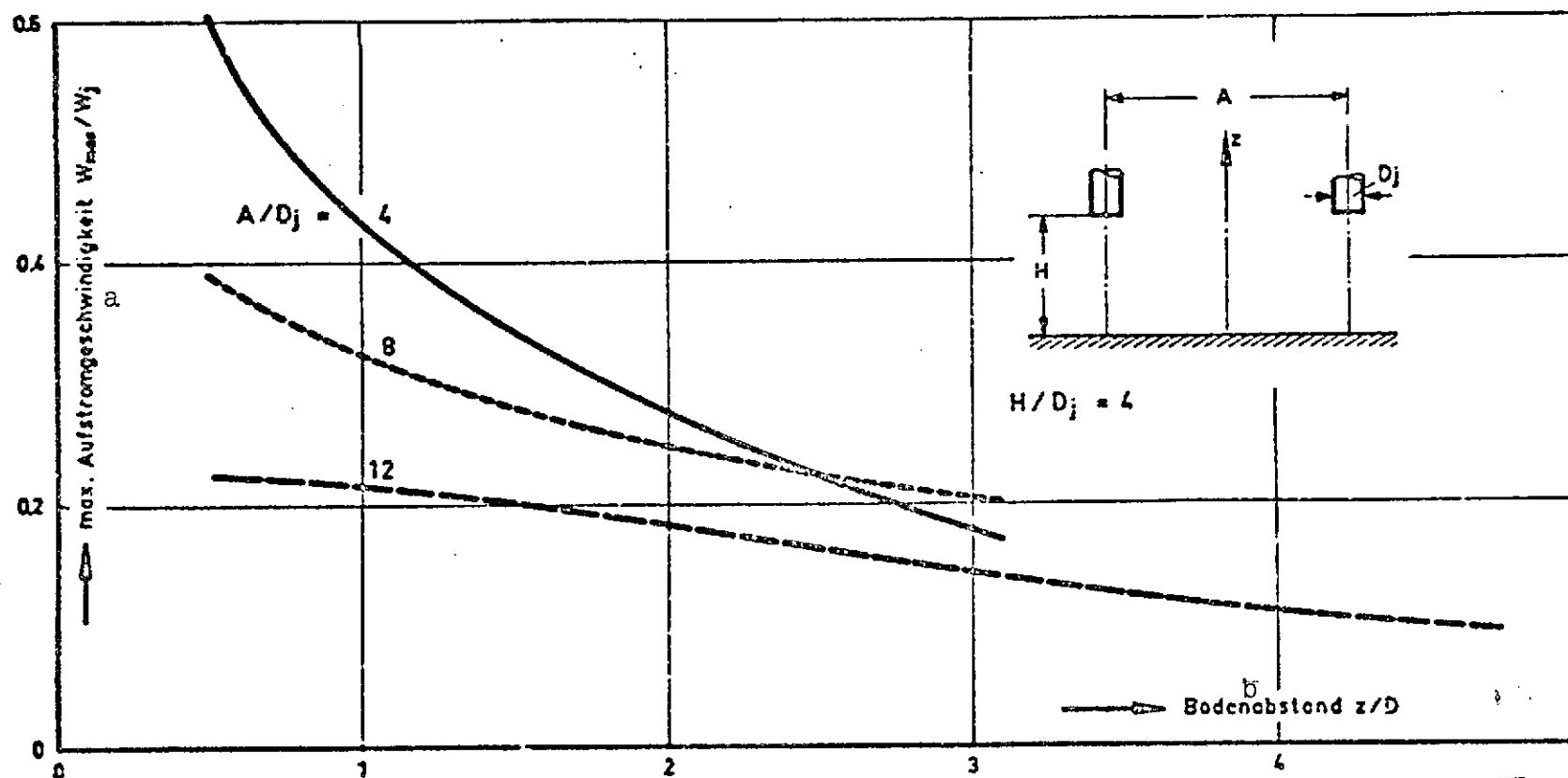


Fig. 5.7. Dropoff in max. velocity of upward flow between a pair of nozzles, from measurements taken from [7].

Key: a. Max. velocity of upward flow
b. Ground distance

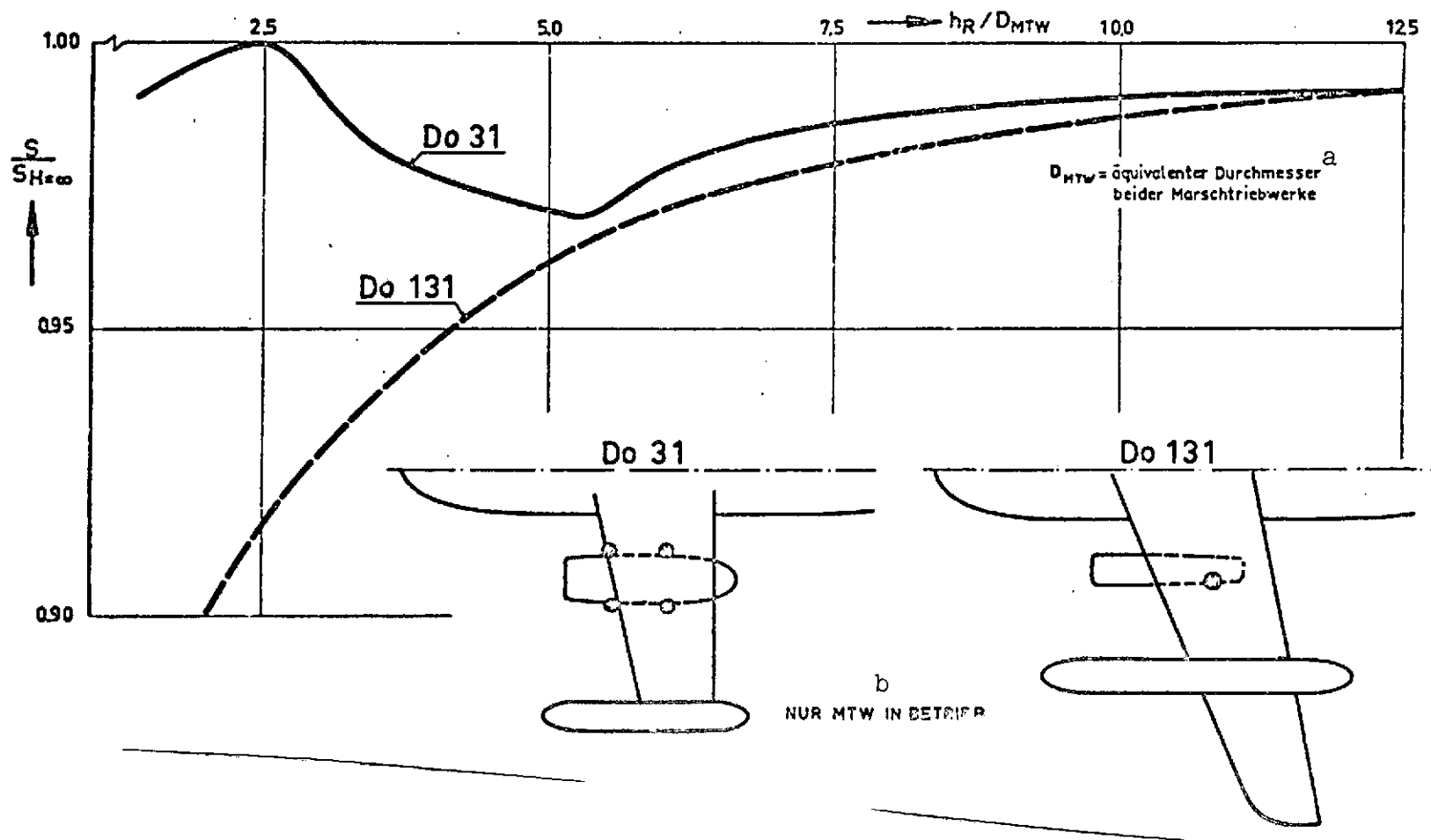
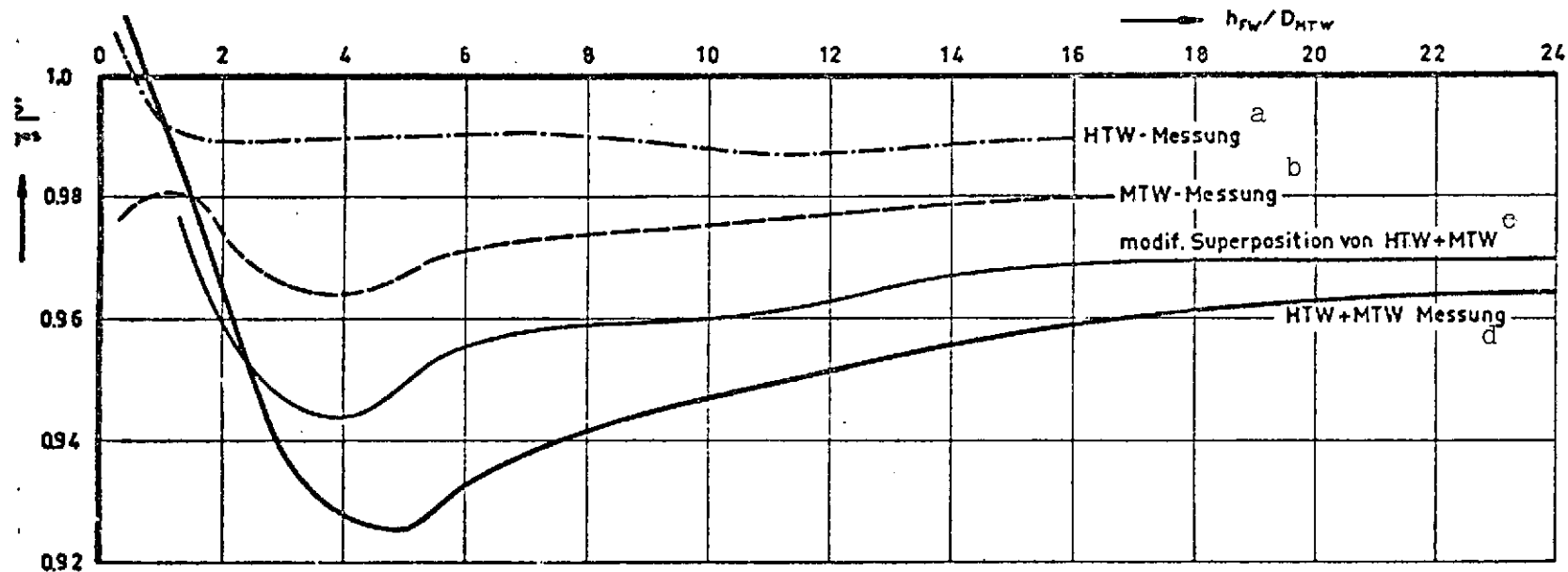


Fig. 5.8. Change in shift close to ground. Do 31 and Do 131 model measurements. Suction and fountain effects superimposed.

Key: a. Equivalent diameter of the two cruising power plants
b. Only cruising power plants operating



h_{FW} = Landing gear - to -
ground distance

D_{MTW} = Equivalent diameter of
the two cruising power
plants

S_{ges} = Takeoff thrust of all
power plants

Fig. 5.9. Do 31: change in thrust in hover as a function of ground distance. All power plants on takeoff thrust. $\theta = 0^\circ$. Cruising power plant nozzle angle $\tau = 90^\circ$

- Key:
- a. Lift power plant measurements
 - b. Cruising power plant measurements
 - c. Modified superposition of lift + cruising power plants
 - d. Lift + cruising power plant measurements

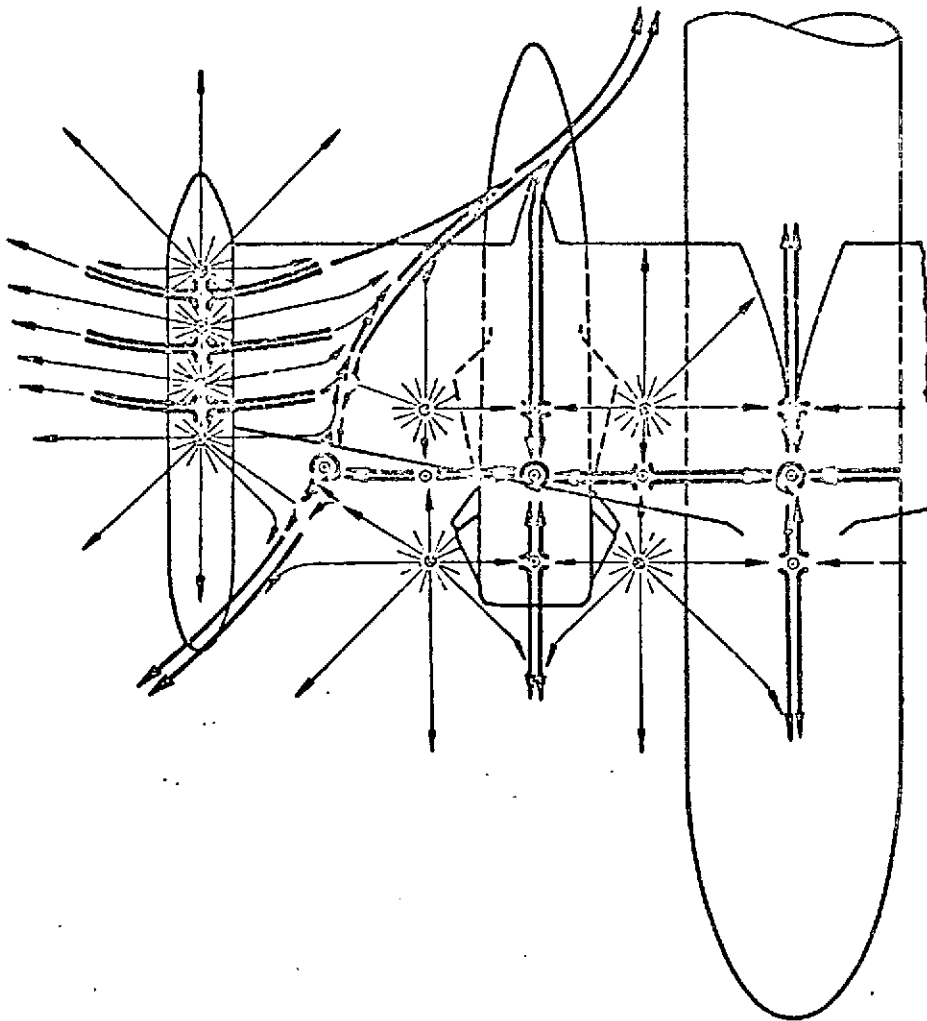


Fig. 5.10. Stagnation points and stagnation lines in ground flow field during Do 31 vertical takeoff.

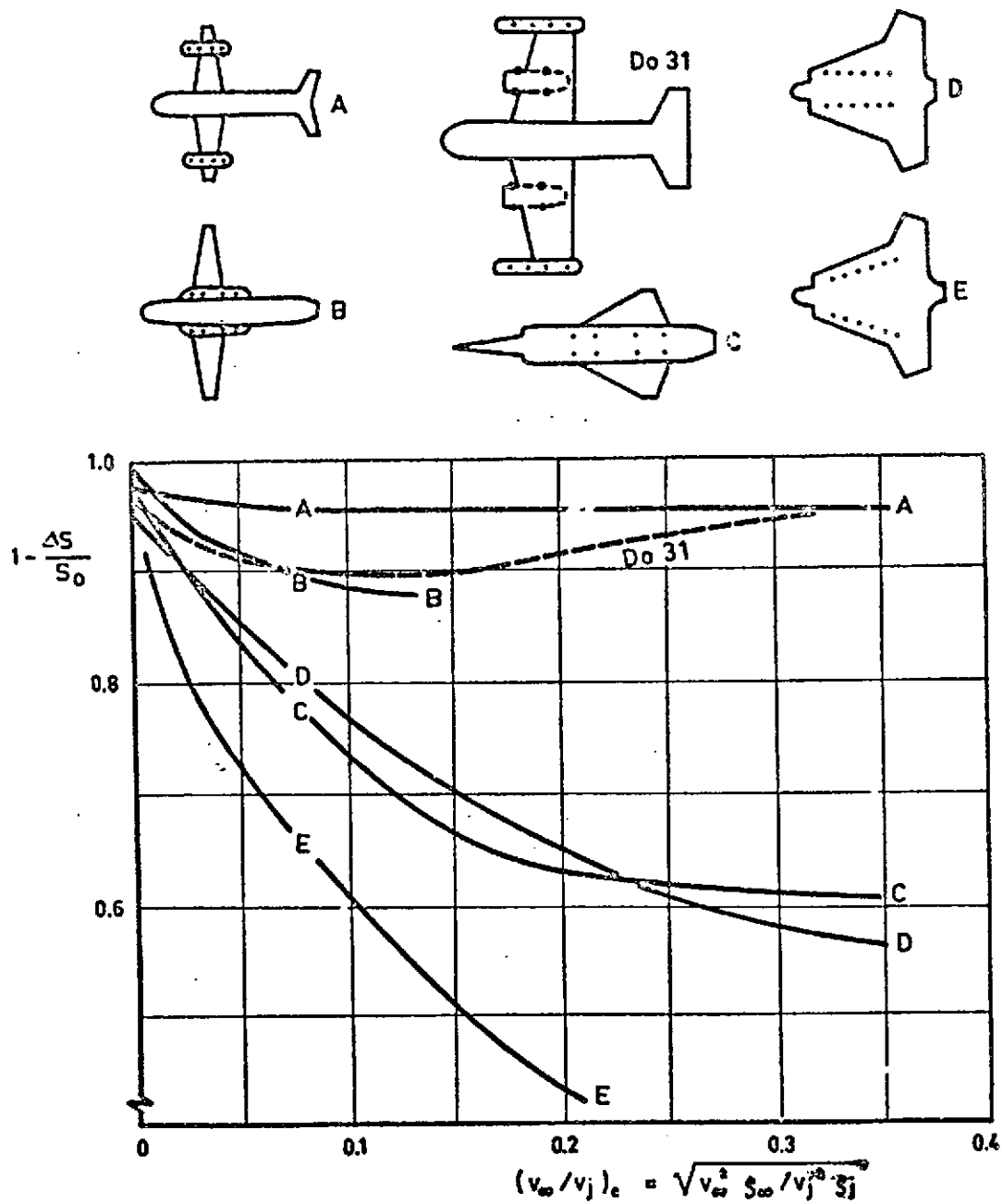


Fig. 5.11. BAC models and Do 31 model with lift and lift/thrust power plants in transition.

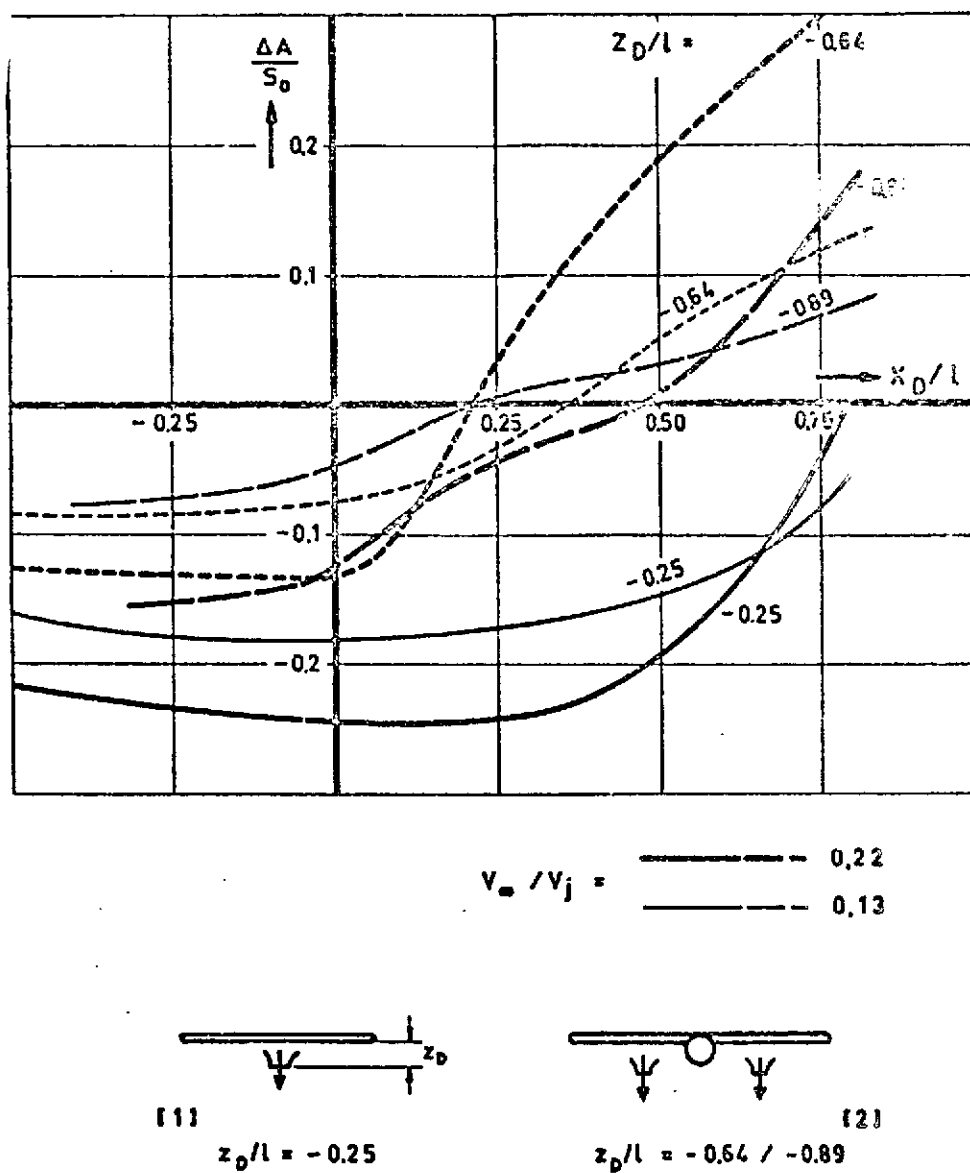


Fig. 5.12. Jet interference for a rectangular wing, from measurements taken from [1] and [2].

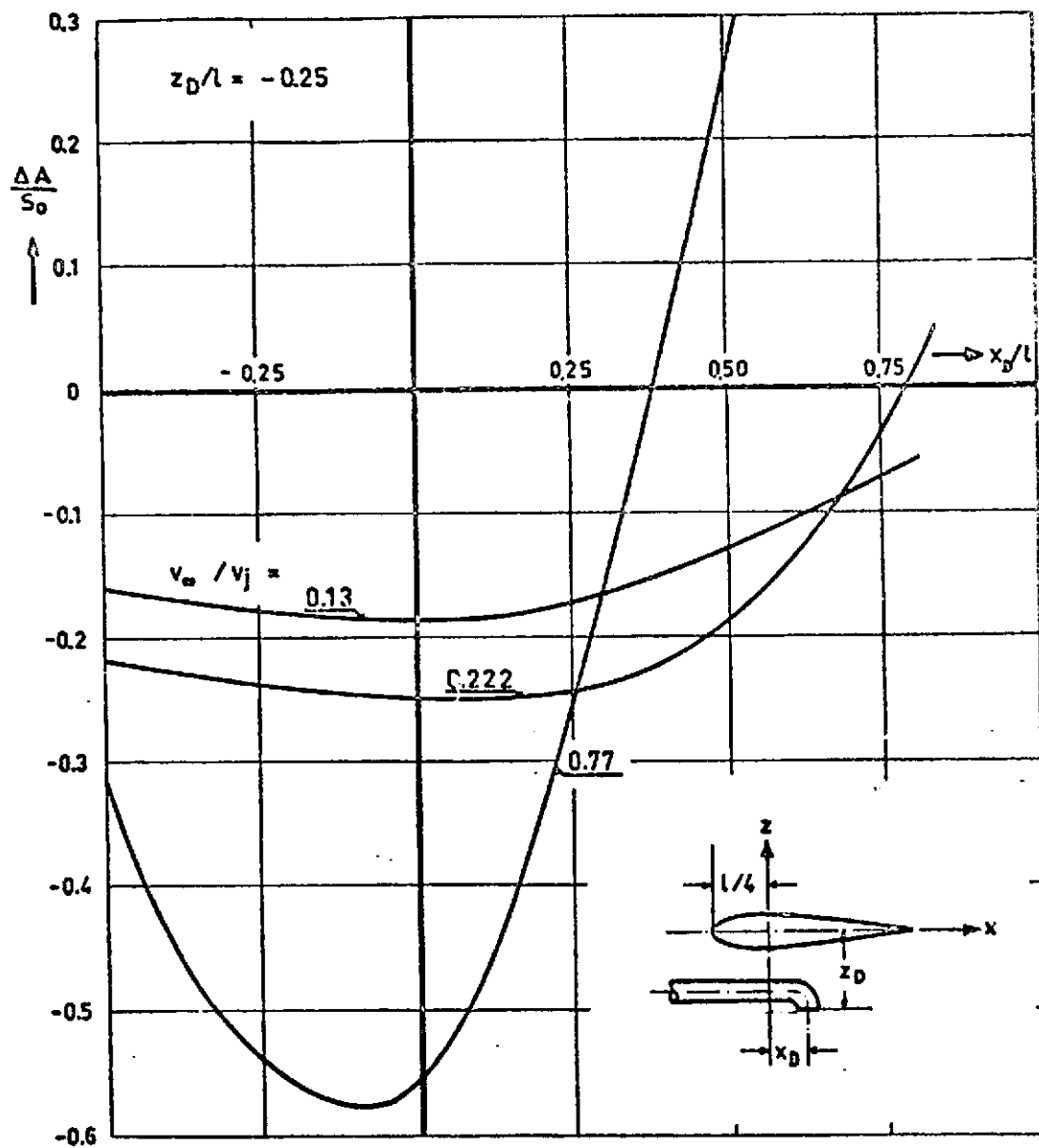


Fig. 5.13. Jet interference for a rectangular wing, from measurements in [1].

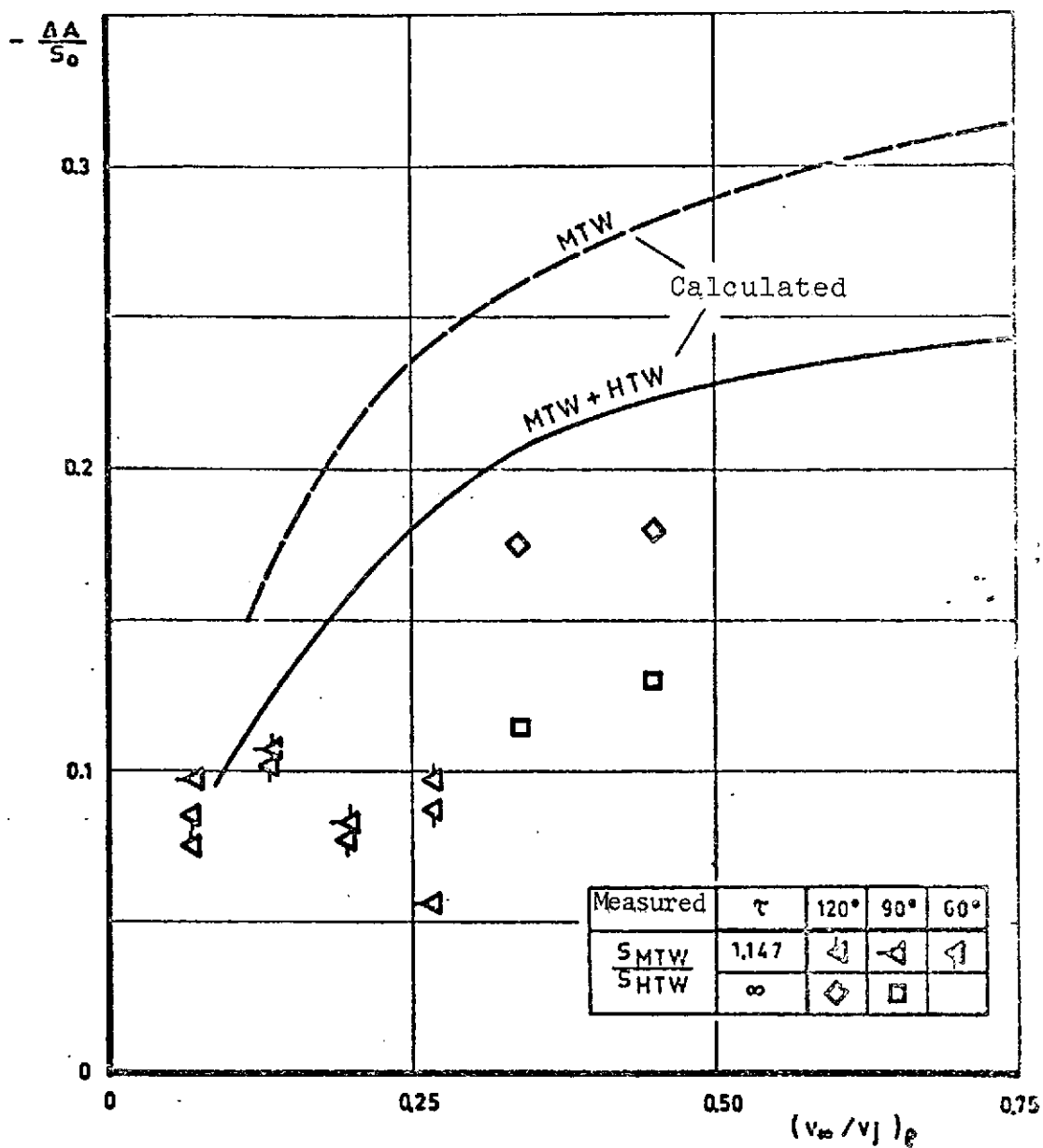


Fig. 5.14. Do 31 jet interference with cruising + thrust power plants. Comparison between measured and calculated values.

6. Summary

/168

This report contains all of the know-how associated with the problems that were solved in connection with jet interference during the development and testing of the Do 31 V/STOL transport aircraft. The most important results of model measurements, covering the complete V/STOL flight profile, are presented. From 1 to 4% lift loss was measured in hover; this increases to a maximum of 8% close to the ground. Jet-induced torques are not appreciable. In transition, the change in normal force can amount to as much as 12% of gross thrust, and the jet-induced tail-heavy torque requires up to 50% of available pitch control torque for compensation under the most unfavorable conditions.

The various model method were critically evaluated. The relatively simple principle of simulating power plant jets by the discharge of compressed air has proven itself in the case of the Do 31 and can also be recommended for future V/STOL development for measurements without forward speed. Due to the relatively high inlet momentum of up-to-date lift fans, both the thrust jet and inlet flow should be simulated for future V/STOL aircraft in jet interference measurements in transition flight.

A series of VTOL transitions by the Do 31 E3 test aircraft are analyzed with respect to jet-induced forces and torques. The data stored on magnetic tape are evaluated with a computer program. More than 120 measurement points had to be interrogated at a frequency of 5 Hz. The precision required for jet interference evaluations cannot always be satisfied, particularly in the measurement of thrusts. Nevertheless, the agreement between model and flight measurements is satisfactory, and it was possible to confirm the model principles which were applied.

The one known semiempirical method for calculating jet-induced normal force in hover is extended to complex configurations such as the Do 31. Points of reference are given for estimating jet interference close to the ground and in transition for future V/STOL aircraft. Model measurements cannot be dispensed with in the future, either.

/169